Specific Functions of ERK/MAPK Signaling in Brain Development and Neurocognition

by

Michael Holter

A Dissertation Presented in Partial Fulfillment
of the Requirements for the Degree
Doctor of Philosophy

Approved October 2019 by the
Graduate Supervisory Committee:

Jason Newbern, Chair
Trent Anderson
Janet Neisewander
Shwetal Mehta

ARIZONA STATE UNIVERSITY

December 2019

ABSTRACT

Development of the cerebral cortex requires the complex integration of extracellular stimuli to affect changes in gene expression. Trophic stimulation activates specialized intracellular signaling cascades to instruct processes necessary for the elaborate cellular diversity, architecture, and function of the cortex. The canonical RAS/RAF/MEK/ERK (ERK/MAPK) cascade is a ubiquitously expressed kinase pathway that regulates crucial aspects of neurodevelopment. Mutations in the ERK/MAPK pathway or its regulators give rise to neurodevelopmental syndromes termed the "RASopathies." RASopathy individuals present with neurological symptoms that include intellectual disability, ADHD, and seizures. The precise cellular mechanisms that drive neurological impairments in RASopathy individuals remain unclear. In this thesis, I aimed to 1) address how RASopathy mutations affect neurodevelopment, 2) elucidate fundamental requirements of ERK/MAPK in GABAergic circuits, and 3) determine how aberrant ERK/MAPK signaling disrupts GABAergic development.

Here, I show that a Noonan Syndrome-linked gain-of-function mutation $Raf1^{L613V}$, drives modest changes in astrocyte and oligodendrocyte progenitor cell (OPC) density in the mouse cortex and hippocampus. $Raf1^{L613V}$ mutant mice exhibited enhanced performance in hippocampal-dependent spatial reference and working memory and amygdala-dependent fear learning tasks. However, we observed normal perineuronal net (PNN) accumulation around mutant parvalbumin-expressing (PV) interneurons. Though PV-interneurons were minimally affected by the $Raf1^{L613V}$ mutation, other RASopathy mutations converge on aberrant GABAergic development as a mediator of neurological dysfunction.

I therefore hypothesized interneuron expression of the constitutively active *Mek1*$^{S217/221E}$ (*caMek1*) mutation would be sufficient to perturb GABAergic circuit development. Interestingly, the *caMek1* mutation selectively disrupted crucial PV-interneuron developmental processes. During embryogenesis, I detected expression of cleaved-caspase 3 (CC3) in the medial ganglionic eminence (MGE). Interestingly, adult mutant cortices displayed a selective 50% reduction in PV-expressing interneurons, but not other interneuron subtypes. PV-interneuron loss was associated with seizure-like activity in mutants and coincided with reduced perisomatic synapses. Mature mutant PV-interneurons exhibited somal hypertrophy and a substantial increase in PNN accumulation. Aberrant GABAergic development culminated in reduced behavioral response inhibition, a process linked to ADHD-like behaviors. Collectively, these data provide insight into the mechanistic underpinnings of RASopathy neuropathology and suggest that modulation of GABAergic circuits may be an effective therapeutic option for RASopathy individuals.

ACKNOWLEDGMENTS

"Just follow your heart kid, and you'll never go wrong."
- Babe Ruth, *The Sandlot*

I would like to give a very special thanks to my family – Mom, Dad, and Kimberly, and Uncle Chris and Aunt Jeannette, who have always been there for me and never missed a big moment. Thank you to Nanny and Poppy who showed me nothing but love and support. These people taught me to follow my dreams and that drive, persistence, and a sense of humor are the keys to a great life.

I would like to thank my advisor Dr. Jason Newbern not only for his outstanding mentorship and friendship, but also for challenging me to become the best scientist I could be. I'd like to thank Dr. Trent Anderson, Dr. Janet Neisewander, and Dr. Shwetal Mehta, who constitute arguably the greatest committee ever created.

I would like to thank all of my friends who made my graduate school career a fantastic experience. Here I have made friendships that will last a lifetime.

Lastly, I would like to thank the many mice that dedicated their lives to these projects for the betterment of human health.

TABLE OF CONTENTS

Page

CHAPTER Page

LIST OF TABLES

LIST OF FIGURES

Figure Page

LIST OF SYMBOLS

(ADHD)	Attention Deficit Hyperactivity Disorder
(ARC)	Activity Regulated Cytoskeletal Protein
(ASD)	Autism Spectrum Disorder (ASD)
(BDNF)	Brain Derived Neurotrophic Factor
(BMP)	Bone Morphogenetic Protein
(caMEK1)	constitutively active MEK1
(CFC)	Cardio-Facio-Cutaneous Syndrome
(CGE)	Caudal Ganglionic Eminence
(CIN)	Cortical GABAergic Interneuron
(CNO)	Clozapine-N-oxide
(CNS)	Central Nervous System
(CR)	Calretinin
(CSPG)	Chondrotin Sulfate Proteoglycan
(CT-1)	Cardiotrophin 1
(CQV)	Coefficient of Quartile Variation
(DREADD)	Designer Receptor Exclusively Activated by Designer Drug
(DTI)	Diffusion Tensor Imaging
(ECM)	Extracellular Matrix
(ERK)	Extracellular Regulated Kinase
(EYFP)	Enhanced Yellow Fluorescent Protein
(FGF8)	Fibroblast Growth Factor 8
(FMI)	Fixed Minimum Interval

(FS)	Fast-spiking
(GABA)	Gamma-amino-butyric Acid
(GDP)	Guanine Diphosphate
(GEF)	Guanine Nucleotide Exchange Factor
(GFAP)	Glial Fibrillary Acidic Protein
(GTP)	Guanine Triphosphate
(HA)	Hemagglutinin
(IRT)	Inter-response Time
(KO)	Knock Out
(LTI)	Latency to Initiate
(LTP)	Long Term Potentiation
(MAPK)	Mitogen Activated Protein Kinase
(MAPK1)	Mitogen Activated Protein Kinase 1
(MAPK3)	Mitogen Activated Protein Kinase 3
(MGE)	Medial ganglionic eminence
(NCFC)	Neuro-Cardio-Facio-Cutaneous
(NF1)	Neurofibromatosis Type 1
(NRG1)	Neuregulin 1
(NRG3)	Neuregulin 3
(OPC)	Oligodendrocyte Progenitor Cell
(PDGFRα)	Platelet Derived Growth Factor Receptor Alpha
(PFC)	Prefrontal Cortex
(PN)	Projection Neuron

(PNN) Perineuronal Net

(POA) Preoptic Area

(PTZ) Pentylenetetrazol

(PV) Parvalbumin

(RBD) RAS Binding Domain

(REF) Reference Memory

(RFP) Red Fluorescent Protein

(RTK) Receptor Tyrosine Kinase

(S1) Somatosensory Cortex

(SOS1) Son of Sevenless

(SST) Somatostatin

(SVZ) Subventricular Zone

(VGAT) Vesicular GABA Active Transporter

(VIP) Vasoactive Intestinal Polypeptide

(VZ) Ventricular Zone

(WMC) Working Memory Correct

(WMI) Working Memory Incorrect

(WRAM) Water Radial Arm Maze

CHAPTER 1

INTRODUCTION

The human brain is the most complex organ assembled through evolution. At its most complicated, the brain orchestrates incredible behavioral feats including the initiation and cessation of motor movement, the integration of sensory experience, and the storage of short- and long-term memories, all while performing basic autonomic functions essential for sustained life. The cerebral cortex is responsible for higher order cognitive functions that make us uniquely human. By volume, the human cortex accounts for approximately 77% of brain weight and is organized into sulci and gyri that allow for improved surface area and enhanced computational power compared to other organisms (*Trends in Neurosciences*, 18:471-474, 1995). The proper formation of the cortex requires advanced coordination of molecular and cellular events during both embryonic and neonatal development.

The activation of specific intracellular signaling cascades is necessary to give rise to the cellular and functional diversity of the cerebral cortex. In particular, the Extracellular Regulated Kinase (ERK/MAPK) pathway is a highly conserved and ubiquitously expressed signaling cascade that coordinates numerous aspects of cortical development including the regulation of neural progenitor cell division, neuronal fate, migration, and survival (Samuels et al., 2009). The ERK/MAPK cascade consists of four core constituents, RAS, RAF, MEK, and ERK, all of which are expressed to different degrees within individual neural cell types. MAPK3/ERK1 and MAPK1/ERK2 constitute the principal kinases of the core cascade and exhibit high levels of sequence homology and functional redundancy (Fremin et al., 2015).

In the brain, the canonical ERK/MAPK pathway is initiated through binding of specific ligands, such as growth factors, to Receptor Tyrosine Kinases (RTKs) in the extracellular space. Factors such as Fibroblast Growth Factor 8 (FGF8) and Brain Derived Neurotrophic Factor (BDNF) are essential for the establishment and refinement of cortical circuits (Huang et al., 1999; Toyoda et al., 2010). Upon ligand binding in the extracellular space, RTKs undergo an intracellular autophosphorylation event that recruits a complex of associated proteins including the Son of Sevenless (SOS) Guanine Nucleotide Exchange Factor (GEF). SOS isoforms facilitate the conversion of GDP- to GTP-bound RAS, leading to a conformational change in RAS to an active state. Through the RAS binding domain (RBD), RAS-GTP then recruits and activates the RAF kinases. The RAF isoforms then phosphorylate the substrates MEK1 and MEK2 (MEK1/2) at serine residues 218/222 (Lavoie and Therrien, 2015). MEK1/2 kinase activity leads to subsequent phosphorylation and activation of the ERK1/2 proteins, the principal kinases of the ERK/MAPK pathway. Phosphorylated ERK1/2 controls many cellular functions through both cytosolic and nuclear targets, allowing the cascade to regulate gene expression through numerous downstream effectors.

Importantly, dysregulation of the ERK/MAPK cascade has been implicated in several neurodevelopmental diseases. Fragile X and Angelman Syndromes, as well as some forms of schizophrenia, have all been indirectly linked to alterations in ERK/MAPK signaling (Fazzari et al., 2010; Filonova et al., 2014; McMillan et al., 2012). In addition, 1% of all Autism Spectrum Disorder (ASD) cases directly involve copy number variants of 16p11.2, a locus of 11 genes which includes the *MAPK3/ERK1* gene (Pucilowska et al., 2018; Pucilowska et al., 2015; Vithayathil et al., 2018). A family of neurodevelopmental

diseases, popularly called Neuro-Cardio-Facio-Cutaneous (NCFC) Syndromes or the "RASopathies," arise from mutations in the core constituents and regulators of the ERK/MAPK cascade (Figure 1) (Tidyman and Rauen, 2016). Collectively, the RASopathies affect approximately 1 in 2000 live births with varying degrees of neurological symptoms. Individuals with mutations in ERK/MAPK pathway components typically exhibit distinct neurological, craniofacial, and cardiac abnormalities. Neurological symptoms consist of intellectual disability, issues with motor commands, autism prevalence, and seizures (Adviento et al., 2014; Rauen et al., 2013). Collectively, abnormal ERK/MAPK pathway activity has emerged as a potential master regulator of neurological phenotypes across multiple disorders. Therefore, therapeutic measures designed to target this cascade may be particularly effective treatment options for a number of individuals suffering from neurological symptoms associated with aberrant ERK/MAPK activity.

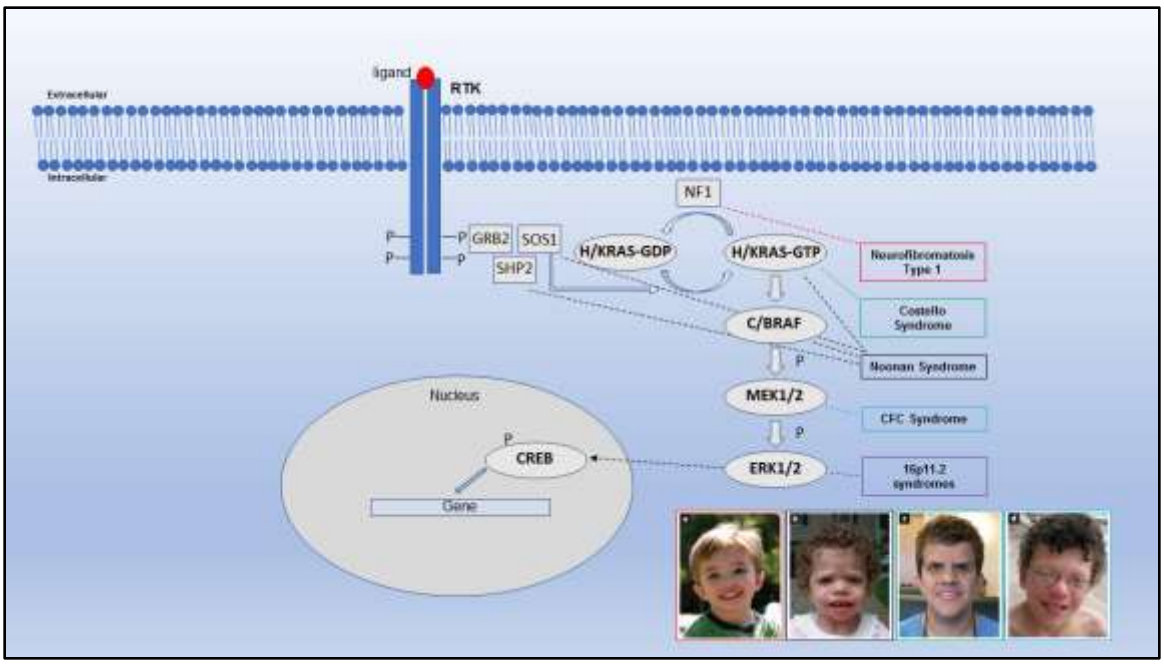

Figure 1. Mutations in regulators and core kinases of the ERK/MAPK cascade lead to the RASopathies. Ligand binding to RTKs in the extracellular space leads to the activation of the RAS isoforms. RAS binding to the RAF isoforms leads to the phosphorylation of MEK, which can then phosphorylate and activate the principal ERK1/2 isoforms. ERK1/2 can affect changes in gene expression through multiple means. Mutations in NF1, SOS1, Shp2, BRAF, CRAF, MEK1, MEK2, ERK1, and ERK2 are linked to a series of neurodevelopmental disorders termed the RASopathies. *Pictures of RASopathy patients are adapted from the laboratory of Katherine A. Rauen (Rauen et al., 2013).*

RASopathy-linked mutations differentially affect CNS cell populations

Despite a common pathogenic mechanism linking numerous developmental disease states to dysregulated ERK/MAPK signaling, the underlying contributions of individual cell types to neurocognitive abnormalities observed in ERK/MAPK-linked disorders remain incompletely understood. Thus, study of the basic requirements of ERK/MAPK in diverse neural cell populations will be necessary to fully understand disease neuropathogenesis. A comprehensive understanding of the cell-specific consequences of altered ERK/MAPK pathway activity on cortical circuitry will be fundamental to the development of new therapeutics for these individuals.

Mutations in nearly all core constituents and regulators of the ERK/MAPK cascade are sufficient to drive neurological dysfunction. In particular, genes such as *SYNGAP1*, *NF1*, *SOS1*, *PTPN11*, *SHOC2*, *K-RAS*, *H-RAS*, *BRAF*, *RAF1*, and *MEK1* have been reported in patient cases of the RASopathies (Pierpont et al., 2009; Rodriguez-Viciana et al., 2006; Tidyman and Rauen, 2016; Tidyman and Rauen, 2009). However, it is unclear how individual cortical cell types are affected by mutations in these genes. This is due in part to the variable expression of ERK/MAPK pathway components in distinct cortical populations. For example, *SYNGAP1* expression is enriched in cortical projection neurons (PNs) but lowly expressed in cortical GABAergic interneurons (CINs) (Mardinly et al., 2016). As a consequence, neurological phenotypes related to changes in SYNGAP1 protein function are severe when PNs are selectively affected (Ozkan et al., 2014). These phenotypes include increased seizure susceptibility, anxiolytic behaviors, and deficits in fear learning. Conversely, no significant neurological abnormalities are observed when

CINs are selectively mutated (Ozkan et al., 2014). Therefore, individual types of cortical neurons may regulate distinct aspects of neuropathogenesis on a mutation-specific basis.

Furthermore, loss of a negative regulator of RAS signaling, neurofibromin, leads to differential neurocognitive outcomes when conditionally deleted from glutamatergic or GABAergic neurons. Intellectual disability is commonly observed in patient cases of NF1 and other RASopathies, and is typically thought to be mediated by changes in hippocampal function (Rauen et al., 2013). Interestingly, loss of NF1 from postmitotic glutamatergic neurons was not sufficient to alter hippocampal-dependent spatial reference memory (Cui et al., 2008). However, conditional deletion of NF1 from post-mitotic GABAergic neurons led to deficits in hippocampal learning and memory and associated defects in long term potentiation (LTP) (Cui et al., 2008). Collectively, these data from two upstream regulators of RAS activity suggest that the neuropathogenesis of specific RASopathy disease states is controlled by distinct populations of neural cell types.

Neurofibromin is highly expressed in non-neuronal glial cell populations, and thus these cells are likely involved in NF1 neuropathogenesis (Loo et al., 2019; Mardinly et al., 2016). This is substantiated by post-mortem patient studies, where brain tissue of individuals with Neurofibromatosis type 1 (NF1) revealed high densities of glial fibrillary acidic protein-expressing (GFAP) reactive astrocytes across multiple brain regions (Nordlund et al., 1995; Rizvi et al., 1999). Indeed, loss of neurofibromin in glial progenitors of the CNS drives reactive astrogliosis and increased risk of tumor formation, another common phenotype observed in clinical cases of NF1 (Rauen et al., 2013; Rauen et al., 2015; Zhu et al., 2005). Loss of NF1 function specifically in post-mitotic neurons is similarly sufficient to increase numbers of $GFAP^+$ astrocytes (Zhu et al., 2001).

Furthermore, oligodendrocyte progenitor cell (OPC) pool expansion is frequently observed in the CNS of NF1 mouse models (Bennett et al., 2003). OPC expansion may lead to changes in myelinogenesis and potentially underlie white matter abnormalities in NF1 patients (Ishii et al., 2013; Koini et al., 2017). Therefore, glia appear to play a central role in the pathogenesis of NF1 and modulation of their functions within neural circuits may alleviate some neurological symptoms.

Despite clear evidence for individual cell type contributions to RASopathy pathogenesis, it is difficult to understand how mutations in genes such as *Syngap1*, *Nf1*, *Sos1*, and the *Ras* isoforms drive neurological defects. Mutations that lead to aberrant RAS signaling drive alterations in pathway activity through multiple intracellular cascades (Figure 2) (Anastasaki and Gutmann, 2014; Brown et al., 2012; Hegedus et al., 2007; Kaul et al., 2015). While ERK/MAPK is often considered the classic kinase pathway activated by RAS, other parallel molecular cascades such as PI3K, Rho/ROCK, and cAMP are often adversely affected (Anastasaki and Gutmann, 2014; Brown et al., 2012; Hegedus et al., 2007; Kaul et al., 2015). Pharmacological modulation of each of these intracellular cascades is sufficient to reverse some aspects of neuropathogenesis.

Studying mutations in upstream regulators of RAS signaling poses difficulty in understanding how unique downstream cascades mediate neurological phenotypes. Mutations in the RAS effector *BRAF*, of which the encoded BRAF protein has selective binding affinity for MEK isoforms, drive profound behavioral deficits in RASopathy individuals with cardio-facio-cutaneous (CFC) Syndrome (Pierpont et al., 2010b). Mutations in *BRAF* are often associated with strong biochemical activation of the MEK and ERK isoforms (Rodriguez-Viciana et al., 2006), which may therefore significantly

alter critical cellular events during brain development. Mutations in other RAF isoforms, such as *RAF1*, have been documented in clinical RASopathy cases (Pandit et al., 2007; Razzaque et al., 2007). These patients often exhibit behavioral deficits, though biochemical activation of downstream ERK/MAPK components in response to *RAF1* mutations appears to be weak relative to most *BRAF* mutations (Rodriguez-Viciana et al., 2006; Wu et al., 2011). In addition, mutations in canonical components of the ERK/MAPK cascade are associated with greater severity of behavioral complications in comparison to mutations in upstream regulators of RAS (Pierpont et al., 2010b). Thus, examining the neurological ramifications associated with mutations in kinases downstream of RAS will be insightful in determining the specific effects of ERK/MAPK signaling to the neuropathogenesis of the RASopathies.

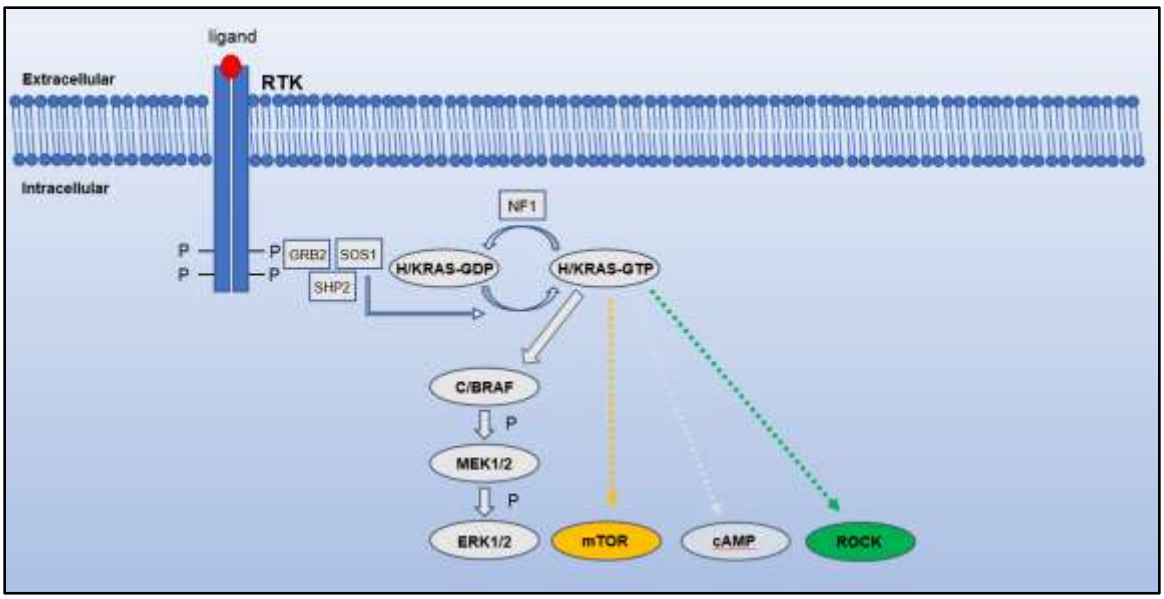

Figure 2. Parallel cascades are affected by mutations upstream of RAS. The majority of RASopathy mutations are found in upstream regulators of the canonical ERK/MAPK pathway. Dysregulation of RAS activity leads to differential activation of other intracellular signaling cascades such as PI3K/AKT/mTOR, cAMP, and Rho/ROCK in addition to canonical ERK/MAPK. It is therefore difficult to understand how each of these cell signaling pathways contributes to the neurological phenotypes observed in the RASopathies.

ERK/MAPK in the CNS – MAP of pallial development

Canonical ERK/MAPK activity instructs the development of cortical cell populations. Previous research has elucidated several roles for the cascade in the development of dorsal-derived cell populations, such as cortical excitatory neurons and glia (Li et al., 2012b; Pucilowska et al., 2012; Pucilowska et al., 2008; Pucilowska et al., 2015; Xing et al., 2016). The dorsal pallium of the cerebral cortex contains fate-restricted radial glia populations that reside in the ventricular and subventricular zones (VZ, SVZ) and give rise to elaborate cortical columns (Haueis, 2016; Mountcastle, 1997; Rakic, 1974). Radial glia divide asymmetrically to produce glutamatergic cortical projection neurons (PNs) in inside-out fashion (Greig et al., 2013). Radial migration of nascent PNs along radial glial fibers generate six functionally diverse cortical layers, where newly born neurons migrate beyond the previously established layer in a process called lamination (Cooper, 2008). Deep layer 5/6 cortical excitatory neurons primarily form long-range subcortical projections, whereas upper layer 2/3 glutamatergic neurons project intra-cortically across the corpus callosum to the opposite hemisphere (Greig et al., 2013). Cortical PNs are produced from E11 to approximately E15.5, where radial glia shift to gliogenesis and begin the production of astrocytes. This neuro/gliogenic "switch" requires complex interactions between extracellular matrix molecules and their coinciding signaling pathways (Miller and Gauthier, 2007). Cardiotrophin 1 (CT-1) activation of JAK-STAT is a key mediator of cortical astrogenesis (Barnabé-Heider et al., 2005). Upregulation of glial genes is also mediated by bone morphogenetic proteins (BMPs) and Delta/Notch signaling (Miller and Gauthier, 2007). Collectively, BMPs and Delta/Notch activate the Smad family of transcription factors, which positively regulate gliogenic genes (Gomes et al., 2003). In

addition, BMP signaling during the gliogenic period upregulates the helix-loop-helix transcription factor Id1, which represses neurogenesis (Nakashima et al., 2001).

The ERK/MAPK signaling cascade is similarly integral to the onset of gliogenesis, as radial glia lacking the kinases MAP2K1 and MAP2K2 (MAP2K1/2) lead to cortices completely devoid of astrocytes (Li et al., 2012b). Reinstatement of the ERK/MAPK target and *Ets* transcription family member, *Erm*, was sufficient to rescue gliogenesis in the developing cortex (Li et al., 2012b). Conversely, expression of a constitutively active MAP2K1 (herein referred to as caMek1) allele in radial glia promoted an early shift into gliogenesis and a significant overproduction of astrocytes, likely at the expense of some cortical PNs (Li et al., 2012b). Although many signaling molecules, kinases, and transcription factors are involved in corticogenesis, ERK/MAPK appears to be a central regulator of cortical cell number and controls crucial temporal aspects of early brain development.

In addition to its roles in neuro- and gliogenesis, ERK/MAPK signaling is required in postnatal processes necessary for cortical maturation. Post-mitotic layer 2/3 PNs require ERK/MAPK for elaborate dendritic complexity and axonal outgrowth processes, though ERK/MAPK is not necessary for their long-term survival (Pucilowska et al., 2012; Xing et al., 2016). Cortices lacking ERK/MAPK fail to form the corpus callosum (Li et al., 2012b), though this may be due to combinatorial effects of not only pallial-generated neurons but also astrocytes and oligodendrocytes. Conversely, canonical ERK/MAPK activity is critical to the survival of layer 5 CTIP2^{+} subcortical PNs, where loss of ERK/MAPK drives the cleaved caspase 3-mediated death of a subset of these cells (Xing et al., 2016). Interestingly, enhanced MEK1 activity delays layer 5 PN axonal extension into the

neonatal spinal cord and increases arborization (Xing et al., 2016). Collectively, normal ERK/MAPK signaling is essential for the early establishment of pallial-derived neurons and glia to produce functional cortical circuits.

CINs are generated in the ganglionic eminences of the embryonic subpallium

Approximately 20% of cortical neurons utilize the neurotransmitter γ-aminobutyric acid (GABA), the primary inhibitory neurotransmitter in the Central Nervous System (CNS) (Sahara et al., 2012). Cortical GABAergic interneurons (CINs) are a population of locally connecting cells provide the inhibitory balance to cortical glutamatergic excitation. CINs have well-defined roles in cortical formation, maintenance of critical period plasticity, and modulation of behavioral output (Hensch, 2005a; Hensch, 2005b; Huang et al., 2007; Lehmann et al., 2012; Markram et al., 2004). An estimated 22 different CIN subtypes exist in the mature cortex which can be classified by their differing biochemical, morphological, and electrophysiological properties in addition to distinct patterns of connectivity (Fino et al., 2013; Rudy et al., 2011). The differences in these properties allow CIN subtypes to perform a variety of functions essential for basic cortical computation.

The rich diversity of CIN subtypes are generated by radial glia inhabiting the medial and caudal ganglionic eminences of the subpallium (MGE and CGE respectively), and to a lesser extent, the preoptic area (POA) (Gelman et al., 2009; Wonders and Anderson, 2006). Progenitors of the MGE require the homeobox transcription factor *Nkx2.1* to generate CINs during embryogenesis (Sussel et al., 1999). *Nkx2.1*$^{-/-}$ mutant mice do not develop the MGE and instead form a single, continuous lateral ganglionic eminence (LGE). In adulthood, mice lacking Nkx2.1 function exhibit a significant reduction in CIN density,

further establishing Nkx2.1 as an essential mediator of the CIN lineage (Sussel et al., 1999; Wonders and Anderson, 2006). Furthermore, mutant cortices exhibit reduced *Lhx6*-expressing cells, another key determinant of the MGE-derived cell fate (Sussel et al., 1999). Nearly 70% of CINs arise from the MGE and can be biochemically classified by non-overlapping expression of the calcium chelator, parvalbumin (PV), or the neuropeptide, somatostatin (SST) (Miyoshi et al., 2015). More recent studies suggest that the location of MGE progenitors within the VZ and SVZ and rostro-caudal location is sufficient to bias nascent CINs toward differential fates (McKenzie et al., 2019; Petros et al., 2015). Interestingly, no known transcriptional markers currently exist to differentiate CIN subtypes in the early stages of neurogenesis (Lim et al., 2018; Mayer et al., 2018; Mi et al., 2018; Sandberg et al., 2018). Transcriptional analyses seem to indicate that unspecified, yet biased progenitors give rise to the rich diversity of mature CINs. Importantly, MGE CIN fates appear to be patterned, at least in part, by non-canonical Wnt signaling from multiple sources across the eminence (McKenzie et al., 2019).

In the adult cortex, PV and SST-CINs comprise the most populous and functionally diverse CIN subtypes. PV-CINs exhibit either a basket or chandelier morphology and high frequency firing rates unlike that of other CINs (Butt et al., 2005; DeFelipe et al., 2013; Rudy and McBain, 2001). Distinct PV-CIN morphologies coincide with differential patterns of connectivity: basket cell axon terminals primarily target the soma of PNs, whereas chandelier synaptic contacts are formed on the PN axon initial segment (Fino et al., 2013). The fast-spiking (FS) properties characteristic of PV-CINs are driven by the expression of fast-inactivating Kv3.1 and Kv3.2 potassium channels (Rosato-Siri et al., 2015; Rudy and McBain, 2001). The differential expression of ion channels is fundamental

to the acquisition of specific firing rates and contributes to the rich diversity of CIN subtypes. The high metabolic demand of the FS firing rate requires PV-CINs to maintain high densities of mitochondria compared to other neuron populations (Kann et al., 2014).

SST-expressing interneurons comprise the second most abundant CIN subtype and can be identified electrophysiologically as burst-spiking nonpyramidal cells or by low threshold-spiking firing patterns (Butt et al., 2005). In contrast to PV basket or chandelier cells, SST Martinotti cells primarily innervate the dendrites of cortical PNs and thus are important for the fine-tuning of neural activity through cortical circuits (Fino et al., 2013). SST-CIN signaling is important for the early activity-dependent maturation of cortical circuits. During neonatal development, GABA signaling exerts "excitatory" properties until the expression of the chloride ion channel KCC2, whereupon GABA exerts inhibitory effects (Ben-Ari, 2002). Premature inhibition by GABA during the first postnatal week disrupts cortical PN dendritic arborization, a process likely mediated by SST-CINs (Cancedda et al., 2007). Thus, the normal development and maturation of SST-CINs is essential to the sculpting of cortical circuits.

In comparison to the MGE, the caudal ganglionic eminence (CGE) generates 30% of CINs that have a distinct genetic profiles and laminar allocations (Miyoshi et al., 2015). Gsh1, ER81, and Prox1 are all crucial to the proper migration and maturation of CGE-derived CINs (Hernandez-Miranda et al., 2010; Miyoshi et al., 2015). Fate-mapping revealed that CINs originating from the CGE integrate primarily into the superficial layers of the cortex (Miyoshi and Fishell, 2011; Miyoshi et al., 2010). These CINs can be distinguished from MGE-derived CINs by expression of *5HTr3A*, in conjunction with other markers such as the calcium binding protein calretinin (CR), Reelin, and Vasoactive

Intestinal Polypeptide (VIP) (Miyoshi et al., 2015). Both MGE- and CGE-derived CINs require expression of *Dlx1/2* and *Dlx5/6* genes, which constitute the master regulators of GABAergic identity. Mice lacking these genes exhibit subtype-specific CIN loss due to alterations in both specification and migration (Cobos et al., 2005; Le et al., 2007; Long et al., 2009; Wang et al., 2010).

CINs utilize distinct migratory trajectories compared to PNs. Nascent CINs undergo an initial wave of tangential migration along the marginal zone and ventricular surfaces of the developing embryonic pallium (Metin et al., 2006). Tangential migration is guided by a series of chemotaxic cues such as Slit1 and Enfa5, which are highly expressed in the VZ of the MGE and function as chemorepellents to direct nascent CINs into the subpallial mantle zones (Marin, 2013; Zimmer et al., 2008). Chemorepulsion by semaphorin/neuropilin signaling is equally essential to CIN migration and inhibit early termination of migratory processes in the striatum (Marin and Rubenstein, 2001). GABAergic progenitors that are unresponsive to these signaling mechanisms tend to acquire a striatal identity and terminate migration in this region (Marin and Rubenstein, 2001).

Tangential migration to the cortex is also mediated by netrin-1, which is required for CIN migration through the cortical plate (Stanco et al., 2009). Classic trophic factors such as BDNF and NT4 function to increase the motility of immature CINs and are thus essential during early migratory stages (Polleux et al., 2002). Sustained tangential migration requires PI3K pathway activity and is not dependent on canonical ERK/MAPK signaling (Polleux et al., 2002). Neuregulin-1 (NRG1) and its associated receptor, ErbB4, act as an early chemorepellent (Li et al., 2012a). ErbB4 is enriched in the GABAergic

progenitors and remains highly expressed in mature PV-CINs. GABAergic precursors shift to radial migration in late embryogenesis to invade the cortical lamina. The shift from tangential to radial migration is mediated by the activation of ERBB4 by neuregulin 3 (NRG3), which drives cortical plate invasion of tangentially-migrating CINs (Bartolini et al., 2017). Cell adhesion mechanisms, such as formation of gap junctions between CINs and the radial glial fibers, are necessary for the shift to radial migration (Elias et al., 2007; Marin et al., 2010). GABAergic precursor leading processes sequester high concentrations of integrins and the connexins Cx43 and Cx26 at contact points with radial glia (Elias et al., 2007; Huang, 2009; Kawauchi, 2015; Marin et al., 2010). CINs in the cortical lamina then undergo activity-dependent pruning, where GABAergic cell number is refined by a wave of Bax-dependent cell death during the first postnatal week (Southwell et al., 2012). This programmed cell death event ensures the proper balance between excitation and inhibition necessary for normal function of the cerebral cortex.

Maturing CINs that survive cortical pruning are important in maturation processes such as critical period plasticity (Hensch, 2005a; Hensch, 2005b; Morishita et al., 2015). The maturation of GABAergic circuits is closely coupled with experience-dependent plasticity in a complex molecular process mediated by BDNF (Castrén et al., 1992; Huang et al., 1999). Indeed, formation of GABAergic perisomatic synapses around cortical PNs is regulated trophic factors such as BDNF and NRG1 (Chattopadhyaya et al., 2004; Fazzari et al., 2010; Huang et al., 1999). Importantly, fast-spiking PV-CIN populations have enriched ERBB4 expression in comparison to other CINs and have high synaptogenic affinity for PN soma and axon initial segments (DeFelipe et al., 2013; Fino et al., 2013; Rudy et al., 2011).

PV-CINs effectively gate the end of critical period plasticity in the CNS. During the second postnatal week, PV-CINs become encapsulated within an ECM structure of sequestered chondroitin sulfate proteoglycans called the perineuronal net (PNN) (Hensch, 2005a). Abnormal onset, extent, and function of the PNN during development is thought drastically perturb critical period plasticity and alter cortical output (Steullet et al., 2017). Disruption of ECM remodeling and PNN formation is commonly observed in many neurodevelopmental disorders and is therefore thought to contribute broadly to human neurocognitive phenotypes (Krencik et al., 2015; Steullet et al., 2017). Furthermore, astrocyte-directed RASopathy mutations drive enhanced PNN sequestering around PV-CINs (Krencik et al., 2015). Thus, it has been proposed that dysregulation of this essential process is a central mediator of RASopathy neuropathogenesis. The GABAergic contributions to this bidirectional process have not been explored in the context of the RASopathies.

How aberrant ERK/MAPK signaling affects brain development and gives rise to neurological symptoms of the RASopathies is poorly understood. Here, I aimed to **1)** address how a unique RASopathy mutation affects brain development, **2)** understand the fundamental requirements of ERK/MAPK in developing GABAergic circuits, and **3)** determine how pathological ERK/MAPK signaling during GABAergic development disrupts function of the mouse cerebral cortex.

To address these aims, I provide the first neurological characterization of a Noonan Syndrome-linked *Raf1*^{L613V} mouse model. I show that *Raf1*^{L613V} mutant mice have modest but significant increases in astrocyte and oligodendrocyte progenitor cell number. Unlike past RASopathy mouse models, *Raf1*^{L613V} mice exhibited enhanced performance in spatial

reference, working, and fear learning, and thus represent the first germline RASopathy mouse model with learning and memory improvements.

Dysfunctional GABAergic circuitry has been broadly implicated as a potential driver of neurological impairments in many neurodevelopmental disorders. To determine how GABAergic circuits contribute to the neurological deficits in the RASopathies, we employed Cre-dependent conditional mutagenesis to either **1)** hyperactivate, or **2)** delete ERK/MAPK within developing GABAergic interneurons. I show that increased ERK/MAPK signaling in developing GABAergic circuits disrupts the establishment of PV-expressing CIN density, with minimal effects on other CIN subtypes. Reduced PV-CIN density was due to an early embryonic cell death event mediated by cleaved-caspase 3 near the ganglionic eminences during neurogenesis. Interestingly, increased MEK1 activity was not sufficient to alter basic physiological development of PV-CINs, which maintained fast-spiking signatures. Hyperactive ERK/MAPK in PV-CINs led to a shocking increase in PNN accumulation, a critical extracellular structure associated with cortical maturation. Hyperactive mutant mice had significant impairments in prefrontal cortex-mediated behavioral response inhibition, a set of behaviors linked to ADHD-like phenotypes.

Conversely, deletion of ERK/MAPK from developing CINs had minimal effects of PV-CINs, but substantial alterations in SST-CIN specification. ERK1/2 deletion from GABAergic circuits resulted in global changes in activity-dependent gene expression, suggesting that normal ERK/MAPK signaling in developing CINs is required for the normal maturation of the cerebral cortex. Taken together, this work argues for increased study of patient specific mutations and implicates defective GABAergic circuits as a

primary contributor to the RASopathies. Thus, modulation of inhibitory signaling may be particularly impactful for treating the neurological symptoms of some RASopathy individuals.

CHAPTER 2

The Noonan Syndrome-linked *Raf1*^{L613V} mutation drives increased glial number in the mouse cortex and enhanced learning.

Authors: Michael C. Holter[1], Lauren. T. Hewitt[1,5,†], Stephanie V. Koebele[2,5], Jessica M. Judd[2], Lei Xing[4], Heather A. Bimonte-Nelson[2,5], Cheryl D. Conrad[2], Toshiyuki Araki[3], Benjamin G. Neel[3], William D. Snider[4], Jason M. Newbern* [1, #]

Affiliations:

[1]School of Life Sciences, [2]Department of Psychology, Arizona State University; Tempe, AZ 85287

[3] Laura and Isaac Perlmutter Cancer Center, NYU Langone Health, NY, NY 10016

[4]University of North Carolina Neuroscience Center, The University of North Carolina School of Medicine; Chapel Hill, NC, 27599

[5]Arizona Alzheimer's Consortium; Phoenix, AZ

[†]Present Address: Interdepartmental Neuroscience Graduate Program, University of Texas; Austin, TX, 78712

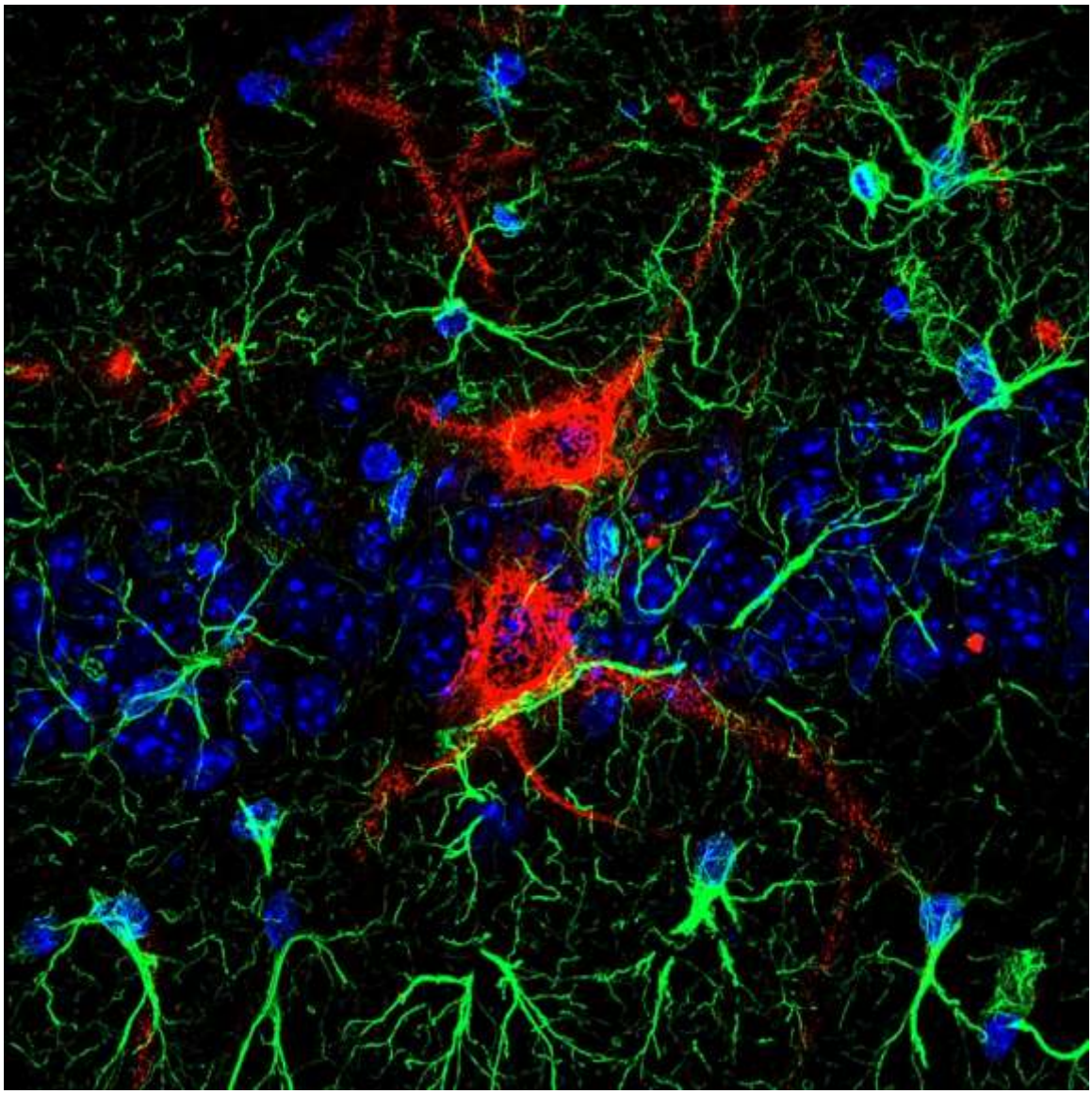

Cover Art Submission. *GFAP-expressing astrocytes (green), the astrocyte-derived PNN (red), and cell nuclei (blue) distributed within CA1 of the Raf1^{L613V} mouse hippocampus.*

Abstract

RASopathies are a family of related syndromes caused by mutations in regulators of the RAS/Extracellular Regulated Kinase 1/2 (ERK1/2) signaling cascade that often result in neurological deficits. RASopathy mutations in upstream regulatory components, such as *NF1, PTPN11/SHP2,* and *RAS* have been well-characterized, but mutation-specific differences in the pathogenesis of nervous system abnormalities remain poorly understood, especially those involving mutations downstream of *RAS*. Here, we assessed cellular and behavioral phenotypes in mice expressing a $Raf1^{L613V}$ gain-of-function mutation associated with the RASopathy, Noonan Syndrome. We report that $Raf1^{L613V/wt}$ mutants do not exhibit a significantly altered number of excitatory or inhibitory neurons in the cortex. However, we observed a significant increase in the number of specific glial subtypes in the forebrain. The density of $GFAP^+$ astrocytes was significantly increased in the adult $Raf1^{L613V/wt}$ cortex and hippocampus relative to controls. $OLIG2^+$ oligodendrocyte progenitor cells were also increased in number in mutant cortices, but we detected no significant change in myelination. Behavioral analyses revealed no significant changes in voluntary locomotor activity, anxiety-like behavior, or sociability. Surprisingly, $Raf1^{L613V/wt}$ mice mutants performed better than controls in select aspects of the water radial-arm maze, Morris water maze, and cued fear conditioning tasks. Overall, these data show that increased astrocyte and oligodendrocyte progenitor cell (OPC) density in the cortex coincides with enhanced cognition in $Raf1^{L613V/wt}$ mutants and further highlight the distinct effects of RASopathy mutations on nervous system development and function.

Introduction

The canonical RAS/RAF/MEK/ERK (aka ERK1/2 or MAPK3/MAPK1) intracellular signaling cascade is a crucial regulator of specific aspects of neural development and synaptic function (Cui et al., 2008; Fremin et al., 2015; Ishii et al., 2013; Kushner et al., 2005; Lee et al., 2014; Li et al., 2012b; Newbern et al., 2008; Xing et al., 2016). Mutations that lead to altered ERK1/2 signaling give rise to a group of human developmental syndromes, commonly referred to as "RASopathies" (Rauen et al., 2013). Cardiac, craniofacial, and neurological abnormalities, such as developmental delay, hypotonia, intellectual/cognitive disability, and epilepsy, are often observed in individuals with RASopathies, in addition to an increased risk of autism (Adviento et al., 2014; Alfieri et al., 2010; Jindal et al., 2015; Mitra et al., 2017). Autism-like phenotypes and changes in ERK1/2 activity have also been detected in mouse models of Angelman (MIM: 105830), Rett (MIM: 312750), and Fragile X (MIM: 300624) syndromes (Filonova et al., 2014; Greer et al., 2010; Michalon et al., 2012; Xu et al., 2014; Yashiro et al., 2009). The majority of RASopathy mutations lead to hyperactive signaling and are concentrated in classic components of Receptor Tyrosine Kinase (RTK)-linked intracellular signaling cascades. These include 'upstream' regulators of multiple cascades (*PTPN11* (MIM: 176876), *NF1* (MIM: 162200), *SHOC2* (MIM: 602775), *SOS1/2* (MIM: 182530, 601247), *SYNGAP1* (MIM: 603384), *SPRED1* (MIM: 609291), *SPRY1* (MIM: 602465), *K/N/HRAS* (MIM: 190070, 164790, 190020)), and relatively 'downstream' kinases in the core ERK1/2 pathway (*BRAF/RAF1* (MIM: 164757, 164760), *MEK1/2* (MIM: 176872, 601263), *ERK1/2* (MIM: 601795, 176948)) (Alfieri et al., 2010; Cesarini et al., 2009; Pierpont et al., 2009; Tartaglia et al., 2011; Tidyman and Rauen, 2016). Individuals with Noonan

Syndrome (MIM: 163950) comprise ~50% of all RASopathy cases and mutations have been observed in multiple genes, including *PTPN11/SHP2*, *SOS1*, *SHOC2*, *KRAS*, *NRAS*, *LZTR1* (MIM: 600574), *RAF1/CRAF*, and *MAP2K1/MEK1* (Chen et al., 2014; Jindal et al., 2015; Tidyman and Rauen, 2016). While the genetic cause for most RASopathies is known, therapeutic options remain limited, due in part to an incomplete understanding of disease neuropathogenesis.

RASopathies are often associated with diminished intellectual functioning and neuropsychiatric impairment, but these phenotypes are highly variable (Jindal et al., 2015; Pierpont et al., 2009; Pierpont et al., 2010b; Pierpont et al., 2013; Tartaglia et al., 2001). Individuals with mutations in kinases downstream of RAS (e.g. *RAF*, *MEK*) generally exhibit more pronounced neurocognitive deficits in comparison to mutations in upstream regulators of RAS activity (Pierpont et al., 2009; Tartaglia et al., 2002; Tartaglia et al., 2001; Zenker et al., 2004). This is perhaps surprising since upstream mutations could lead to abnormalities in multiple parallel signaling cascades, including AKT/mTOR, RHO/ROCK, and PKA, in addition to ERK1/2 (Anastasaki and Gutmann, 2014; Brown et al., 2012; Castellano and Downward, 2011; Kaul et al., 2015). Pharmacological modulation of ROCK, NOTCH, PKC, or cAMP/PKA signaling appear to mitigate select cellular defects in animal models, indicating ERK1/2-independent contributions to RASopathy pathogenesis (Anastasaki and Gutmann, 2014; Brown et al., 2012; Langdon et al., 2012; López-Juárez et al., 2017; Titus et al., 2017). Nonetheless, animal model studies have demonstrated that pharmacological inhibitors of hyperactive ERK1/2 signaling reverse many RASopathy-linked phenotypes. It is unclear whether ERK/MAPK inhibitors should be utilized in response to mutations that are linked to variable neurocognitive outcomes.

For example, *RAF1*^{L613V} individuals mostly present with intellectual impairment (Denayer et al., 2010; Pandit et al., 2007; Razzaque et al., 2007), but *RAF1*^{L613V} individuals with normal IQ (Kobayashi et al., 2010) and even increased IQ (E. Ciara et al., 2009, ASHG, abstract) have also been observed. Further study of mutated components downstream of RAS (i.e., RAF or MEK) might assist in defining the specific contributions of altered ERK1/2 signaling to the cellular and behavioral defects in RASopathies.

Studies of the developmental effects of ERK1/2 and RASopathy mutations in model organisms have identified alterations in embryonic stages of neurogenesis and gliogenesis (Gauthier et al., 2007; Li et al., 2012b; Li et al., 2012c; Paquin et al., 2009; Pucilowska et al., 2012; Pucilowska et al., 2008; Samuels et al., 2008). Abnormalities in cortical neuron morphology and synaptic plasticity during postnatal periods have also been implicated in learning deficits (Brown et al., 2012; Cui et al., 2008; Kushner et al., 2005; Lee et al., 2014; Lush et al., 2008; Paquin et al., 2009; Pucilowska et al., 2012; Sanchez-Ortiz et al., 2014; Thomas and Huganir, 2004; Xing et al., 2016). ERK1/2 activation in neurons promotes specific forms of synaptic plasticity and learning (Thomas and Huganir, 2004). When expressed selectively in mature glutamatergic neurons, the Costello Syndrome-associated *Hras*$^{G12V+/-}$ mutation enhanced phosphorylated-ERK1/2 (p-ERK1/2) levels, increased LTP, and resulted in improved performance in spatial learning and contextual fear conditioning (Kushner et al., 2005). However, germline *Hras*^{G12V} mice do not exhibit differences in LTP and display diminished spatial learning capabilities (Schreiber et al., 2017). These findings hint at distinct contributions of neuronal vs non-neuronal changes to plasticity and learning in the RASopathies that likely vary at different stages of development.

Glial cells are critical for the proper formation, maturation, and plasticity of neural circuits (Molofsky et al., 2012). ERK1/2 signaling is an important mediator of gliogenesis, glial proliferation, and function (Andreadi et al., 2012; Breunig et al., 2015; Gauthier et al., 2007; Gutmann et al., 2001; Hegedus et al., 2007; Krencik et al., 2015; Li et al., 2012b; Nordlund et al., 1995). For example, a hallmark feature of post-mortem Neurofibromatosis Type 1 (NF1) (MIM: 162200) patient forebrains and mouse models of NF1 is an increased number of $GFAP^{+}$ reactive astrocytes (Gutmann et al., 1999; Nordlund et al., 1995; Rizvi et al., 1999; Zhu et al., 2005). Additionally, diffusion tensor imaging (DTI) analyses have identified white matter differences in individuals with NF1 and the autism-linked 16p11.2 microduplication (MIM: 614671), which includes ERK1 (Filges et al., 2014; Koini et al., 2017). Collectively, these data speak to an important, yet poorly understood role for astrocyte and oligodendrocyte dysfunction in RASopathy neuropathogenesis.

Here we studied the establishment of neuronal and glial number and behavior in mice heterozygous for a $Raf1^{L613V}$ variant linked to Noonan Syndrome in humans (Pandit et al., 2007; Razzaque et al., 2007; Wu et al., 2011). $Raf1^{L613V/wt}$ heterozygous mice exhibit embryonic lethality on a pure C57Bl/6J background but survive on a mixed C57Bl/6J x 129S1 background with notable deficits in cardiac and craniofacial development (Wu et al., 2011; Wu et al., 2012). Even though Noonan Syndrome is associated with a range of neurological abnormalities, nervous system development has not been evaluated in $Raf1^{L613V/wt}$ mouse mutants. Here, we report increases in $GFAP^{+}$-astrocyte and $OLIG2^{+}$-oligodendrocyte-progenitor cell (OPC) density in the mature forebrains of $Raf1^{L613V/wt}$ mice without a significant difference in cortical neuron density. Remarkably, $Raf1^{L613V/wt}$ mutant mice exhibit moderate enhancements in spatial reference memory, spatial working

memory, and fear learning tasks. Taken together, our data show that the Noonan Syndrome-linked *Raf1*$^{L613V/wt}$ mutation increases the number of two glial subtypes and enhances distinct aspects of cognition.

Materials and Methods

Mice and Genotyping

Animal experiments were performed in accordance with NIH guidelines for the use and care of laboratory animals and established protocols approved by the Institutional Animal Care and Use Committee at the University of North Carolina–Chapel Hill and Arizona State University (Protocol#17-1521R). All mice examined in this study were euthanized via CO2 inhalation or fully anesthetized with avertin prior to transcardial perfusion as described in the AVMA Guidelines on Euthanasia. The generation of mice harboring the $Raf1^{L613V}$ knock-in mutation has been previously described (Wu et al., 2011). Due to embryonic lethality when backcrossed onto the C57Bl/6J genetic background (Wu et al., 2011), these experiments utilized mice maintained on a C57Bl/6J x 129S1 mixed background (JAX Stock # 101043). Mice were housed under standard laboratory conditions with *ad libitum* access to food and water on a 12-hour light/dark cycle in vivaria at UNC and ASU. For PCR genotyping, we utilized a single primer set to amplify a 560bp fragment of the $Raf1^{L613V}$ allele and a 500bp wild-type allele from genomic DNA samples (Forward (5'-3'): AGTCAGCCTAGAGGCCACTGTTA, Reverse (5'-3'): CTCCAATTTTCACCGTGAGGC).

Tissue Preparation and Immunohistochemistry

Mice were fully anesthetized and transcardially perfused with cold 4% PFA in 1X PBS. Brains were then dissected, post-fixed overnight, mounted in a 3% agarose block, and sectioned on a EMS 7000smz-2 vibrating microtome. For most experiments, brains from a littermate control/mutant pair were sectioned, immunolabeled, and imaged in

parallel. Tissue sections were collected in PBS, permeabilized in 0.2% Triton X-100 in PBS, and incubated in a blocking solution consisting of 5% Normal Donkey Serum and 0.2% Triton X-100 in PBS. Primary antibodies were then diluted in blocking solution and incubated with tissue sections at 4C for 24-48 hours while rocking gently. The primary antibodies used were: rabbit anti-p-ERK (1:1000, Cell Signaling 4370), mouse anti-RBFOX3/NeuN (1:1000, Millipore MAB377), goat anti-Parvalbumin (1:1000, Swant PVG-214), rabbit anti-GFAP (1:1000, Abcam ab7260), rabbit anti-ACSBG1 (1:500, Abcam ab65154), mouse anti-S100β (1:1000, Sigma SAB1402349), rabbit anti-IBA1 (1:1000, Wako 019-19741), rabbit anti-OLIG2 (1:1000, Millipore AB9610), rat anti-MBP (1:1000, Abcam ab7349), rabbit anti-PDGFRα (1:1000, Santa Cruz sc-338), rabbit anti-NG2 (1:500, Millipore AB5320), mouse anti-CC1 (1:500, Calbiochem), rabbit anti-Arc (1:1000, Synaptic Systems 156 003), rabbit anti-TNFα (1:2000, Bio-Rad), and biotinylated WFA (20µg/mL, Vector). Tissue sections were then washed in 0.2% Triton in PBS and incubated in fluorescently-conjugated secondary antibodies including donkey anti-rabbit, donkey anti-rat, donkey anti-mouse, and donkey anti-goat IgGs conjugated to Alexa Fluor 488, 555, 568, or 647 dyes (Invitrogen). For WFA labeling, a streptavidin-conjugated 488 secondary antibody was used. Brain slices were then slide mounted, coverslipped in Fluoromount (EMS #17984), and stored at 4C prior to imaging.

Electron Microscopy

P60 mice were anesthetized, transcardially perfused with 2% paraformaldehyde, 2% glutaraldehyde in 0.1M PB and post-fixed overnight. A 3mm x 1mm x 1mm block was sub-dissected from the genu of the corpus callosum for myelination assessment. Tissue

blocks were then washed 3x with PB before a 2 hr secondary fixation with 1% osmium tetroxide in 0.1M PB. Tissue blocks were washed 3x with deionized water and stored at 4C overnight. The next day, the tissue blocks were returned to room temperature and dehydrated in a series of three acetone washes, increasing in 20% increments per wash. The tissue blocks were then infiltrated with Spurr's epoxy resin three times at increasing increments of 25% pure resin, and sectioned in a Leica Ultracut-R microtome at a section thickness of 70nm, stained with 2% uranyl acetate in 50% ethanol for six minutes, and then moved to Sato's lead citrate for four minutes. Genu sections were visualized in a Philips CM12 TEM at 80kV, and images were captured with a Gatan model 791 slow-scan CCD camera in the Biological Electron Microscopy Facility at Arizona State University.

Image Analysis and Quantification

For immunofluorescent analyses, images were collected on a Leica SP5 or Zeiss LSM800 confocal microscope from at least three different tissue sections per mouse and at least three mice per group. Confocal optical sections for quantification are typically collected from a z-axis region between 5-15 μm from the surface of the tissue section. Following optimization of image brightness and contrast, regions of interest (ROI) were outlined in images of anatomically matched sections using standard neuroanatomical boundaries. The number of labeled cells was determined by a blinded observer in at least three individual ROIs per mouse spanning all layers of a cortical or hippocampal column contained within a specified sub-region. The number of cells was divided by the area of the ROI and averaged across all ROIs from an individual brain to estimate the density of labeled cells in a single mouse brain. To calculate relative density, the average density was

normalized to the age-matched littermate control processed in parallel. Results were analyzed for statistical significance using the Students t-test.

For myelination analysis, electron micrographs within a cross-section of the genu of the corpus callosum were assessed for axon area, g-ratio, and the proportion of myelinated to unmyelinated axons. Axon g-ratios were calculated as the cross-sectional diameter of the axon excluding the myelin sheath, divided by the total diameter of the axonal fiber including the myelin sheath. The numbers of myelinated and unmyelinated axons were counted within a given image, and the proportion of myelinated to unmyelinated axons was calculated for mutants and controls. Results are reported as the average ± SEM and compared using the Student's t-test.

Western Blotting

Cortices were dissected and lysed in RIPA buffer (0.05M Tris-HCl, pH 7.4, 0.5M NaCl, 0.25% deoxycholic acid, 1% NP-40, and 1mM EDTA, Millipore), supplemented with 0.1% SDS, protease inhibitor cocktail (Sigma) and phosphatase inhibitor cocktails II and III (Sigma). Lysates were cleared by centrifugation, and protein concentration was determined. Equal amounts of protein were denatured in reducing sample buffer, separated by SDS-PAGE gels, and transferred to PVDF membranes (Bio-Rad). Blots were blocked with 5% BSA in TBS containing 0.5% Tween 20 (TBS-T) for 1 h at room temperature, then incubated overnight at 4°C with primary antibodies. The primary antibodies used were: rabbit anti-p-ERK1/2 (Thr202/Tyr204) (Cell Signaling Technology, Inc), rabbit anti-ERK1/2 (CST), rabbit anti-MEK1/2 (Ser217/221) (CST), rabbit MEK1/2 (CST), rabbit anti-DUSP6 (Abcam ab76310), rabbit anti-SPRY2 (Abcam ab85670), and anti-GAPDH

(Cell Signaling Technology, Inc.). After washing with TBS-T, membranes were incubated with HRP-conjugated secondary antibodies in 5% milk in TBS-T for 2 h at room temperature. Blots were washed with TBS-T, and detection was performed with SuperSignal West Pico chemiluminescent substrate (Thermo Scientific).

Behavior

All behavior experiments were performed at ASU with mice kept on a standard light cycle in a room dedicated to behavioral assessment. The experimenter was blinded to the mouse genotype during animal testing and data analysis. No statistically significant difference was observed between male and female mice; therefore, results were pooled for presentation.

Open Field, Elevated Plus, and Social Approach Assay

The open field, elevated plus, and social approach tests were performed on 23 control (6 male, 17 female) and 31 mutant (16 male, 15 female) mice with at least three days between different behavioral assays. The open field was used to test voluntary locomotive and anxiety-like behaviors. The apparatus consisted of a 40x40cm arena enclosed by 30cm high opaque walls. A single 60W bulb was positioned to brightly illuminate the center of the chamber with dim lighting near the walls. Mice were placed into the apparatus and video recorded for a total of 10 minutes. Video data were analyzed for distance traveled and time spent in the center quadrant.

The elevated plus maze was constructed from black Plexiglas, elevated 81cm off the ground, and oriented in a plus formation with two 12x55cm open arms and two

12x55cm closed arms extending from an open 12x12cm center square. Closed arm walls were 40cm high extending from the base of the arm at the center square. The apparatus was lit with a 60W bulb with light concentrated on the center square. At the beginning of each trial, mice were placed in the center square, facing the south open arm, and recorded while freely exploring for 5 minutes.

The social approach apparatus contained three 20x30x30cm chambers (total dimensions 60x30x30cm) connected by open doorways. Prior to experimental social trials, mice were habituated to the apparatus and allowed to freely explore all three chambers for 5 minutes. At the end of the 5 minutes, mice were removed and placed in their home cage. A sex- and age-matched stimulus mouse was then placed into a small empty cage in chamber 1 of the apparatus. The experimental mouse was reintroduced to the center chamber (chamber 2) of the apparatus and recorded while freely exploring for 10 minutes. The time spent in the chamber with the stimulus mouse (chamber 1) or the empty chamber (chamber 3) was then measured.

Video recordings of the open field, elevated plus, and social approach tests were collected and quantified in ImageJ using publicly available plugins (Komada et al., 2008) followed by statistical analysis using the Student's t-test.

Water Radial-Arm Maze

The water radial-arm maze (WRAM) was used to evaluate spatial working and reference memory (Bimonte-Nelson, 2015; Hyde et al., 2000). The maze consisted of an eight-arm apparatus (each arm 38.1 × 12.7cm) filled with opaque, room temperature water. Water temperature was consistently between 18–20°C for testing. Extra maze spatial cues

were present to aid mice in spatial navigation. In the win-shift version of WRAM, mice (n = 19 control, 15 mutant, all female) were required to find hidden platforms (10 cm diameter) submerged at the end of four out of the eight arms. Platform location patterns were assigned to each subject and stayed constant for a particular mouse across all testing days, but varied among subjects. Mice received four trials per day for 18 days.

Trials began with the subject being released from the start arm and given 2 min to locate a platform. Arm entries were manually recorded when the mouse's body crossed the threshold of the mouth of the arm. Once a platform was found, the animal remained on it for 15 seconds and was returned to its heated testing cage for a 30s inter-trial interval (ITI). During the ITI, the just-found platform was removed from the maze, and the water was cleaned to remove any debris and obscure olfactory cues. The mouse was then placed back into the start arm and given another 2 min trial to locate a platform. Because a platform is removed from the maze for the remainder of the day after discovery, mice must maintain several items of information in order to effectively solve the task, thus increasingly taxing the working memory system as trials progress within a day. The number of arm entries into non-platformed arms is quantified as errors as the dependent measure of spatial memory in the task (Fig. 7B). Errors are further divided into particular error types. Working Memory Correct (WMC) errors are defined as all entries into arms that previously contained a platform within a day. Reference Memory (RM) errors are first entries into arms that never contained a platform, and Working Memory Incorrect (WMI) errors are all subsequent entries into arms that never contained a platform within a day. WMC, REF, and WMI errors are summed for a total error score. All errors were quantified using orthogonal measures of working and reference memory, as previously reported (Bimonte-Nelson et al., 2015;

Hyde et al., 2000). Data were analyzed using Statview statistical software with a repeated measures ANOVA followed by Fisher's LSD *post-hoc* test, when indicated.

Morris Water Maze

Five days after the last day of WRAM testing, spatial reference memory was evaluated in the same cohort of mice using the Morris water maze (MM) (n = 19 control, 15 mutant, all female). The apparatus was a round tub (188cm diameter) filled with opaque, room temperature water (18–20°C), and contained a submerged platform (10cm diameter) in the northeast quadrant. The platform location remained fixed across all days and trials, with spatial cues available to aid the animals in spatial navigation, testing spatial reference memory (Morris et al., 1982). Mice received four trials per day for five days. At the beginning of each trial, mice were placed into the tub from one of four starting points (north, south, east or west). The order of the drop-off location varied semi-randomly across days, but was the same within a day for all subjects. MM performance was recorded using a video camera and tracking system (Ethovision; Noldus Instruments; Wageningen, The Netherlands). Mice had 60s to locate the platform, where they remained for 15s before being placed back into a heated cage for an ITI of 5–8min. A probe trial was given on the fifth day of testing, during which the platform was removed and mice were given 60s to swim freely in the maze. Following the first probe trial day, a reversal task was carried out for two consecutive days. Specifically, the platform location was moved from the northeast quadrant to the opposite, southwest quadrant, where it remained across all reversal task trials. Mice then received four trials per day for two days. A second probe trial followed the last baseline trial on day two of the reversal task. For acute behavioral stimulation of

Arc expression, a separate subset of mice (n=4 mutants, 4 controls) were placed in the Morris maze for 5-trials with 15 minutes between trials in one day and sacrificed 60 minutes after the end of the 5th trial for immunohistochemical analyses. Data were analyzed using Statview statistical software with a repeated measures ANOVA followed by Fisher's LSD *post-hoc* test, when indicated.

Visible platform task

After completion of cognitive behavioral testing on the WRAM and MM, mice were evaluated using the visible platform control task to assess locomotor and visual performance. The apparatus was a rectangular tub (100 × 60cm) filled with clear room temperature water (18–20°C). A black platform (10cm wide) was positioned 4cm above the surface of the water. A ring of opaque curtains surrounded the tub, blocking all obvious spatial cues. Animals received three trials in one day. The drop off location remained the same across trials; however, the platform location varied semi-randomly across three locations. Each mouse had 90s to locate the platform, where it remained for 15s before being placed back into a heated cage for an ITI of 5–8min.

Fear Conditioning

Control (n=11, 3 male, 8 female) and *Raf1*$^{L613V/wt}$ (n=9, 2 male, 7 female) adult mice were placed in test cages (12"Wx10"Dx12"H: Coulbourn Instruments, E10-18TC) housed within a sound-attenuating cabinet (Coulbourn, E10-23, white, 31.5" W x 21" D x 20" H) with an attached video camera that recorded behavior for offline scoring of all fear conditioning procedures. Seventy-five (75) dB tones of 30 second duration were produced

by a frequency generator (Coulbourn, E12-01 or H12-07) and delivered through a speaker (Coulbourn, H12-01R) on the side panel. Video recordings were analyzed for the number of seconds mice spent freezing, a species-typical fear response that is defined by the absence of all movement except those associated with respiration, during the 30 sec prior to, and during, tone presentation. An animal shock generator (Coulbourn, H13-15) produced an electrical current (0.25mA, 1 sec) evenly delivered to metal bars in the cage flooring (Coulbourn, E10-11R/M-TC-SF). All stimuli were controlled using Graphic State software (v 3.0) installed on a computer connected to a stimuli output controller system (Coulbourn, H02-08).

Training and testing were performed in two distinct contexts (A and B) with varying rooms and investigator appearance. Context A had silver, metal walls on the sides, clear Plexiglas front and back with yellow paper located outside, metal bar shock floor, white drop pan, and cleaned with grapefruit scented cleaner (Method®, Target Inc.). For testing in context B, the chambers had walls covered with vertical black and white striped inserts, a cross-hatched non-shock metal grid floor, black drop pans, and cleaned with 70% isopropyl alcohol. Mice were acclimated to the testing room for 20 min and to each of the two contexts for 10 min on the three days prior to training. In the training session for Context A, mice were presented with three trials of an auditory tone that co-terminated with presentation of a foot shock. Twenty-four (24) and 48 hours later, mice were tested for memory by undergoing three tone-only trials in context B at each time point. Mice then underwent an extinction paradigm where tones were repeatedly presented (maximum of 16) until total freezing was less than 10 seconds during tone presentation. One week later, spontaneous recovery was assessed by presenting them with three presentations of the tone

to determine whether freezing to tone was due to associative or non-associative processes. After this testing was complete, we performed a shock intensity test, where shocks were gradually increased from a minimum of 0.08mA until the mouse elicited a clear startle response. Statistical analysis was conducted using Students t-test or repeated measures ANOVA, followed by *post-hoc* tests in SPSS.

Results

Cortical neuron number is normal in Raf1$^{L613V/wt}$ mutant mice

We generated *Raf1*$^{L613V/wt}$ heterozygous mice on mixed C57Bl/6J x 129S1 background. Past work has shown that embryonic and cardiac fibroblasts from *Raf1*$^{L613V/wt}$ mice do not exhibit a difference in basal ERK1/2 activity but show a significant stimulus-dependent increase in levels of p-ERK1/2 following treatment with different RTK-linked trophic cues, including EGF, FGF2, PDGF, and IGF-1 (Wu et al., 2011; Wu et al., 2012). Western blot assessment of whole cortical lysates revealed no relative difference in basal p-MEK, MEK, p-ERK1/2 or total ERK1/2 levels between *Raf1*$^{L613V/wt}$ and control adult mice (Fig. 1A, n = 5). Moreover, we detected no change in the negative feedback regulators SPRY2 and DUSP6 in cortical lysates from *Raf1*$^{L613V/wt}$ and control mice (Supplemental Fig. 1A; n = 5). *Raf1*$^{L613V/wt}$ and control mice also showed comparable patterns of hippocampal p-ERK1/2 labeling (Supplemental Fig. 1B, C). A subpopulation of layer 2 cortical excitatory neurons receives high levels of glutamatergic input, a known activator of ERK1/2 signaling, and expresses increased levels of FOS, an immediate early gene product regulated, in part, by ERK1/2 activity (Thomas and Huganir, 2004; Yassin et al., 2010). In agreement with previous work, we noted many p-ERK1/2-labeled neurons in layer 2/3 of sensory cortex in adult control mice (Cancedda et al., 2003; Pham et al., 2004; Suzuki et al., 2004). However, mutant mice exhibited a significantly larger number of p-ERK1/2 labeled neurons in layer 2 of the sensory cortex compared to age-matched controls (Fig. 1B-E, F; $n = 4$, $p < 0.01$). These data are consistent with the anatomically restricted, local increases in p-ERK1/2 observed in *HRas*^{G12V} mice (Schreiber et al., 2017), and suggest that

the *Raf1*^{L613V} mutation drives an increase in stimulus-dependent ERK1/2 signaling in a subset of endogenously active cortical neurons.

ERK1/2 signaling in radial glia regulates the trajectory of cortical neurogenesis and cortical excitatory neuron number (Li et al., 2012a; Lush et al., 2008; Pucilowska et al., 2012). We assessed the number of cells in *Raf1*$^{L613V/wt}$ and control cortices expressing a well-established neuronal marker, RBFOX3/NeuN, which is highly expressed in nearly all excitatory neurons in the cortex (Fig. 1G-J). The relative density of RBFOX3/NeuN^{+} neurons in the adult sensory cortex was unchanged, suggesting no significant alterations to neurogenesis (Fig. 1K; n = 3). GABAergic neurons comprise ~20% of the total neuron population in the cortex and express relatively low levels of RBFOX3/NeuN. We immunolabeled for parvalbumin (PV) and somatostatin (SST) to assess the density of the two largest cortical GABAergic neuron subpopulations. PV-expressing GABAergic neurons were distributed normally in cortical layers with no significant alterations in density (Fig. 1L-O, P; n = 3). Taken together, our data indicate that the *Raf1*$^{L613V/wt}$ mutation does not alter the distribution and number of mature excitatory and inhibitory neurons in the adult cortex.

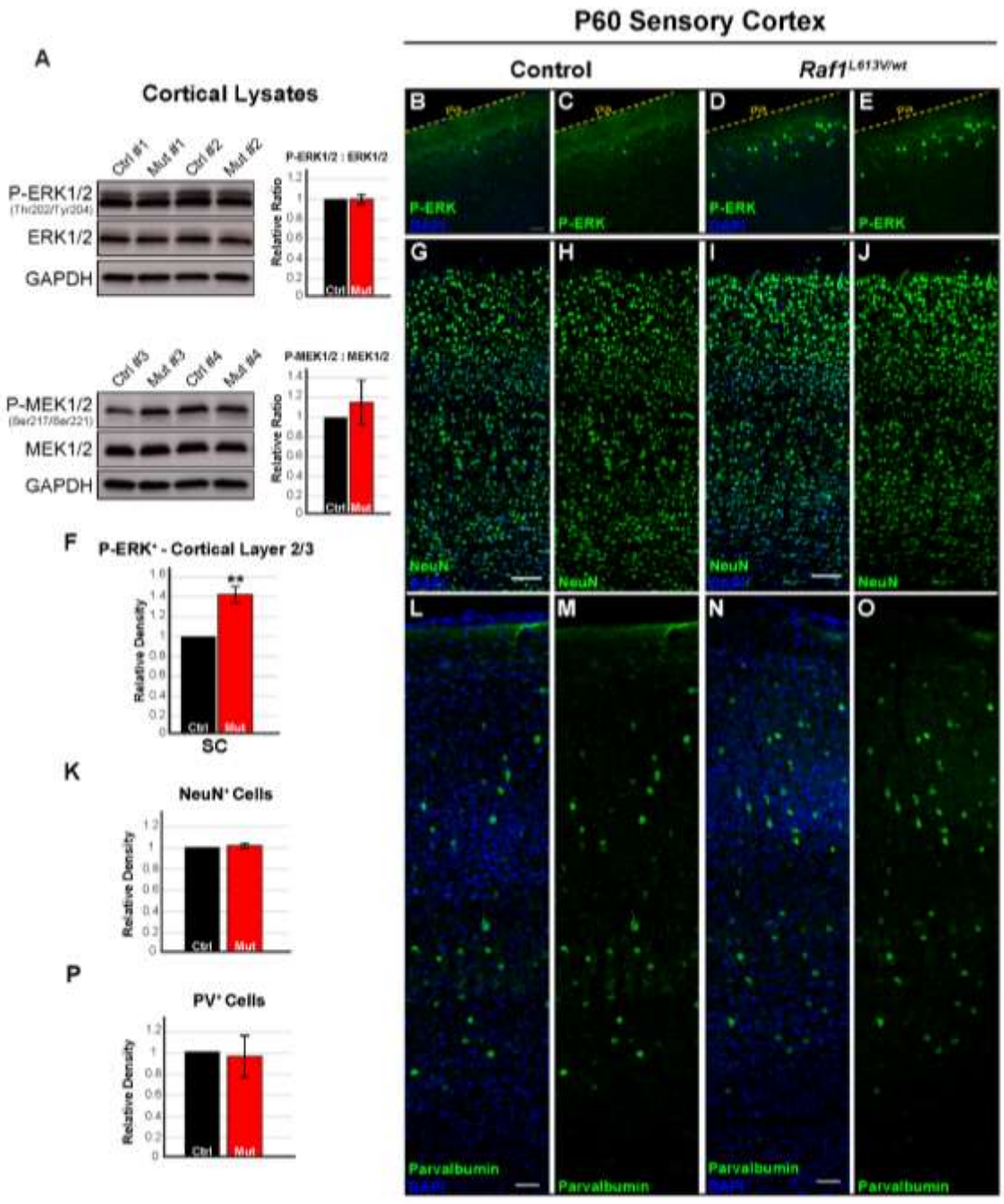
A
Cortical Lysates
Ctrl #1
Mut #1
Ctrl #2
Mut #2
P-ERK1/2
(Thr202/Tyr204)
ERK1/2
GAPDH
P-ERK1/2 : ERK1/2
Relative Ratio
Ctrl
Mut
Ctrl #3
Mut #3
Ctrl #4
Mut #4
P-MEK1/2
(Ser217/Ser221)
MEK1/2
GAPDH
P-MEK1/2 : MEK1/2
F
P-ERK+ - Cortical Layer 2/3
Relative Density
SC
K
NeuN+ Cells
P
PV+ Cells
P60 Sensory Cortex
Control
Raf1L613V/wt
B
C
D
E
P-ERK
G
H
I
J
NeuN
L
M
N
O
Parvalbumin

Figure 1. *Raf1*$^{L613V/wt}$ mutants do not exhibit significant alterations in cortical neuron density. **A**: Western blots of P21 whole cortical lysates from *Raf1*$^{L613V/wt}$ cortices exhibit no relative change in the total levels of MEK1/2 or ERK1/2 or the phosphorylation of MEK1/2 or ERK1/2, as measured by the ratio of phosphorylated to total protein (mean ± SEM, n = 5). **B-F:** Representative confocal images of p-ERK1/2 immunolabeling in adult (P60) sensory cortex reveals an increased density of p-ERK1/2-expressing pyramidal cells in mutant layer 2 (D-E), compared with littermate controls (B-C); quantification in F (mean ± SEM, n=3, $p < 0.01$). **G-K:** Representative immunolabeled sections of sensory cortex showing NEUN-labeled neurons and DAPI-labeled nuclei. *Raf1*$^{L613V/wt}$ (I-J) cortical NEUN$^+$ density does not significantly differ from controls (G-H), as quantified in K (mean ± SEM, n = 3). **L-P:** Quantification of Parvalbumin-labeled cortical GABAergic neurons in control (L-M) and mutant (N-O) cortices reveals no significant alterations in cell density (P) (mean ± SEM, n = 3). All scale bars = 50μm.

Increased density of GFAP$^+$ astrocytes in Raf1$^{L613V/wt}$ forebrains

Altered glial number and function are observed in response to RASopathy-linked *Nf1*, *Ptpn11/Shp2*, and *Ras* mutations (Gutmann et al., 1999; Gutmann et al., 2001; Krencik et al., 2015; Li et al., 2012a; Nordlund et al., 1995; Rizvi et al., 1999). To determine if *Raf1*$^{L613V/wt}$ mutant mice display alterations in glial development, we immunolabeled for glial fibrillary acidic protein (GFAP) and Acyl-CoA synthetase bubblegum family member 1 (ACSBG1), markers of fibrous and protoplasmic astrocytes, respectively, and the glial marker S100β (Cahoy et al., 2008). Astrocytes expressing these canonical markers were clearly labeled in adult forebrains from control and mutant mice (Fig. 2A-J). In control cortices, GFAP$^+$ astrocytes were enriched in the white matter, upper layer 1-2, and layer 6, though labeled profiles were occasionally detectable in the remaining cortical layers. We found a significantly increased density of GFAP$^+$ astrocytes in *Raf1*$^{L613V/wt}$ sensory cortices across all layers, relative to littermate controls (Fig. 2A-D, M; n = 3, $p < 0.05$). In comparison to the cortex, GFAP$^+$ astrocytes are present at a relatively higher abundance throughout the wild-type hippocampus. Assessment of the GFAP$^+$ astrocyte population in

the CA1 region of the mutant hippocampus also revealed an increase in density (Fig. 2E-H, M; n = 3, $p < 0.01$) in mutant mice. These data demonstrate that $GFAP^+$ astrocyte number is increased in *Raf1*$^{L613V/wt}$ mutants across multiple brain regions.

In states of injury, gliosis is often characterized by an increased density of $GFAP^+$ astrocytes, which usually coincides with microglial activation and proliferation (Molofsky et al., 2012). We therefore labeled for the activated microglia marker, IBA1, to assess the effects of *Raf1*$^{L613V/wt}$ in the cortex and hippocampus. We found that the density and distribution of $IBA1^+$ activated microglia were evenly distributed across the cortical grey matter and did not significantly differ in density in mutants relative to littermate controls (Fig. 2K, L, N; n = 3). Additionally, no change in the relative density of activated microglia was observed in the mutant hippocampus (Fig. 2N; n = 3). In summary, the *Raf1*$^{L613V/wt}$ mutation is sufficient to induce an increased density of $GFAP^+$ astrocytes, but not neurons or microglia.

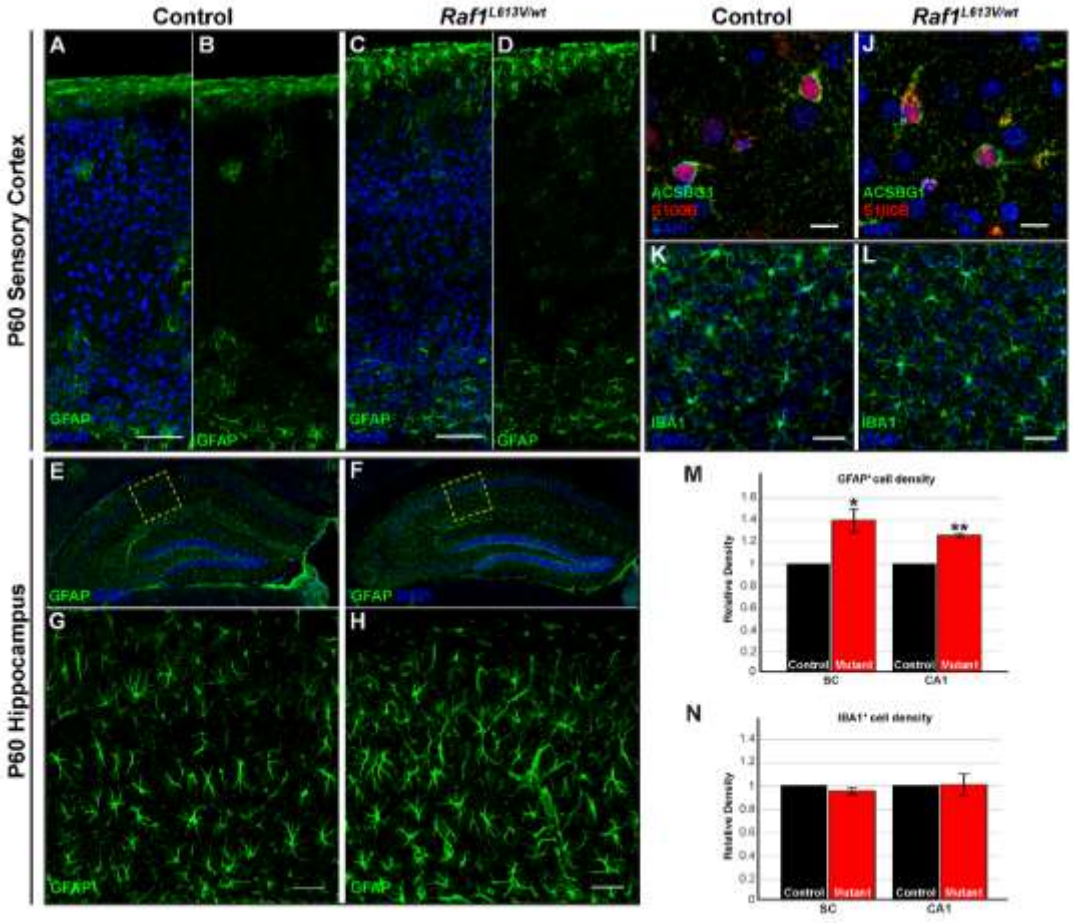

Figure 2. Increased density of GFAP$^+$ astrocytes, but not IBA1$^+$ microglia, in *Raf1$^{L613V/wt}$* cortex and hippocampus. A-D: Representative confocal images of GFAP-immunolabeled control (A-B) or mutant (C-D) sensory cortices show a significantly increased density of GFAP$^+$ astrocytes across cortical layers (M) of mutant mice (mean ± SEM, n = 3, *p < 0.05) (scale bar = 100μm). **E-F:** Coronal cross-sections of control (E, inset in G) and *Raf1$^{L613V/wt}$* (F, inset in H) hippocampus following immunostaining for GFAP. Mutant hippocampal CA1 sub-regions demonstrate a significantly increased relative density of GFAP$^+$ astrocytes, relative to littermate controls (M) (mean ± SEM, n = 3, *p < 0.01) (scale bar = 50μm). **I-J:** Triple-labeled representative images of control (I) and mutant (J) cortex following staining for the grey matter astrocyte marker ACSBG1, pan-glial marker S100β, and DAPI (n=3). **K-L, N:** No significant change in the density of microglia in the cortex is observed in mutant mice (L) relative to controls (K); quantification in N (mean ± SEM, n = 3) (scale bar = 25um).

$Raf1^{L613V}$ drives enhanced oligodendrocyte progenitor cell density in the cortical grey and white matter but does not alter myelination

Past work has linked hyperactive ERK1/2 signaling to alterations in oligodendrocyte development, including proliferation, differentiation, and myelination (Ehrman et al., 2014; Ishii et al., 2013; Newbern et al., 2011). We first assessed the density of OPCs expressing PDGFRα in the adult $Raf1^{L613V/wt}$ cortex. Immunolabeling for PDGFRα revealed an increased density of OPCs in the adult sensory cortex (Fig. 3A-F, M; $n = 3$, $p < 0.01$). PDGFRα is downregulated by mature oligodendrocytes; thus, we also examined the relative number of cells expressing Olig2, an independent marker of the oligodendrocyte lineage. We found increased numbers of $Olig2^+$ cells in the cortical grey matter of adult $Raf1^{L613V/wt}$ mutant mice (Fig. 3I, L, M; $n = 7$, $p < 0.01$), but not the hippocampus (control relative density 1; mutant relative density 1.06; $p = 0.66$; $n = 3$). Olig2 is expressed by oligodendrocyte progenitor cells (OPCs) and mature oligodendrocytes. We distinguished between myelinating and immature oligodendrocyte lineage cells by co-labeling with the mature myelinating oligodendrocyte marker, CC1 (Fancy et al., 2009). As expected, all $CC1^+$ cells present in the cortical grey matter co-expressed Olig2, but a subpopulation of $Olig2^+$ cells did not express detectable levels of CC1, consistent with immature OPCs. $Raf1^{L613V/wt}$ brains also had significantly increased densities of $Olig2^+/CC1^-$ cells in the corpus callosum as compared to littermate controls (Fig. 3M-P, R; $n = 5$, $p < 0.05$). Even though there was an increase in oligodendrocyte progenitors, we detected no significant difference in the density of CC1-labeled mature myelinating oligodendrocytes in $Raf1^{L613V/wt}$ mutant cortices (Fig. 3H, K, Q; $n = 3$).

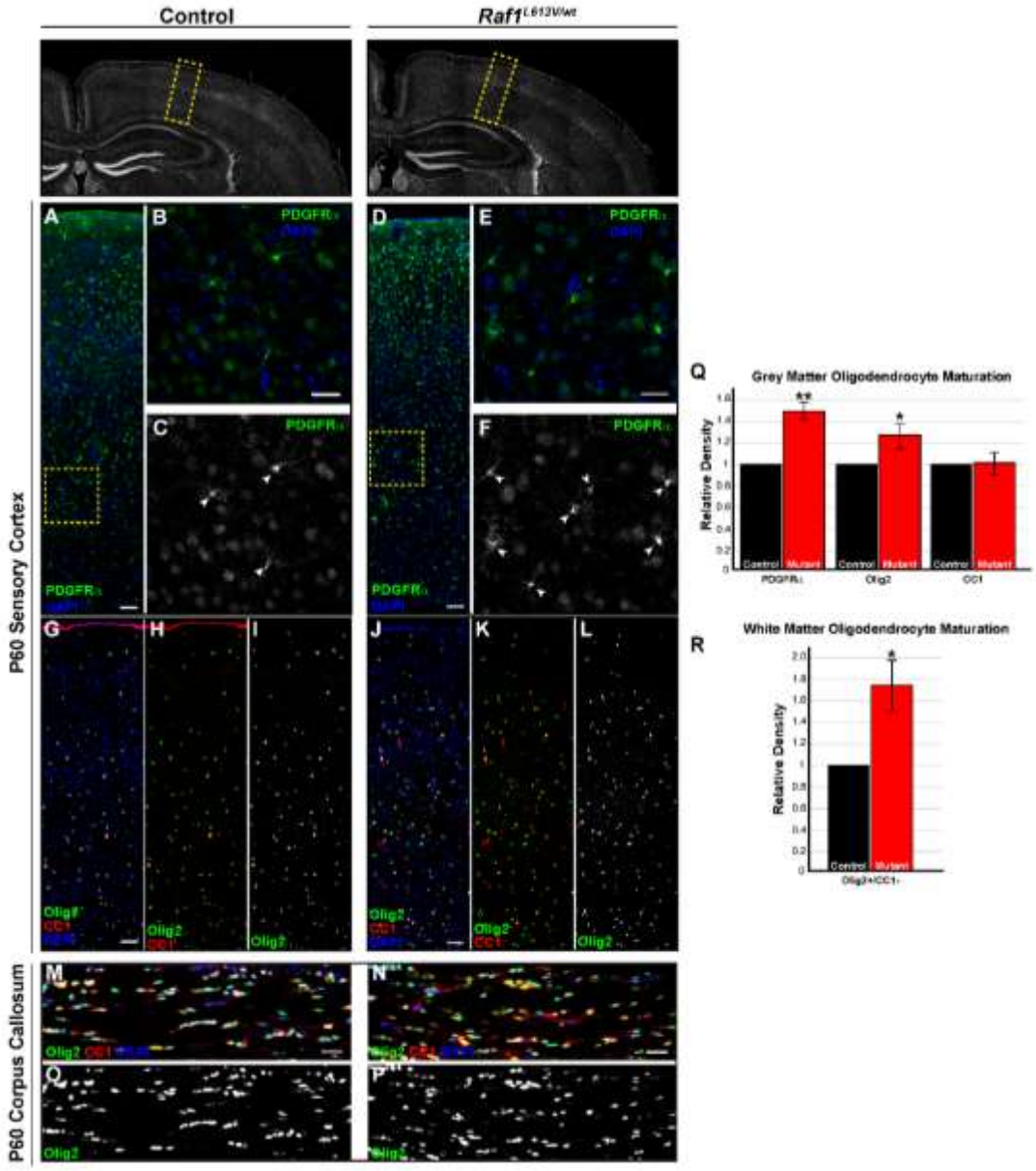
Control
Raf1L613V/wt
P60 Sensory Cortex
P60 Corpus Callosum
A
B
C
D
E
F
G
H
I
J
K
L
M
N
O
P
PDGFRα
Olig2
CC1
Q
Grey Matter Oligodendrocyte Maturation
Relative Density
Control
Mutant
PDGFRα
Olig2
CC1
R
White Matter Oligodendrocyte Maturation
Olig2+CC1+

Figure 3. *Raf1*$^{L613V/wt}$ mutants show increased numbers of OPCs but not myelinating oligodendrocytes. **A-F**: Representative immunolabeled sections of control (A, inset in B-C) and mutant (D, inset in E-F) sensory cortices reveal a significant relative increase in the number of PDGFRα^{+} cells in mutant mice (white arrow heads, mean ± SEM, n = 3, *p < 0.01). **G-L:** Triple-labeled representative images of staining for the pan-oligodendrocyte marker, Olig2, mature myelinating marker, CC1, and DAPI. Note the increased density of Olig2^{+} cells in the *Raf1*$^{L613V/wt}$ sensory cortex (J-L), relative to controls (G-I), as quantified in M (mean ± SEM, n = 7, *p < 0.01). By contrast, analysis of CC1^{+} cells reveals no changes in the number of presumably mature, myelinating oligodendrocytes (Q) (mean ± SEM, n = 4). **M-P:** Assessment of Olig2^{+}/CC1^{-} oligodendrocyte lineage cells revealed a significant increase in the density in the mutant (N, P) medial corpus callosum relative to age-matched controls (M, O) (R; n = 5, p < 0.05). All scale bars = 50μm.

Strong gain-of-function ERK1/2 signaling drives increased myelination in adult animals (Ishii et al., 2013). However, the pattern of myelin basic protein (MBP) immunolabeling in P60 *Raf1*$^{L613V/wt}$ cortices was indistinguishable from that of controls (Fig. 4A-B). We also observed no difference in cortical MBP immunolabeling between mutants and controls at P14, an early stage of cortical myelination (Supplemental Fig. 4A-D). To quantify myelin thickness, we examined myelinated axons in the genu of the corpus callosum by electron microscopy (Fig. 4C-D). We did not detect a significant change in average axon area (Fig. 4E; n = 3) or the proportion of myelinated to unmyelinated axons (Fig. 4F; n = 3) in adult *Raf1*$^{L613V/wt}$ mutants. Moreover, we did not observe a significant difference in g-ratio, a normalized measure of myelin thickness that takes into account differences in axon diameter (Fig. 4G-H; n = 3). Collectively, these data indicate an increased number of OPCs in the mutant cortex without alterations in mature oligodendrocyte number or myelination.

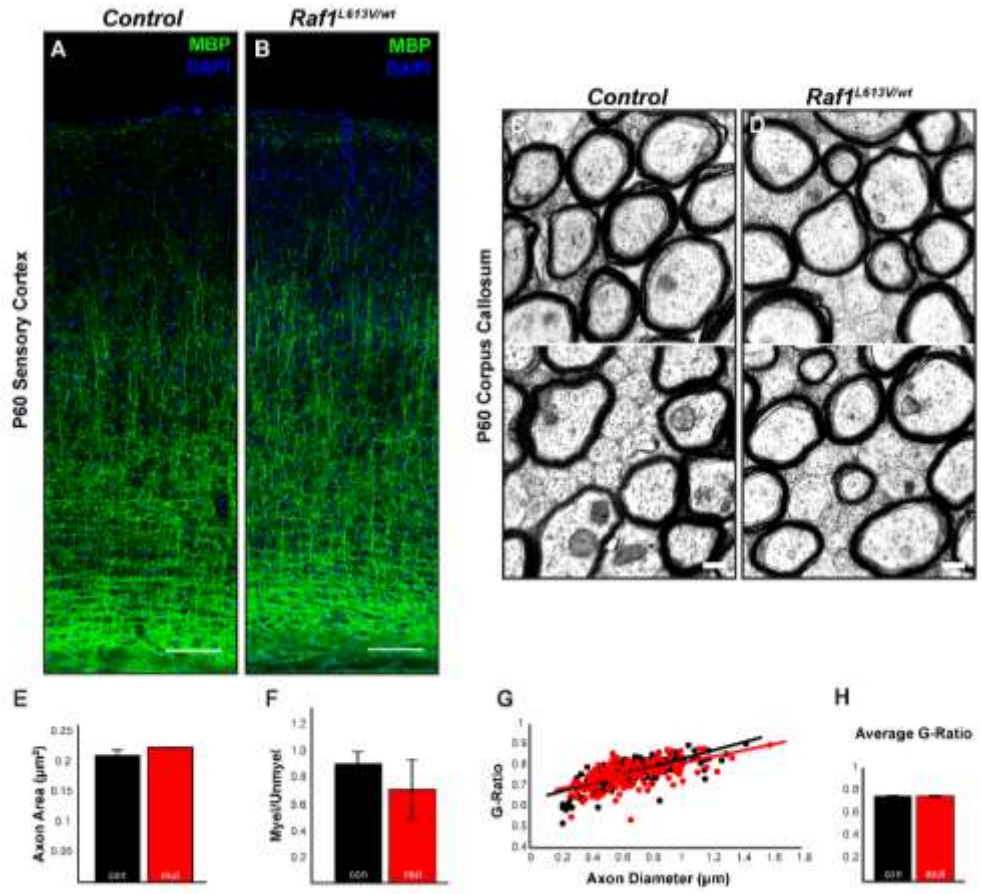

Figure 4. Raf1$^{L613V/wt}$ cortices display normal myelination patterns. A-B: MBP-labeled regions of adult sensory cortices reveal no qualitative differences in the extent or pattern of myelination (n=3) (scale bar = 50µm). **C-D:** Representative electron micrographs of the genu of the corpus callosum in control (C) and mutant (D) mice reveal no difference in axon area (E) or the proportion of myelinated to unmyelinated axons (F) (mean ± SEM, n = 3) (scale bar = 200nm). **G-H:** Myelination, as quantified by g-ratio, was not significantly different in mutant mice relative to controls (mean ± SEM, n = 3).

To better understand the timing of increased OPC density in the adult cortex, we examined the cortical OPC pool in juvenile, P14 *Raf1*$^{L613V/wt}$ mice. Immunolabeling for PDGFRα (Fig. 5A-D; n = 3) and Olig2 (Fig. 5E-H; n = 3) revealed no significant differences in OPC number in the cortex between P14 mutant mice and littermate controls (Fig. 5O). Analysis of NG2-labeled, presumptive oligodendrocyte progenitors at P30 similarly yielded no significant difference in density (Fig. 5I-L, P; n = 3). However, we detected a significant increase in the density of PDGFRα-expressing cells at P30, indicating that the OPC pool expansion occurs post-adolescence (Fig. 5 M, N, P; n = 3; $p < 0.05$).

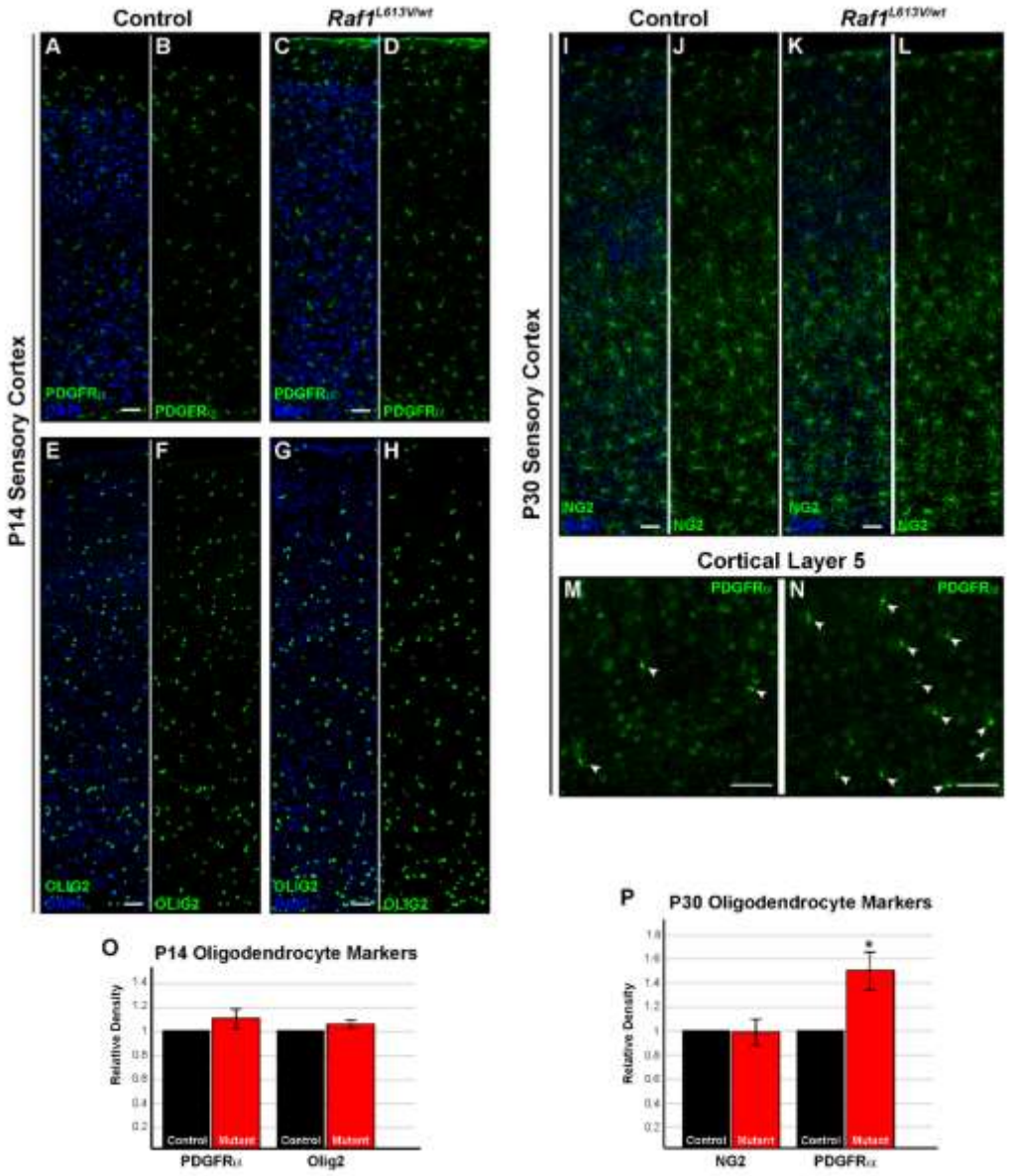

Figure 5. P14 mutant cortices do not display increased densities of PDGFRα^{+} or OLIG2^{+} cells. A-H: Sensory cortices from P14 control (A-B, E-F, I-J) and *Raf1*$^{L613V/wt}$ (C-D, G-H, K-L) mice, immunolabeled for PDGFRα (A-D) or OLIG2 (E-H), show no relative difference in OPC cell density (M) (mean ± SEM, n = 3). **I-L:** Immunolabeling for an alternate marker of OPCs, NG2, in P30 control (I-J) and mutant (K-L) brains also results in no changes in relative density of labeled cells (M) (mean ± SEM, n = 3). All scale bars = 50μm.

$Raf1^{L613V/wt}$ animals exhibit enhanced learning and memory

Individuals affected by the *$Raf1^{L613V}$* mutation present with variable levels of intellectual function (Pandit et al., 2007; Razzaque et al., 2007; Denayer et al., 2010; Kobayashi et al., 2010; E. Ciara et al., 2009, ASHG, abstract). The neurobehavioral characteristics of *$Raf1^{L613V/wt}$* mutant mice are unknown. RASopathies are often associated with behavioral phenotypes seen in autism, such as increased anxiety, decreased sociability, and locomotor impairments. We therefore exposed *$Raf1^{L613V/wt}$* mutant mice to a behavioral battery to assess these behaviors, as well as learning and memory performance.

Adult *$Raf1^{L613V/wt}$* mutant displayed no abnormalities in three distinct tasks meant to assess anxiety-like behaviors, sociability, and locomotion compared to wild-type mice (Fig. 6) (Crawley, 1999; Silverman et al., 2010). In the open field assay, mutant mice did not display a significant difference in total distance traveled (Fig. 6A) or time spent in the center quadrant, demonstrating no deficit in voluntary locomotor ability or anxiety-like behavior (Fig. 6B-C; n=23 controls, 31 mutants). These data were consistent with a separate test of locomotor activity and anxiety, the elevated plus maze, where no significant change in locomotor activity (Fig. 6D) or time spent in the open arm was detected (Fig. 6E-F; n=23 controls, 31 mutants). Finally, the social approach assay did not reveal a significant difference between mutant and control mice in total entries (Fig. 6G) or the time spent exploring the chamber with a novel mouse, indicating no deficit in sociability (Fig. 6H-I; n=21 controls, 31 mutants).

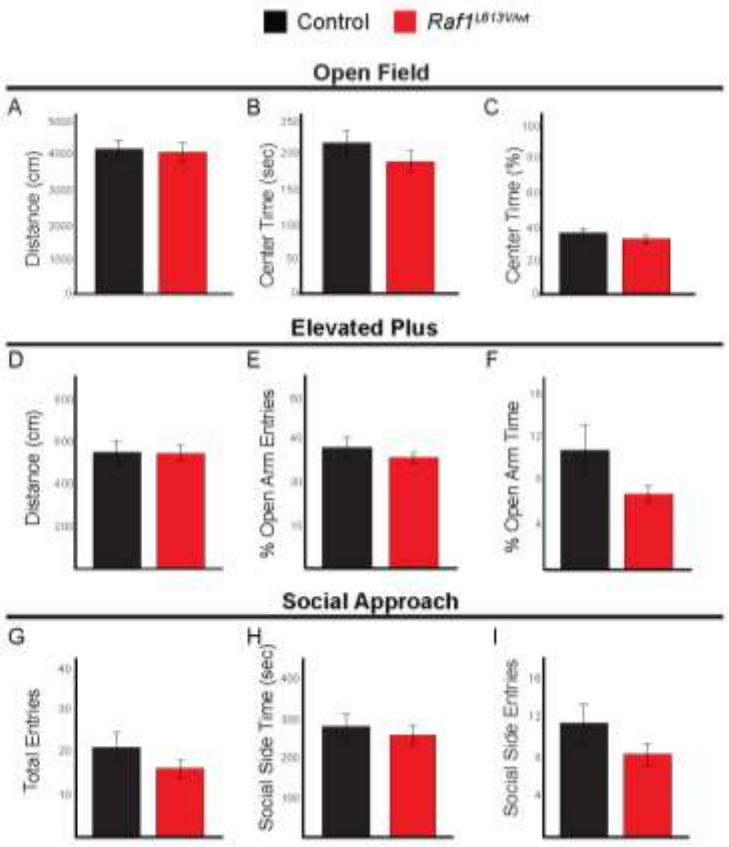

Figure 6. *Raf1*$^{L613V/wt}$ mice have normal locomotor capabilities, anxiety-like behaviors, and sociability. Control (n=23) and *Raf1*$^{L613V/wt}$ (n=31) mice were tested on a battery of behavioral tasks including the open field, elevated plus, and social approach assays. **A-C:** In the open field test, controls and *Raf1*$^{L613V/wt}$ mice do not exhibit a difference in total distance traveled (**A**), center time (**B**) and percent center time (**C**) (mean ± SEM). **D-F:** Elevated plus maze testing of controls and *Raf1*$^{L613V/wt}$ mice reveals that total distance (**D**), percent open arm entries (**E**), and open arm stay time (**F**) are unaltered in mutant mice (mean ± SEM). **G-I:** In the social approach task, controls and *Raf1*$^{L613V/wt}$ mutants display similar performance, as measured by total entries (**G**), time in social side (**H**), and entries on social side (**I**) (mean ± SEM).

We next asked if *Raf1*$^{L613V/wt}$ mutant mice displayed altered performance in an eight-armed water radial-arm maze (WRAM) swim task (Fig. 7A). Control (n=19) and mutant (n=15) mice both showed a statistically significant decrease in the number of total errors over 18 days of testing (main effect of day [$F_{(17, 544)} = 9.87$, $p < 0.0001$]). Surprisingly, however, *Raf1*$^{L613V/wt}$ mutant mice committed significantly fewer total errors in the acquisition phase (days 1-6) in comparison to controls (Fig. 7B, main effect of genotype [$F_{(1, 32)} = 4.87$, $p < 0.05$] *=Fisher's PLSD $p < 0.05$). When errors were assessed by type, mutant mice made fewer working memory correct (WMC) errors, related to reentering an arm that previously had a platform within a day (Supplemental Fig. 7A) (main effect of genotype [$F_{(1, 32)} = 8.94$, $p < 0.01$] *=Fisher's PLSD $p < 0.01$). Moreover, we detected a marginal trial by treatment interaction for WMC errors during the acquisition phase, indicating that as working memory load increases, mutants tended to make fewer WMC errors than controls (Supplemental Fig. 7B) (marginal interaction of trial by genotype [$F_{(2, 64)} = 2.83$, $p = 0.07$], Trial 3 Only: [$F_{(1, 32)} = 6.83$, $p < 0.05$], Trial 4 Only: [$F_{(1, 32)} = 5.82$, $p < 0.05$]). Neither working-memory incorrect (WMI) nor reference memory (REF) errors significantly differed between genotypes during the acquisition phase (Supplemental Fig. 7C; WMI [$F_{(1, 32)} = 2.05$, $p = 0.16$], REF [$F_{(1, 32)} = 0.41$, $p = 0.53$]). We did not observe significant differences between genotypes during the learning and asymptotic phases, once mice have successfully acquired the task and solve the maze at peak performance (i.e. asymptotic phase) (Fig. 7B; learning: [$F_{(1, 32)} = 0.05$, $p = 0.82$]; asymptotic: [$F_{(1, 32)} = 2.26$, $p = 0.14$]).

Five days following the completion of WRAM testing, the same cohort of mice was tested in the Morris water maze. Control and *Raf1*$^{L613V/wt}$ mutant mice exhibited improved

performance over time (Fig. 7C, main effect of day [$F_{(4, 128)} = 71.58$, $p < 0.0001$]). However, mutant mice displayed enhanced performance relative to controls, as measured by swim distance to platform across all five days of testing (Fig. 7C [$F_{(1, 32)} = 4.59$, $p < 0.05$] inset * = Fisher's PLSD post-hoc $p < 0.05$). Analysis of individual days revealed that mutant mice performed better than controls on days 3, 4, and 5, as predicted by the enhanced performance during WRAM acquisition (Fig 7C, * = one-tailed t-test, $p < 0.05$). Mutant mice also demonstrated reduced swim distance to the platform on day 2 of reversal learning (Fig. 7D; * = one-tailed t-test, $p < 0.05$). Controls and mutants both displayed the expected target quadrant preference, as indicated by a significantly higher percent of total swim distance in the previously platformed quadrant during the probe trial for baseline and reversal task testing (Fig. 7E, Supplemental Figure 7D-E). Additionally, mutants and controls did not exhibit significant differences in the visible platform test, indicating intact visual and motoric capacity (Fig. 7F).

We employed a tone-cued fear conditioning paradigm to examine amygdala-dependent learning and memory. Control (n=11) and mutant (n=9) mice were placed in a testing cage fitted with a shock floor, and given a 30-second auditory tone, immediately followed by a foot-shock, for a total of three tone-foot shock pairings. Control and mutant mice displayed similar shock thresholds (Fig. 7H) and baseline time freezing during the 30-second tone immediately prior to the first foot shock pairing (Fig. 7G). Control and mutant mice both exhibited an increase in average time freezing during the subsequent two tone presentations of the training phase (Fig. 7G; main effect of trial [$F_{(3, 54)} = 36.47$, $p < 0.001$] LSD post-hoc $p < 0.001$). No difference in freezing between genotypes was detected during training (Fig 7G; [$F_{(1, 18)} = 0.59$, $p = 0.45$]). Twenty-four (24) and 48-hrs after

acquiring the tone-foot shock association, mice were placed in a different context and tested for freezing behavior in response to the auditory tone without the paired foot shock. *Raf1*$^{L613V/wt}$ mice displayed significantly increased time freezing to tone in comparison to controls 24-hrs post-training (Fig. 7G; interaction between genotype and trial ([$F_{(3,54)}$ = 3.43, $p < 0.05$] * = LSD post-hoc $p < 0.05$), but not at 48-hrs (Fisher's LSD post-hoc $p = 0.11$). A significant difference in time spent freezing to tone was not observed during extinction learning or in spontaneous recovery seven days post-extinction (Fig. 7I, Supplemental Fig 7F). Taken together, *Raf1*$^{L613V/wt}$ mice demonstrate moderately enhanced performance in hippocampal-dependent spatial working and reference memory tasks and amygdala-dependent fear memory.

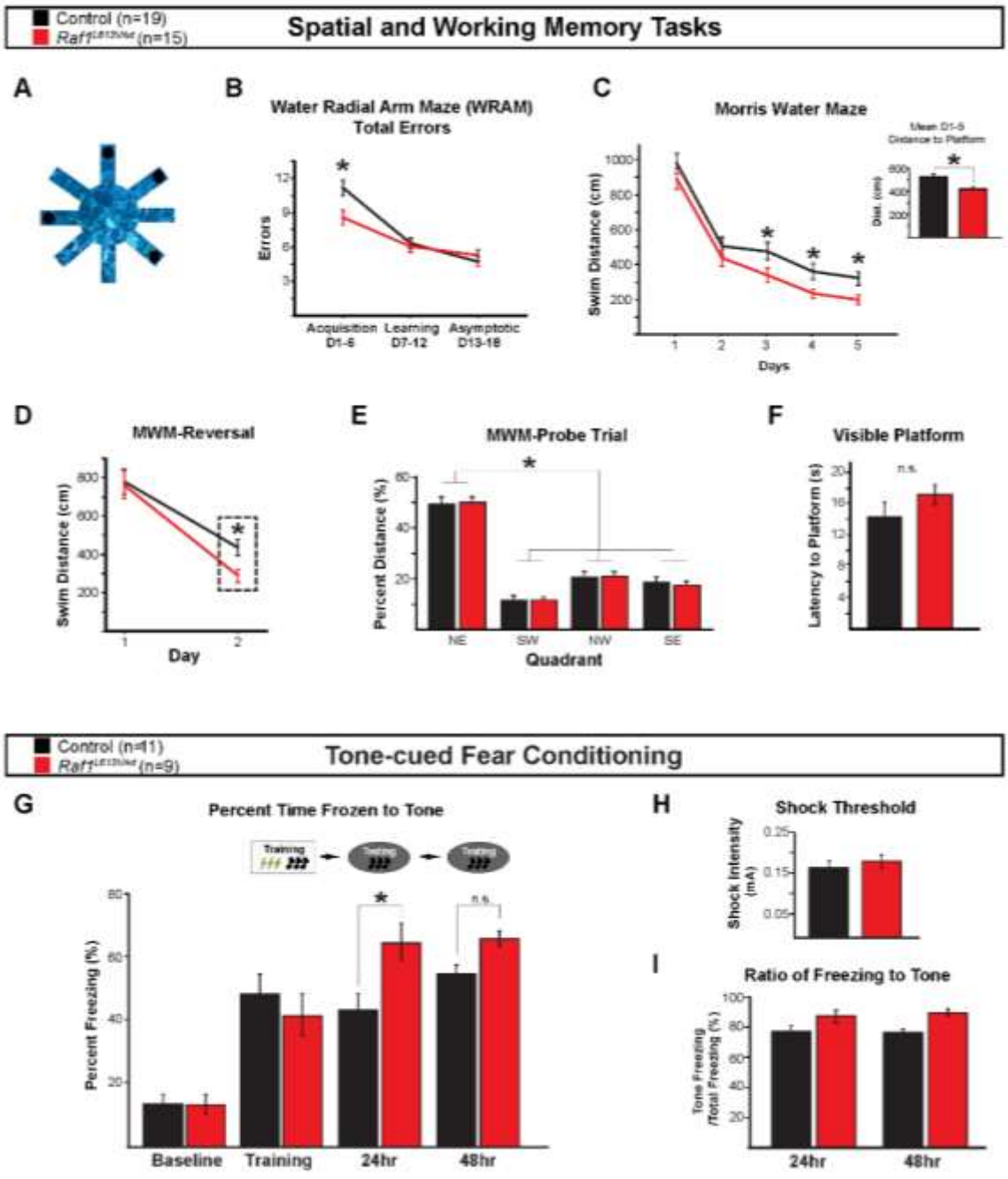
Control (n=19)
Raf1L613V/wt (n=15)
Spatial and Working Memory Tasks
A
B
Water Radial Arm Maze (WRAM)
Total Errors
Errors
Acquisition D1-6
Learning D7-12
Asymptotic D13-18
C
Morris Water Maze
Swim Distance (cm)
Days
Mean D1-5 Distance to Platform
Dist. (cm)
D
MWM-Reversal
Swim Distance (cm)
Day
E
MWM-Probe Trial
Percent Distance (%)
NE
SW
NW
SE
Quadrant
F
Visible Platform
Latency to Platform (s)
n.s.
Control (n=11)
Raf1L613V/wt (n=9)
Tone-cued Fear Conditioning
G
Percent Time Frozen to Tone
Training
Tested
Percent Freezing (%)
n.s.
Baseline
Training
24hr
48hr
H
Shock Threshold
Shock Intensity (mA)
I
Ratio of Freezing to Tone
Tone Freezing /Total Freezing (%)
24hr
48hr

Figure 7. *Raf1*$^{L613V/wt}$ animals exhibit enhanced spatial and working memory and fear learning. A: Schematic of an 8-armed water radial-arm maze (WRAM) used to examine adult control (n=19) and *Raf1*$^{L613V/wt}$ (n=15) mice. **B:** During the acquisition phase of WRAM testing between days 1-6, mutants execute significantly fewer total errors than controls (mean ± SEM, main effect of genotype [$F_{(1, 32)} = 4.87$, $p < 0.05$] *=Fisher's PLSD $p < 0.05$). **C:** In the Morris water maze (MWM), *Raf1*$^{L613V/wt}$ mice show a reduction in swim distance to platform on days 3, 4, and 5 relative to controls (mean ± SEM, * = one-tailed t-test, $p < 0.05$). The inset graph shows the average across all 5 days of testing (mean ± SEM, [$F_{(1, 32)} = 4.59$, $p < 0.05$] * = Fisher's PLSD $p < 0.05$). **D:** In the Morris maze reversal task, *Raf1*$^{L613V/wt}$ mice demonstrate reduced swim distance to platform on day 2 (mean ± SEM, * = one-tailed t-test, $p < 0.05$). **E:** Probe trial analysis demonstrated significant preference for the NE target quadrant (mean ± SEM, [$F_{(3, 96)} = 89.90$, $p < 0.0001$] * = Fisher's PLSD $p < 0.0001$). **F:** In the visible platform task, we did not detect a significant effect of genotype (mean ± SEM, [$F_{(1, 32)} = 1.31$, $p = 0.26$]). **G:** Naïve control (n=11) and mutant (n=9) animals were tested in tone-cued fear conditioning. Mutant animals do not differ significantly from controls in freezing behavior during the baseline or training phase; however, *Raf1*$^{L613V/wt}$ mice spent a significantly greater amount of time frozen to tone 24-hours post training (mean ± SEM, [$F_{(3,54)} = 3.429$, $p < 0.05$] * = Fisher's LSD post-hoc $p < 0.05$). No effect was detected 48-hours post training (mean ± SEM, Fisher's LSD post-hoc $p = 0.109$). **H:** No significant differences in shock threshold were detected (mean ± SEM). **I:** Ratio *of freezing to tone was unchanged at 24- and 48-hours post-training (mean ± SEM).*

Alterations in regulators of synaptic plasticity are not detectable in Raf1$^{L613V/wt}$ *mutant mice*

To identify the mechanisms that drive enhanced behavioral performance in learning and memory assays in *Raf1*$^{L613V/wt}$ mice, we assessed the expression of ARC, TNFα, and perineuronal net components, known regulators of synaptic plasticity that have also been linked to altered ERK1/2 signaling (Han et al., 2013; Thomas and Huganir, 2004). We subjected behaviorally naïve adult mice to five trials in the Morris water maze to activate the hippocampal circuit. Brains were collected 1 hour after the final trial and the number of ARC^{+} cells were assessed in the cortex and hippocampus. *Raf1*$^{L613V/wt}$ mice did not exhibit significant differences in ARC expression in comparison to controls in the cortex (Fig. 8A-D, n=4), or in the granule cell layer of the dentate gyrus (Fig. 8E-I, n = 4).

We also examined the expression of putative astrocyte-derived modulators of synaptic plasticity. The astrocyte-secreted molecule, TNFα, is a major contributor to learning and memory (Camara et al., 2015; Camara et al., 2013; Han et al., 2013), and astrocyte-mediated perineuronal net formation around PV^+ GABAergic neurons is thought to contribute to RASopathy phenotypes (Krencik et al., 2015). We therefore assessed behaviorally-naïve *Raf1*$^{L613V/wt}$ mice for the expression of TNFα and a perineuronal net marker, *wisteria floribunda* agglutinin (WFA), in the hippocampus. Qualitative analysis of hippocampal TNFα revealed no apparent changes to the pattern of expression in the hippocampal region globally or in mutant $S100\beta^+$ glia (Fig. 8J-O). We next examined the extent of WFA-labeling surrounding PV^+ GABAergic neurons within the CA1 region of the hippocampus (Fig. 8P-U). We found that *Raf1*$^{L613V/wt}$ PV^+ GABAergic neurons within the hippocampus displayed a similar extent and amount of WFA-labeling in comparison to controls (Fig. 8P-U, W; n = 35 mutant and 37 control neurons from 3 independent pairs). Therefore, *Raf1*$^{L613V/wt}$ mutant mice do not exhibit significant alterations in the expression of these three mediators of synaptic plasticity.

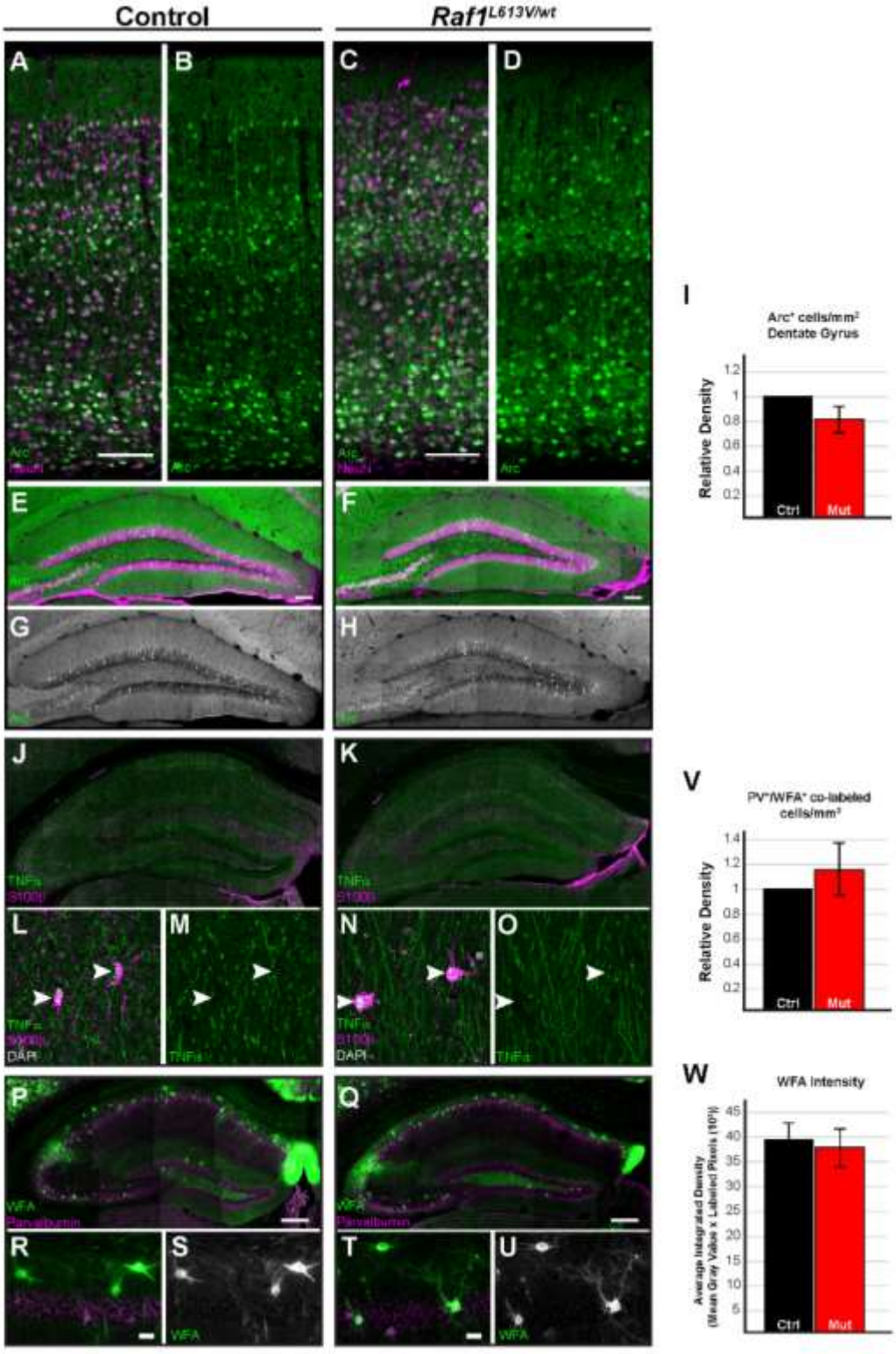
Control
Raf1L613V/wt
A
B
C
D
E
F
G
H
J
K
L
M
N
O
P
Q
R
S
T
U
I
Arc+ cells/mm2
Dentate Gyrus
Relative Density
Ctrl
Mut
V
PV+/WFA+ co-labeled
cells/mm2
Relative Density
Ctrl
Mut
W
WFA Intensity
Average Integrated Density
(Mean Gray Value x Labeled Pixels (10^3))
Ctrl
Mut

Figure 8. Normal expression of markers of synaptic plasticity in *Raf1*$^{L613V/wt}$ neurons and astrocytes. A-H: Control and mutant mice were subjected to a single 5-trial day of Morris Water Maze testing and collected 1-hour after completion of the 5th trial (n = 4). **A-D:** Double immunolabeled sections of sensory cortex for the activity-dependent gene ARC and mature neuronal marker NEUN. We did not detect any differences in the pattern of Arc labeling in the cortex. (scale bar = 100 µm) **E-I:** Counts of labeled cells in the granular layers of the dentate gyrus reveal no change in the density of ARC^{+} cells (mean ± SEM, n = 4). **J-W:** Assessment of markers of astrocyte function in behaviorally naïve mice. **J, K:** Representative coronal sections of hippocampus immunolabeled for TNFα and S100β. **L-O:** Confocal micrographs (63x) of TNFα- and S100β-labeled astrocytes indicates no qualitative change in the levels of TNFα in mutant hippocampi (n = 3). **P, Q:** Double immunolabeled coronal sections of hippocampus, stained with PV and the perineuronal net marker WFA (scale bar = 250µm). **R-U:** Representative images of CA1 hippocampal WFA-labeled neurons show no significant differences in the extent of perineuronal net formation (scale bar = 25µm). **V:** No significant differences in the number of WFA-labeled PV cells are seen (mean ± SEM, n = 3). **W:** Mutant (n = 35) and control (n = 37) PV neurons have a similar extent of surrounding WFA-labeled pixels (mean ± SEM).

Discussion

Our study provides insight into the cellular and behavioral processes affected by a Noonan Syndrome-linked *Raf1*^{L613V} mutation. In contrast to RASopathy-linked *PTPN11* or *RAS* mutants, we found little evidence that *Raf1*^{L613V} expression significantly alters global cortical excitatory or PV-expressing inhibitory neuron number (Gauthier et al., 2007; Paquin et al., 2009; Rooney et al., 2016). However, we detected an increased density of GFAP^{+} astrocytes in the mutant cortex and hippocampus (Gauthier et al., 2007; Li et al., 2012a; Li et al., 2012b; Paquin et al., 2009; Pucilowska et al., 2008; Pucilowska et al., 2012; Pucilowska et al., 2015; Samuels et al., 2008). OPC number was also increased in mutant cortices, though no significant change was observed in mature oligodendrocyte density or myelination. The increase in select glial subtypes did not correlate with a significant difference in locomotor ability, anxiety, or sociability. In contrast to many NF1 and Noonan Syndrome mouse models, *Raf1*$^{L613V/wt}$ mice displayed moderately enhanced performance in three different learning and memory tasks. Overall, these data show that the 'downstream' RASopathy-linked *Raf1*^{L613V} mutation increases the number of GFAP^{+} astrocytes and OPCs and improves aspects of learning and memory without significant alterations in basal behavioral measures of anxiety or sociability.

Pharmacological inhibitors of RAS and MEK1/2 reverse several aspects of nervous system dysfunction in many RASopathy rodent models (Costa et al., 2002; Lee et al., 2014; Sanchez-Ortiz et al., 2014; Wu et al., 2011). However, clinical trials with pathway inhibitors, primarily statins in NF1 patients, have had limited success, possibly due to ERK1/2-independent pathways modified in response to mutations at the level of or upstream of RAS (Acosta et al., 2011; Anastasaki and Gutmann, 2014; Brown et al., 2012;

Hegedus et al., 2007; Kaul et al., 2015; Krab et al., 2008; Mainberger et al., 2013; Payne et al., 2016; van der Vaart et al., 2013). Defining the effects of mutations at multiple levels of the cascade may help resolve which processes are suitable for therapeutic targeting in all RASopathies or in a personalized, mutation-specific fashion. We show that a RASopathy mutation downstream of RAS, *Raf1*^{L613V}, drives an increase in the number of GFAP^{+} astrocytes and OPCs. A CFC-Syndrome linked *MEK1*^{Y130C} mutant has recently been shown to exhibit a comparable glial phenotype (Aoidi et al., 2018). *Raf1*^{L613V} and *Mek1*^{Y130C} mutations lead to enhanced ERK1/2 activity in biochemical assays, but to a lesser degree than many other RASopathy mutations (Jindal et al., 2017; Rodriguez-Viciana et al., 2008; Wu et al., 2011). *Nf1* and *Ptpn11/Shp2* mutants show altered glial properties as well, including increased GFAP labeling and OPC number (Ehrman et al., 2014; Nordlund et al., 1995; Rizvi et al., 1999; Zhu et al., 2005). Enhanced expression of glial markers may contribute to these results, but developing glia are known to utilize ongoing NF1 (MIM: 613113), PTPN11/SHP2, and ERK1/2 signaling to regulate glial proliferation (Ehrman et al., 2014; Rhee et al., 2016; Tien et al., 2012). In summary, our data further support the idea that astrocyte and OPC development is highly sensitive to upstream or downstream RASopathy mutations of varying strengths.

The precise aspect of glial development disrupted in RASopathies is not completely understood. Mutations that hyperactivate ERK1/2 signaling in neural stem cells have been shown to initiate premature gliogenesis, often at the expense of neurogenesis (Li et al., 2014; Li et al., 2012a; Wang et al., 2012). Recent work on Costello Syndrome-associated *H-Ras*^{G12V} iPSCs also detected precocious astrocyte differentiation (Krencik et al., 2015). We found little evidence that cortical neuron density was altered in *Raf1*$^{L613V/wt}$ adult mice,

and multiple glial markers were relatively unchanged in P14 mutant cortices. Estimates of cellular density in RASopathy mutants by our group and others often rely upon two-dimensional based approaches, which may be prone to certain technical and analytical artifacts. More rigorous systematic analysis with three-dimensional stereological methods, such as the optical fractionator or the recently developed isotropic fractionator, may be better-suited to reliably detect modest changes in cell number in samples of RASopathy brains. In the least, our data indicate the modification in the density of $GFAP^{+}$ astrocytes and OPCs may occur during the late juvenile-young adult period in $Raf1^{L613V/wt}$ mutants. It is unclear whether the increased glial density arises from a deficit in ongoing glial progenitor proliferation or aberrant development of progenitor pools in the SVZ. The expression of genes important for glial maturation has yet to be evaluated, such as the transient expression of Olig2 in GFAP-expressing astrocytes (Cai et al., 2007). Finally, it will be important to examine whether the increase in glial density is cell autonomous and reversed by administration of pharmacological MEK1/2 inhibitors in adulthood.

Noonan Syndrome is typically linked to intellectual disability and other neuropsychiatric conditions that vary in severity depending on the specific mutation (Rauen, 2013; Jindal et al., 2015; Pierpont et al., 2009). $RAF1^{L613V}$ patients exhibit hallmark RASopathy features, such as hypertrophic cardiomyopathy and hypertelorism, but variable effects on intellectual capabilities that typically include impairment (Pandit et al., 2007; Razzaque et al., 2007; Denayer et al., 2010), but normal IQ (Kobayashi et al., 2010). However, $RAF1^{L613V}$ individuals with increased IQ have also been reported (E. Ciara et al., 2009, ASHG, abstract). Therefore, we asked whether $Raf1^{L613V/wt}$ mice exhibit aberrant neurobehavioral properties. We found that $Raf1^{L613V/wt}$ mutants had no significant

deficits in measures of locomotor, anxiety, or sociability that are often disrupted in models of neurocognitive syndromes. Additional behavioral characterization using paradigms employed in other mouse models of neurocognitive syndromes will be important in future studies, such as novel object recognition, sensory gating assays, or more detailed analyses of sociability that take into account novelty-related preference. However, we did observe somewhat unexpected effects in three behavioral learning and memory assays, where mutant mice exhibited enhanced performance during specific phases. Our results show relatively improved performance of *Raf1*$^{L613V/wt}$ mutants during the early acquisition, but not late, stages of the WRAM, consistent with enhanced learning during the acquisition of this task. However, mutants exhibit signs of enhanced memory following tone-cued fear conditioning, but not during the learning, or training, phase of this task. Further experimentation will be necessary to define how this mutation affects learning versus memory processes in specific circuits. However, to our knowledge, the *Raf1*$^{L613V/wt}$ mutant represents the first germline RASopathy mouse to display enhanced performance in these tasks. It should be noted that hyperactivation of ERK1/2 has been linked to enhanced plasticity in certain contexts. Costello Syndrome patients with *HRAS* mutations exhibit increased TMS-induced plasticity (Dileone et al., 2010). Moreover, *H-Ras*^{G12V} overexpression specifically in *CaMKII*-expressing cortical and hippocampal excitatory neurons has been shown to enhance LTP and Morris water maze performance in mice (Kushner et al., 2005). *Raf1*$^{L613V/wt}$ mice may provide another useful genetically-defined model to identify novel mechanisms of cognitive enhancement.

Our data raise important questions regarding the contributions of RASopathic non-neuronal cells to plasticity and learning. Most studies suggest the glial alterations seen in

RASopathies are detrimental to nervous system function. GFAP upregulation is a hallmark sign of reactive gliosis, which is associated with multiple neuropathological conditions and observed in post-mortem *NF1* brain tissue and mouse models (Nordlund et al., 1995; Rizvi et al., 1999; Gutmann et al., 1999). *H-Ras*^{G12S}-expressing astrocytes disrupt perineuronal net formation and constrain critical period plasticity (Krencik et al., 2015). Diffusion Tensor Imaging (DTI) of individuals diagnosed with a RASopathy have detected enlarged white matter tracts and aberrant myelination, presumably due to changes in oligodendrocytes, that often correlate with learning disability (Koini et al., 2017; Legius et al., 1995; Loitfelder et al., 2015; Mayes et al., 2013; North et al., 1994). Oligodendrocyte-specific NF1 deletion in mice has recently been shown to drive myelin decompaction and sensory gating defects (López-Juárez et al., 2017). Both astrocytes and OPCs, however, are critical for maintaining nervous system homeostasis and promoting plastic changes important for learning and memory (Gibson et al., 2014; Han et al., 2013; Haydon and Nedergaard, 2014; McKenzie et al., 2014). Additionally, reactive gliosis is a graded response associated with specific pro-regenerative effects (Liddelow and Barres, 2017). It seems plausible the relatively subtle biochemical effect of the *Raf1*$^{L613V/wt}$ mutation may have led to mild changes in astrocyte function that minimized the negative consequences of complete activation of reactive gliosis. In support of this, we saw little change in microglial number, which often coincides with increases in GFAP labeling, and we were unable to detect a difference in perineuronal net formation in adult *Raf1*$^{L613V/wt}$ forebrains. Secondly, the increase in OPC number did not lead to changes in mature myelinating oligodendrocyte density or overt deficits in myelination. Our results indicate that moderately enhanced GFAP^{+} astrocyte and OPC number is clearly not sufficient to impair

learning in *Raf1*$^{L613V/wt}$ mice. Additional studies of conditional, glial-specific models will be important for evaluating to what extent the *Raf1*^{L613V}-mediated increase in glial number is involved in enhancing cognition.

The biological basis of heterogeneity between different RASopathy mutations is not completely understood (Jindal et al., 2015; Pierpont et al., 2009; Schreiber et al., 2017). Diverse levels of kinase activation between disease-linked mutations and the precise location of the mutated gene in the signaling network clearly contribute (Pierpont et al., 2009; Rodriguez-Viciana et al., 2008; Rodriguez-Viciana et al., 2006). For example, studies of Noonan Syndrome-associated cardiac defects reveal that hypertrophic cardiomyopathy is observed in less than 20% of cases linked to *PTPN11/SHP2* or *SOS1* mutations (Roberts et al., 2007; Sznajer et al., 2007), but greater than 90% of *RAF1* mutations (Pandit et al., 2007; Razzaque et al., 2007). Neurocognitive phenotypes tend to be more variable but 'downstream' mutations in BRAF, MEK1, or MEK2 generally result in more severe cognitive deficits than 'upstream' mutations (Cesarini et al., 2009; Pierpont et al., 2009; Pierpont et al., 2010b; Pierpont et al., 2013). Quantitative comparisons of common cellular phenotypes using IPSC-derived samples from individuals with different RASopathy mutations would be particularly useful (Krencik et al., 2015). Nonetheless, the variability in neurocognitive function between individuals with the same gene mutation is significant. For example, two siblings with a P491S mutation in PTPN11 have been shown to have wide variation in language ability scores; one with severe impairment, the other just below average (Pierpont et al., 2010b). Individuals with an L613V mutation in *RAF1* show a broad range of IQ scores that range from impairment to possibly higher than average (E. Ciara et al., 2009, ASHG, abstract; Denayer et al., 2010; Kobayashi et al., 2010;

Pandit et al., 2007; Razzaque et al., 2007). Genetic modifiers are likely influential, but difficult to identify in RASopathies due to extensive mutation heterogeneity. Further investigation of known strain-specific differences in RASopathy phenotypes provides a sensible alternative to identifying candidate modifiers (Schreiber et al., 2012; Wu et al., 2011). Gene-environment interactions almost certainly modify neurocognitive outcomes but are poorly studied in the RASopathies. For example, the mildy higher basal state of astrocyte activation in *Raf1*$^{L613V/wt}$ mice may render increased susceptibility to damage following exposure to environmental intoxicants or neuropathogenic viral infections.

Past studies have noted complex, sometimes paradoxical, changes in ERK1/2 activity in response to pharmacological and genetic manipulations in specific contexts. In the fly embryo, gain-of-function mutations in *Mek* induce unanticipated decreases in ERK1/2 activity in certain body segments (Goyal et al., 2017). Studies of RAF inhibitors in cancer led to the discovery of complex compensatory interactions between BRAF and RAF1 that drive a paradoxical increase in ERK1/2 activation (Hatzivassiliou et al., 2010; Heidorn et al., 2010; Poulikakos et al., 2010). Indeed, the same compensatory upregulation of BRAF activity contributes to ERK1/2 hyperactivation in response to select kinase-impairing *Raf1*^{D486N} mutations (Wu et al., 2012). MEK1/2 inhibitors are clearly capable of reversing craniofacial and cardiac defects in *Raf1*$^{L613V/wt}$ mutant mice (Wu et al., 2011). In light of the enhanced learning and memory performance we observed in this strain, it will be interesting to examine whether pharmacological inhibitors of ERK1/2 signaling result in relative neurocognitive impairment in *Raf1*$^{L613V/wt}$ mutants. Overall, our data provide further support for mutation-specific approaches to the development of RASopathy therapeutics.

Acknowledgements: We thank Johan Martinez, Cassandra Roose, Chris Wedwick, members of the Newbern lab, and the ASU Keck Bioimaging and EM Core for technical assistance. All immunohistochemical experiments were performed by Michael C. Holter. Behavioral testing and expertise was conducted in the labs of Heather Bimonte-Nelson by Stephanie Koebele and Lauren Hewitt (Morris Water Maze; Water Radial Arm Maze) and Cheryl Conrad by Jessica Judd and Lauren Hewitt (Fear conditioning). All figures were prepped for presentation by Michael C. Holter. This research was supported by NIH grant R00NS076661 and R01NS097537 to JMN, Children's Tumor Foundation Young Investigator Award #2015-01-013 to LX, and R01CA49152 to BN.

Supplemental Figures

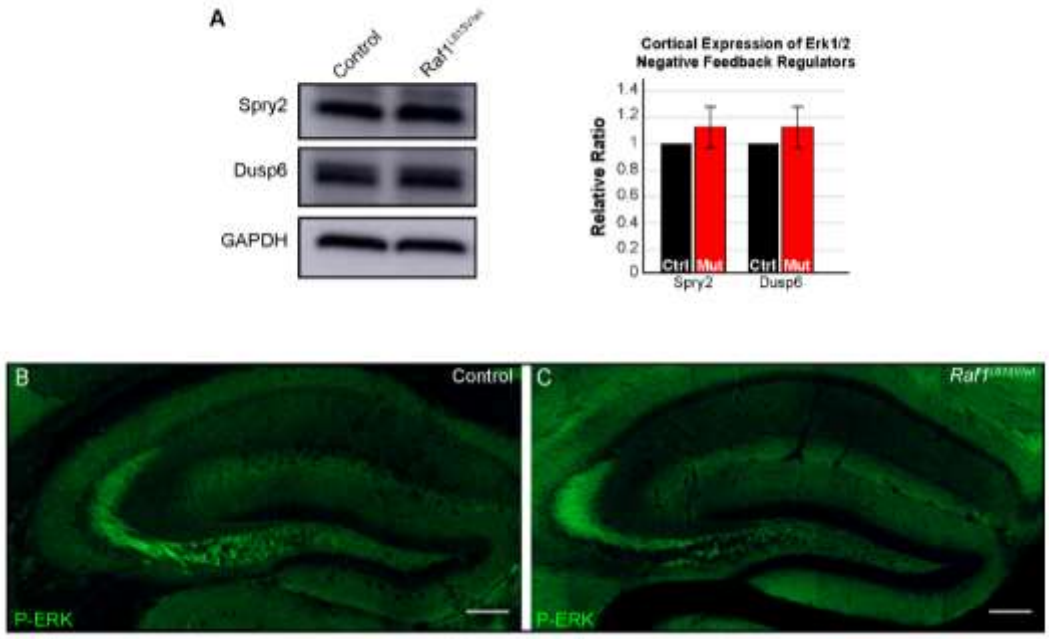

Supplemental Figure 1 (S1). Normal patterns of P-ERK1/2 expression in Raf1$^{L613V/wt}$ brains. A: Western blots of P21 whole control and *Raf1*$^{L613V/wt}$ cortical lysates showed no significant differences in the relative expression of SPRY2 or DUSP6 (mean ± SEM, n = 5). **B-C:** Control (B) and *Raf1*$^{L613V/wt}$ (C) hippocampi displayed a similar pattern of p-ERK1/2 immunolabeling. Scale bar = 200 µm.

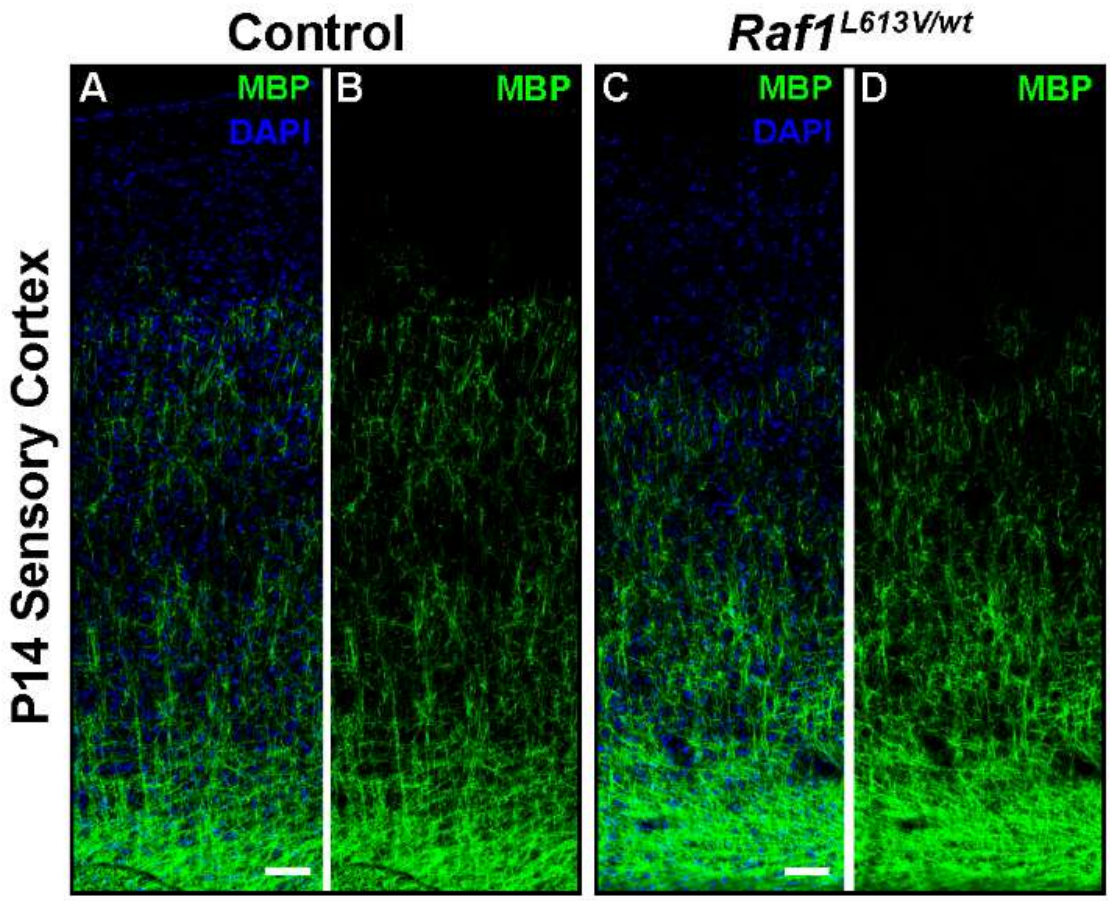

Supplemental Figure 4 (S4). Juvenile Raf1$^{L613V/wt}$ cortices show normal extent of myelination. A-D: Representative double immunolabeled sections of P14 sensory cortex for MBP and DAPI showed no qualitative differences in the pattern of myelination between control (A, B) and mutant (C, D) cortices (scale bar = 50µm).

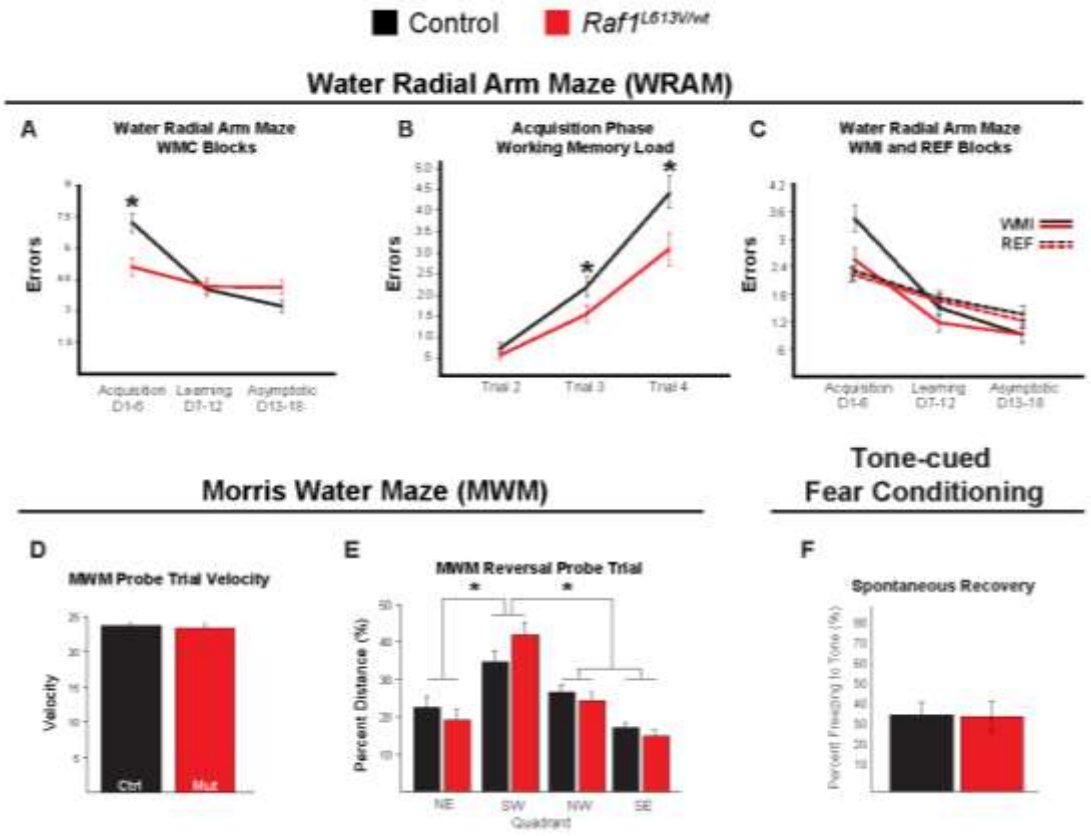

Supplemental Figure 7 (S7). Mutant mice exhibit enhanced spatial reference and working memory. A: *Raf1*$^{L613V/wt}$ animals commit significantly fewer working memory correct errors during the acquisition phase (mean ± SEM, main effect of genotype, acquisition [$F_{(1,32)}$ =8.94, p=0.005] *=Fisher's PLSD $p < 0.05$; learning [$F_{(1,32)}$ = 0.05, p=0.82]; asymptotic [$F_{(1,32)}$ = 2.26, p=0.14]). **B:** Evaluation of working memory correct (WMC) errors during the acquisition phase indicate a marginal interaction of trial by genotype (solid lines) (mean ± SEM, [$F_{(2, 64)}$ = 2.83, p = 0.07]). Individual analysis of trials 3 and 4 reveal a main effect of genotype (Trial 3: [$F_{(1, 32)}$ = 6.83, $p < 0.05$], Trial 4: [$F_{(1, 32)}$ = 5.82, $p < 0.05$]). **C:** Mutant and control animals commit comparable numbers of working memory incorrect errors (mean ± SEM, acquisition [$F_{(1,32)}$ =2.04, p=0.16]; learning [$F_{(1,32)}$ = 0.43, p=0.51]; asymptotic [$F_{(1,32)}$ = 0.002, p=0.98]). Similarly, we observed no differences in reference memory errors between genotypes during the testing period (mean ± SEM, acquisition [$F_{(1,32)}$ =0.41, p=0.52]; learning [$F_{(1,32)}$ = 0.03, p=0.85]; asymptotic [$F_{(1,32)}$ = 0.17, p=0.68]). **D:** No differences between mutant and control velocity were observed during the probe trial. **E:** Quadrant preference in the reversal probe trial is similar between mutant and control mice. **F:** No differences in spontaneous recovery are observed between control and *Raf1*$^{L613V/wt}$ animals after extinction.

CHAPTER 3

Hyperactive Mek1 signaling in cortical GABAergic interneurons causes embryonic parvalbumin-neuron death and defects in behavioral inhibition

Authors: Michael C. Holter[1], Lauren T. Hewitt[1,#], Kenji J. Nishimura[1,#], George R. Bjorklund[1], Shiv Shah[1], Noah R. Fry[1], Katherina P. Rees[1], Tanya A. Gupta[2], Carter W. Daniels[2,†], Guohui Li[3], Steven Marsh[4], David M. Treiman[4], M. Foster Olive[2], Trent R. Anderson[3], Federico Sanabria[2], William D. Snider[5], Jason M. Newbern[1, *]

Affiliations:

[1]School of Life Sciences, [2]Department of Psychology, Arizona State University; Tempe, AZ 85287, USA

[3]College of Medicine, University of Arizona; Phoenix, AZ 85004, USA

[4]Barrow Neurological Institute; Phoenix, AZ 85013, USA

[5]University of North Carolina Neuroscience Center, The University of North Carolina School of Medicine; Chapel Hill, NC, 27599, USA

[#]Present Address: Interdepartmental Neuroscience Graduate Program, University of Texas; Austin, TX, 78712, USA

[†]Present Address: Department of Psychiatry, Columbia University, New York, NY 10032, USA

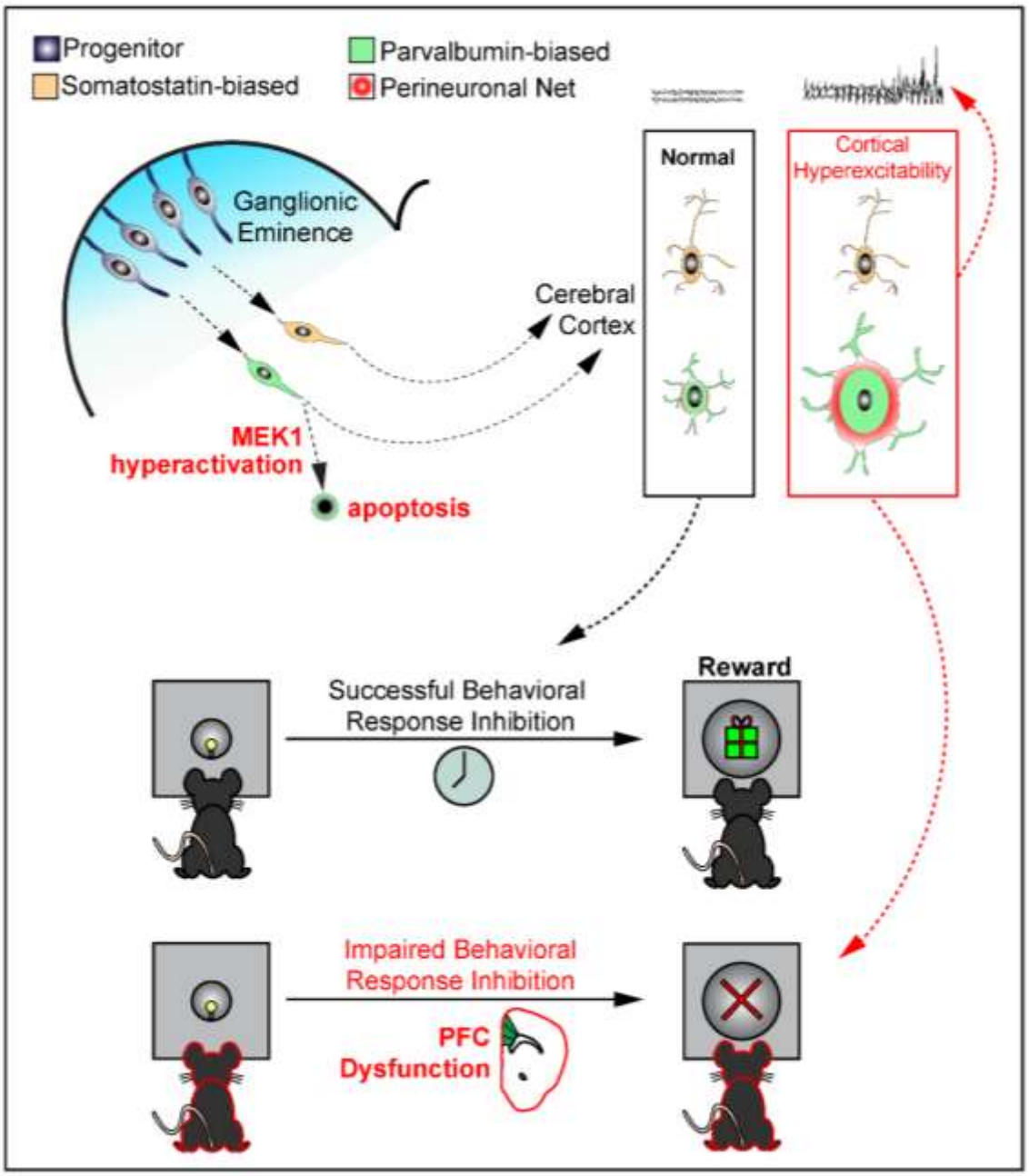

Graphical Abstract. *Hyperactive Mek1 signaling in cortical GABAergic interneurons causes embryonic parvalbumin-neuron death and defects in behavioral inhibition.*

Abstract

Abnormal ERK/MAPK pathway activity is an important contributor to the neuropathogenesis of many disorders including Fragile X, Rett, 16p11.2 Syndromes, and the RASopathies. Individuals with these syndromes often present with intellectual disability, ADHD, autism, and epilepsy. However, the pathological mechanisms that underly these deficits are not fully understood. Here, we examined whether hyperactivation of MEK1 signaling modifies the development of GABAergic cortical interneurons (CINs), a heterogeneous population of inhibitory neurons necessary for cortical function. We show that GABAergic-neuron specific MEK1 hyperactivation *in vivo* leads to increased cleaved caspase-3 labeling in a subpopulation of immature neurons in the embryonic subpallium. Adult mutants displayed a significant loss of mature parvalbumin-expressing (PV) CINs, but not somatostatin-expressing CINs, during postnatal development and a modest reduction in perisomatic inhibitory synapse formation on excitatory neurons. Surviving mutant PV-CINs maintained a typical fast-spiking phenotype and minor differences in intrinsic electrophysiological properties. These changes coincided with an increased risk of seizure-like phenotypes. In contrast to other mouse models of PV-CIN loss, we discovered a robust increase in the accumulation of perineuronal nets, an extracellular structure thought to restrict plasticity in the developing brain. Indeed, we found that mutants exhibit a significant impairment in the acquisition of a behavioral test that relies on behavioral response inhibition, a process linked to ADHD-like phenotypes. Overall, our data suggests PV-CIN development is particularly sensitive to hyperactive MEK1 signaling which may underlie neurological deficits frequently observed in ERK/MAPK-linked syndromes.

Significance Statement

The RASopathies are a family of neurodevelopmental syndromes caused by mutations that lead to increased RAS/RAF/MEK/ERK signaling and are associated with intellectual disability, epilepsy, and ADHD. We do not fully understand how distinct neuronal subtypes are affected in these syndromes. Here, we show that increased MEK signaling in developing mice promotes the embryonic death of a specific subset of cortical inhibitory neurons that express parvalbumin. Surviving mutant parvalbumin neurons also show significant changes in crucial maturation processes, which coincide with increased seizure susceptibility and profound deficits in behavioral inhibition. These data suggest that deficits in inhibitory circuit development contribute to RASopathy neuropathogenesis and indicate that therapeutic strategies targeting inhibitory interneuron dysfunction may be beneficial for these individuals.

Introduction

Multiple developmental disorders are caused by genetic mutations linked to perturbation of kinase activity and altered intracellular signaling. The RAS/RAF/MEK/ERK (ERK/MAPK) pathway is a well-known, ubiquitous signaling cascade that is dynamically activated during development (Krens et al., 2006; Samuels et al., 2009). Mutations in classic RAS/MAPK signaling pathway components or upstream regulators, such as *PTPN11/SHP2*, *NF1*, or *SYNGAP1*, cause a family of related syndromes, known collectively as the RASopathies (Tidyman and Rauen, 2016). Moreover, *MAPK3/ERK1* is present in a frequently mutated region of 16p11.2 linked to Autism Spectrum Disorder (ASD) and animal models of Fragile X, Rett, and Angelmann Syndromes also exhibit changes in ERK/MAPK signaling activity (Kumar et al., 2008; Pucilowska et al., 2015; Vorstman et al., 2006). These disorders are often associated with intellectual disability, neurodevelopmental delay, ADHD, autism, and epilepsy. Clearly, aberrant ERK/MAPK activity is an important molecular mediator of neurodevelopmental abnormalities, however, therapeutic approaches for these conditions are lacking, due in part to a limited understanding of the developmental stage- and cell-specific functions of ERK/MAPK signaling in the brain. Delineating the precise consequences of altered ERK/MAPK activity on specific neuronal subtypes in the developing forebrain may provide insight into the neuropathogenesis of multiple neurodevelopmental diseases.

Coordinated interactions between multiple cell types are necessary for normal brain function, but deficits in select cellular subtypes often mediate specific neurodevelopmental phenotypes. Past work has shown that ERK/MAPK signaling regulates the development of dorsal cortex-derived glutamatergic cortical projection neurons (PNs) and glia (Aoidi et

al., 2018; Ehrman et al., 2014; Ishii et al., 2013; Li et al., 2012b). Upstream regulators, such as *Syngap1*, are also crucial for the early development of cortical glutamatergic neuron structure, excitability, and cognition (Clement et al., 2012; Ozkan et al., 2014). In contrast, NF1 mutations have been shown to impair aspects of spatial learning and memory via disruption of GABAergic, but not glutamatergic, neuron function (Cui et al 2008). Abnormal GABAergic circuitry is thought to be a key feature in the neuropathogenesis of various other neurodevelopmental disorders (Chao et al., 2010; Cui et al., 2008; Paluszkiewicz et al., 2011; Zhang et al., 2010). GABAergic neuron-directed *Syngap1* loss modulates GABAergic output but does not drive major abnormalities in mouse behavior or seizure threshold (Berryer et al., 2016; Ozkan et al., 2014). Mutations in signaling components upstream of *Ras* differentially modulate multiple downstream pathways and do not provide a clear delineation of ERK/MAPK function (Anastasaki and Gutmann, 2014; Brown et al., 2012). Here, we have hyperactivated MEK1 specifically in GABAergic cortical interneurons (CINs) to better understand the effects on inhibitory circuit development.

In the mature cortex, locally connected parvalbumin- (PV) and somatostatin-expressing (SST) CINs comprise the most populous and functionally diverse GABAergic subtypes (Kessaris et al., 2014). Reduced PV-CIN number is often observed in mouse models of multiple neurodevelopmental diseases, however, the mechanism of loss is poorly understood (Chao et al., 2010; Cui et al., 2008; Steullet et al., 2017). PV- and SST-CINs are generated in spatiotemporal fashion primarily from the medial ganglionic eminence (MGE) and migrate tangentially to the cortical plate (Gelman et al., 2009; Gelman and Marín, 2010; Lavdas et al., 1999; Marin and Rubenstein, 2001, 2003; Parnavelas, 2000;

Tamamaki et al., 1997; Wichterle et al., 1999; Wichterle et al., 2001; Wonders and Anderson, 2006). Tangential migration and early GABAergic circuit development is regulated by BDNF/TRKB, GDNF/GFRα1, HGF/MET, and NRG/ERBB4 signaling, which activate multiple Receptor Tyrosine Kinase (RTK)-linked intracellular kinase cascades, including ERK/MAPK (Bae et al., 2010; Fazzari et al., 2010; Flames et al., 2004; Perrinjaquet et al., 2011; Pozas and Ibanez, 2005). While the transcriptional basis of GABAergic neuron development has been well-studied (Lim et al., 2018; Mayer et al., 2018; Mi et al., 2018; Paul et al., 2017), the kinase cascades that mediate GABAergic development in response to critical extracellular cues have received less attention.

Here, we show that GABAergic neuron-specific expression of constitutively-active MEK1$^{S217/221E}$ (caMEK1) led to caspase-3 activation in a subset of embryonic GABAergic neurons. Even though caMEK1 is expressed in all CINs, we only observed a significant reduction in the number of mature PV-CINs, but not SST-CINs. In contrast with past models exhibiting PV-CIN loss, we found a surprising increase in the extent of perineuronal net (PNN) accumulation around these cells (Steullet et al., 2017). We observed an increased risk of spontaneous epileptiform activity and mild seizure-like activity in a subset of mutant mice that coincided with a reduction in inhibitory synapses on pyramidal neurons. Mutant mice exhibited normal locomotor, anxiety-like, and social behaviors, but we discovered deficits in behavioral response inhibition capacity, a process linked to ADHD-like phenotypes. Our findings indicate that GABAergic-specific MEK1 hyperactivation is sufficient to drive widespread changes in cortical development relevant to cognitive phenotypes observed in RASopathies. Together, these data define the precise

functions of ERK/MAPK signaling in CIN development and suggest preferential contributions of PV-CIN pathology to ERK/MAPK-linked disorders.

Materials and Methods

Mice

All mice were handled and housed in accordance with the guidelines of the Institutional Animal Care and Use Committee, kept on a daily 12-hour light-dark cycle, and fed ad libitum. CaMek1 mice were kindly provided by Dr. Maike Krenz and Dr. Jeffrey Robbins while the source of the other mouse strains is listed in Table S1. Genomic DNA was extracted from tail or toe samples for standard genotyping by PCR using the following primer combinations: (listed 5'-3'): Cre – TTCGCAAGAACCTGATGGAC and CATTGCTGTCACTTGGTCGT to amplify a 266 bp fragment; caMek1S217/221E - GTACCAGCTCGGCGGAGACCAA and TTGATCACAGCAATGCTAACTTTC amplify a 600 bp fragment; Ai3/Ai9 – AAGGGAGCTGCAGTGGAGTA, CCGAAAATCTGTGGGAAGTC, ACATGGTCCTGCTGGAGTTC, and GGCATTAAAGCAGCGTATCC amplify a 297 bp wt Rosa26 segment and a 212 bp Ai3/Ai9 allele.

Table S1. Mouse Strains

Mouse Strain	**Reference**	**Stock Number**
Nkx2.1-Cre	Xu et al., 2008	Jax labs #008661
Slc32A1-Cre	Vong et al., 2011	Jax labs #028862
Dlx5/6-Cre	Monory et al., 2006	Jax labs #008199
Map2k1$^{S217/221E}$ (*caMEK1*)	Krenz et al., 2008	
Ai9 (Cre-dependent RFP)	Madisen et al., 2010	Jax labs #007909
Ai3 (Cre-dependent GFP)	Madisen et al., 2010	Jax labs #007903

Immunostaining and Image Analysis

Free floating or slide-mounted sections were rinsed in PBS and blocked in a buffer containing 0.05 - 0.2% Triton 5% Normal Donkey Serum (NDS) in PBS before incubating in primary antibody solution. The primary antibodies used in these experiments are listed in Table S2. Sections were then rinsed and incubated in fluorescently-conjugated secondary antibody solutions containing Alexa-Fluor 488, 568, or 647 conjugated anti-rabbit, anti-goat, or anti-chicken antibodies diluted in blocking solution. Tissue was rinsed in PBS and cover-slipped for microscopic analysis. Streptavidin-conjugated fluorophores were used to visualize WFA labeling.

Table S2. Antibodies

Antibodies	**Manufacturer**	**Catalog Number**
Goat anti-Parvalbumin	Swant	PVG213
Rabbit anti-Somatostatin	Peninsula	T-4103
Biotinylated *Wisteria Floribunda Agglutinin*	Vector	B-1355
Chicken anti-GFP	Aves	GFP-1020
Chicken anti-RFP	Rockland	600-901-379
Rabbit anti-MEK1	Abcam	Ab32091
Rabbit anti-ERK2	Abcam	Ab32081
Rabbit anti-P-ERK1/2	Cell Signaling	4370
Mouse anti-NEUN	Millipore	Mab377
Rabbit anti-cleaved caspase 3	Cell Signaling	9664L
Rabbit anti-GFAP	Abcam	Ab7260
Rabbit anti-VGAT	Synaptic Systems	131 003
Mouse anti-8-oxo-dg	R&D Systems	4354-MC-050

Confocal images of at least three anatomically matched sections that include a brain region of interest were quantified for labeled cell density by observers blind to genotype. For estimating labeled cell density in the cortex, a column spanning all cortical layers was defined, the cross-sectional area measured, and the number of labeled cells was assessed. The proportion of cells co-labeled with Cre-dependent fluorescent reporters was also determined for select experiments. Quantification of cellular labeling was averaged across

all images collected from an individual mouse. At least three mice were collected for each genotype and results were analyzed using Student's t-tests unless indicated otherwise.

We quantified the extent of inhibitory synapse labeling in the perisomal domain of excitatory neurons from confocal images of VGAT/NEUN/GFP co-labeled sections. Confocal images were collected using optimal Airyscan settings for a 63x 1.4 NA objective on a Zeiss LSM800 with the same acquisition parameters, laser power, gain, and offset for VGAT detection. NEUN+/GFP- neurons in S1 layer 2/3 with a pyramidal morphology and residing 5-10μm from the tissue section surface were randomly selected by a blinded observer. NEUN+ soma were outlined in Photoshop and a ring 1.8μm in thickness was then established to specify the perisomatic space. VGAT-immunolabeling from perisomatic regions of interest were imported into ImageJ where the autothreshold algorithm, "Moments", was utilized to define the total area of perisomatic VGAT-labeling in an unbiased manner. The perisomal VGAT-labeled area was then normalized to the total perisomatic area for that neuron. A total of 48 control and 53 mutant neurons from three different mice were analyzed. A similar approach was utilized to quantify VGAT labeling in areas enriched in dendrites by analyzing randomly selected regions of the layer 2/3 neuropil that did not contain any NEUN-labeled soma.

Slice electrophysiology

Brain slicing and preparation was performed as reported previously (Nichols et al., 2018). Mice were deeply anesthetized by isoflurane inhalation before decapitation. Brains were quickly removed and the coronal slices (350 μM) of the somatosensory cortex were produced on a vibratome (VT 1200; Leica, Nussloch, Germany) in fully oxygenated (95%

O2, 5% CO2), ice-cold artificial cerebral spinal fluid (aCSF) containing (in mM): 126 NaCl, 26 NaHCO3, 2.5 KCl, 10 glucose, 1.25 Na2H2PO4·H2O, 1 MgSO4·7H2O, 2 CaCl2·H2O, pH 7.4. The slices were incubated in the same aCSF at 32ºC for 30min before being allowed to recover at room temperature for an additional 30 min before patch clamp recordings were started.

After recovery, slices were transferred into recording chamber and perfused continuously with aCSF of 32ºC at a rate of 1-2 ml/min. Then whole-cell patch clamp recordings were performed on tdTomato-positive fast-spiking (FS) interneurons in the somatosensory cortex layer V/VI (L5/6) by using an Axon 700B amplifier. The FS neurons were identified by lack of an emerging apical dendrite and their intrinsic firing response to current injection (Agmon & Connors, 2018; Anderson et al., 2010; McCormick et al., 1985). Clampex 10.6 (Molecular Devices) was used to collect data and pipettes (2-5 MΩ) were pulled from borosilicate glass (BF150-110-10, Sutter Instruments) by using sutter puller (Model P-1000, Sutter Instruments), filled with an internal solution that contains (in mM): 135 K-Gluconate, 4 KCl, 2 NaCl, 10 HEPES, 4 EGTA, 4 Mg ATP and 0.3 Na Tris. The stability of the recordings was monitored during the experiments, and only the recordings with the series resistances (Rs) less than both 25 MΩ and 20% of the membrane resistances were chosen for analysis. For the input resistance calculation, the steady plateau of the voltage responding to the current input of -50 pA step with 1 s duration was used and intrinsic parameters were measured as previously reported (Nichols et al., 2018). Adaptation index was calculated as the ratio of the 1st interspike interval over the last (i.e. F1st ISI/Flast ISI). The frequency (F) – current (I) slope was calculated as the number of induced action potentials (APs) divided by the current step (number of APs at 150pA-

number of APs at 100pA)/(150pA-100pA). Unpaired Student's t-test and two-way ANOVA with Bonferroni post hoc tests were used for statistical analysis.

Behavioral Testing

Open Field Testing

The open field test was used to test voluntary locomotor capabilities and anxiety-like behavior. The apparatus consisted of a 40x40cm arena enclosed by 30cm high opaque walls. A single 60W bulb was positioned to brightly illuminate the center of the chamber with dim lighting near the walls. Mice were placed into the apparatus and recorded for a total of 10 minutes. Video data were analyzed for total distance traveled and time spent in the center quadrant.

Elevated Plus Maze

The elevated plus maze was constructed from black polycarbonate, elevated 81cm off the ground, and oriented in a plus formation with two 12x55cm open arms and two 12x55cm closed arms extending from an open 12x12cm center square. Closed arm walls were 40cm high extending from the base of the arm at the center square. The apparatus was lit with a 60W bulb with light concentrated on the center square. At the beginning of the trial, mice were placed in the center square, facing the south open arm, and recorded while freely exploring for 5 minutes.

Social Approach Assay

The social approach apparatus was made of transparent plexiglass and contained three 20x30x30cm chambers (total dimensions 60x30x30cm) connected by open doorways. Prior to experimental social trials, mice were habituated to the apparatus and allowed to freely explore all three chambers for 5 minutes. At the end of the 5 minutes, mice were removed and placed in their home cage. A sex- and age-matched stimulus mouse was then placed into a small empty cage in chamber 1 of the apparatus. The experimental mouse was reintroduced to the center chamber (chamber 2) of the apparatus and recorded while freely exploring for 10 minutes. The time spent in the chamber with the stimulus mouse (chamber 1) or the empty chamber (chamber 3) was then measured.

Fixed Minimum Interval (FMI)

Twenty-four adult mice (12 Slc32A1:Cre mice: 5 males, 7 females; 12 caMek1, Slc32A1:Cre mice: 6 males, 6 females) were kept on a 12-hour reverse light-dark cycle. Animals had free access to water in their home cages, but access to food was gradually reduced in the week prior to behavioral training, where 1 hr of food access was provided 30 min after the end of each daily training session. Body weights were maintained such that mice lost no more than 15% of starting body weight. Behavioral testing was conducted in eight MED Associates (St. Albans, VT, USA) modular test chambers (240 mm length □ 200 mm width □ 165 mm height; ENV-307W). Each chamber was enclosed in a sound- and light-attenuating cabinet (ENV-022V) equipped with a fan for ventilation that provided masking noise of approximately 60dB (ENV-025-F28). The back wall and hinged front door of each chamber were made of Plexiglas. The side walls of the chamber were made

of aluminum, and the right wall contained the manipulanda and reward receptacle. The floor was composed of thin metal bars. A circular reward receptacle was positioned in the center of the front panel and equipped with a head entry detector (ENV-302HD), a liquid dipper (ENV-302W-S), and a yellow LED (ENV-321W). The reward receptacle was flanked by a nose-poke device including an LED-illuminator (ENV-314M). The chamber was fitted with a house light (ENV-315W) at ceiling level above the back wall (ENV-323AW) and a 4.5kHz tone generator (ENV-323HAM). Experimental programs were arranged via a MED PC interface connected to a PC controlled by MED-PC IV software. All behavioral sessions were 30 min long, including a 3-min warm-up period during which no stimuli were activated.

Reinforcement Training and Autoshaping. Mice were first trained to obtain 0.1 cc of diluted sweetened condensed milk from the liquid dipper (the reinforcer) in the reward receptacle. Following the 3-min warmup period, a reinforcer was made available, followed by consistent reinforcer delivery at variable, pseudo-randomly selected inter-trial intervals (ITIs) for the remainder of the session (mean = 45 s). No stimuli were activated during ITIs. When the dipper was activated and a reinforcer was available, a 2.9-kHz tone, the head-entry LED, and the house light were turned on. The reinforcer remained available until it was obtained by the mouse, which deactivated the 2.9-kHz tone, the LED, and house light. The dipper remains activated for 2.5s after the mouse obtains the reinforcer. Following 5 sessions of reinforcement training, the procedure was modified for 5 autoshaping sessions which, in the last 8s of each ITI, the LED inside of the nose-poke device was turned on. The nose-poke LED was then turned off and reinforcement was delivered as described. If the mouse nose-poked the device during the time when the LED

was on, it was turned off and reinforcement was delivered immediately. The autoshaping procedure was then modified for another 5 sessions such that reinforcement delivery was contingent upon a single nose-poke to the nose-poke device when its LED was illuminated and the ITI was reduced to 10s.

Fixed-Minimum Interval Training. Mice were then trained on the fixed-minimum interval (FMI) schedule. After the 3-min warmup period, the houselight was deactivated. A nose-poke (initiating response) activated the nose-poke LED and marked the beginning of the inter-response time (IRT). A subsequent head entry into the reward receptacle (terminating response) terminated the IRT. Reinforcement was delivered only if the IRT was longer than the criterion time, which was dependent upon the FMI schedule. IRTs shorter than the criterion time terminated without reinforcement, deactivated the nose-poke LED, and another trial could be immediately initiated. IRTs greater than or equal to the criterion time resulted in delivery of reward, deactivation of the nose-poke LED, a 2.5s duration 2.9kHz tone, and subsequent removal of the liquid dipper. Houselights were then activated for a 10s ITI, after which houselight deactivation indicated a new trial could be initiated via nose-poke. The time between the end of the ITI and the nose-poke initiating response was measured and termed the latency to initiate (LTI). All mice were initially trained on an FMI schedule with a criterion time of 0.5s (FMI 0.5s) until stability was achieved. The FMI 0.5s condition was implemented to acclimate mice to the task and is not used to evaluate response inhibition capacity. Performance was considered stable when a non-significant linear regression for mean median IRTs across 5 consecutive sessions was achieved, using a significance criterion of .05. Following stability on the FMI 0.5s schedule, subjects experience FMI 2s, 4s, and 8s. Each subject was trained to stability.

Data Analysis. Four parameters were tracked on a session-by-session basis: median latency-to-initiate trials (LTI), median inter-response time (IRT), the coefficient of quartile variation (CQV) of IRTs (difference between 1st and 3rd quartile divided by their sum), and the number of obtained reinforcers (ORs). The acquisition phase of each parameter was defined as the mean performance during the first five sessions of each schedule, while the asymptote was defined as the mean during the last five sessions. ANOVAs were conducted to assess statistical significance of time and genotype on FMI schedule and Student's t-tests were conducted to examine parameter differences based on genotype.

Results

Differential expression of ERK/MAPK components in CINs

The ERK/MAPK cascade is a commonly utilized intracellular signaling pathway that is dynamically activated during embryogenesis and in adulthood. In the embryonic ventricular zone, neural progenitors typically show high levels of P-ERK1/2 relative to immature post-mitotic neurons (Pucilowska et al., 2018; Stanco et al., 2014). In adult cortices, elevated P-ERK1/2 labeling is enriched in a heterogeneous set of excitatory PNs, primarily in layer 2, and plays a critical role in long-range PN development (Cancedda et al., 2003; Gauthier et al., 2007; Holter et al., 2019; Pham et al., 2004; Pucilowska et al., 2012; Suzuki et al., 2004; Xing et al., 2016). The activation of ERK1/2 in CINs has not been well characterized. We generated mice expressing *Slc32A1:Cre* and the Cre-dependent red fluorescent protein (RFP) reporter, *Ai9* (Madisen et al., 2010; Vong et al., 2011) (Figure1A-D). As expected, brain regions abundant with GABA-expressing neurons robustly expressed *Ai9* (Figure 1A). Immunolabeling for MAP2K1 (MEK1) revealed relatively lower expression in CINs in comparison to $NEUN^{+}/RFP^{-}$ presumptive PNs (Figure 1E-G). Layer II/III CINs also expressed low levels of MAPK1/ERK2 in comparison to PNs (Figure 1H-J). In agreement with previous studies, high levels of P-ERK1/2 were observed in a subset of PNs in cortical layer II/III (Cancedda et al., 2003; Pham et al., 2004; Suzuki et al., 2004). However, examination of P-ERK1/2 immunolabeling in RFP^{+} CINs revealed qualitatively lower levels of P-ERK1/2 in comparison to PNs (Figure 1K-M). In summary, CINs express relatively lower levels of MEK1, ERK2, and P-ERK1/2 than excitatory neurons in the adult cortex, raising the possibility of functionally distinct roles for this cascade between cortical neuron subtypes.

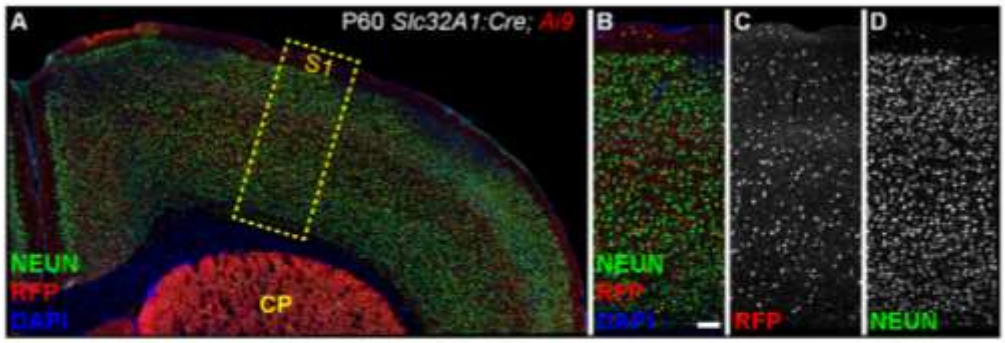

Slc32A1:Cre; Ai9 S1 Layer II/III

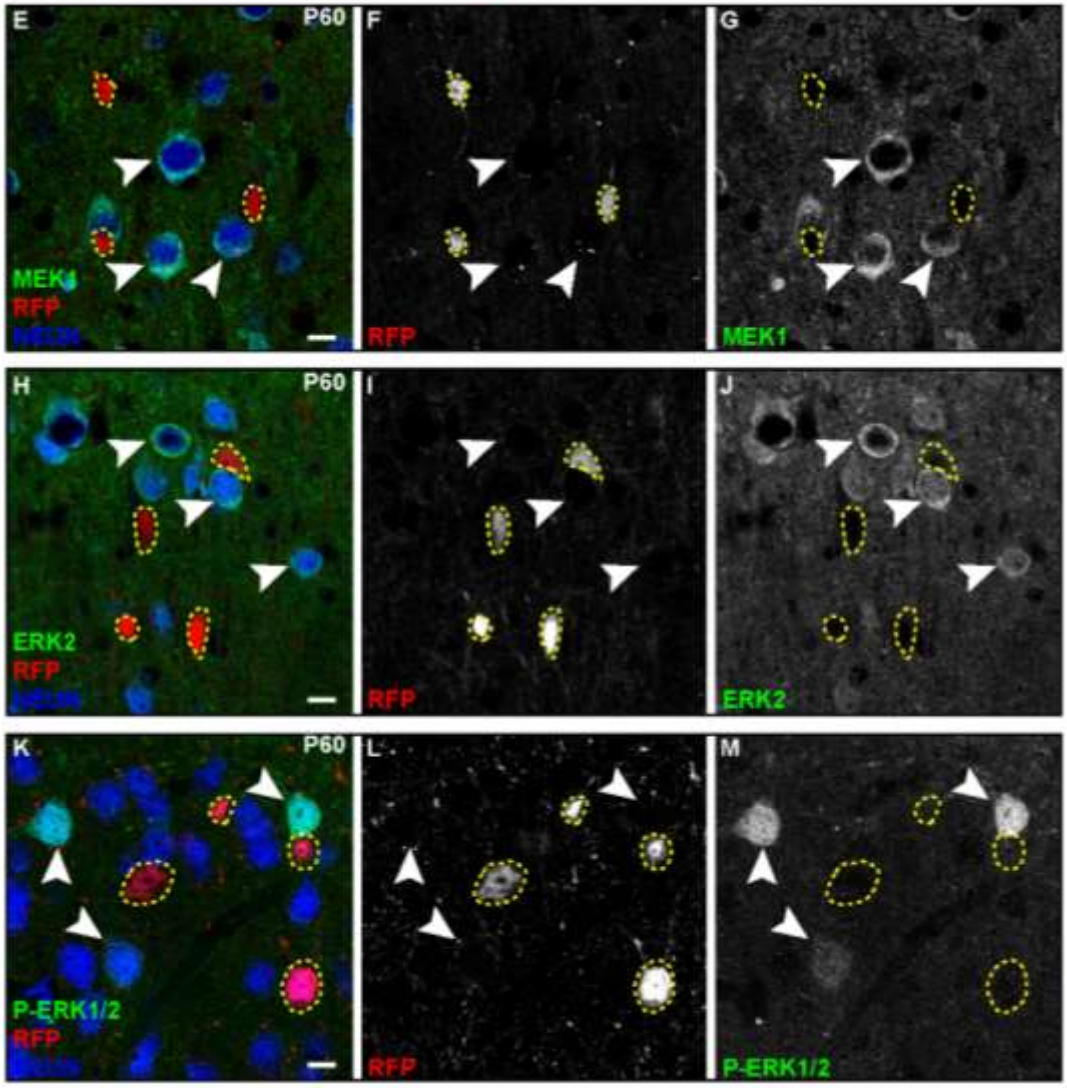

Figure 1. **CINs exhibit low levels of ERK/MAPK expression and activity.** (**A-D**) Representative confocal images of Slc32A1:Cre, Ai9 sensorimotor cortex. Note the robust expression of RFP in brain regions with high densities of GABAergic neurons. (Scale bar = 100 µm) (**E-M**) Immunolabeling for MEK1 (**E-G**) and ERK2 (**H-J**) showed comparatively low expression in inhibitory CINs (yellow outlines) when compared to NEUN+/Ai9- excitatory neurons (arrowheads) in layer II (n=3). Relatively lower expression of P-ERK1/2 was also detected in inhibitory CINs when compared to excitatory neurons (n=3). (Scale bar = 10 µm).

GABAergic-autonomous caMEK1 expression decreases PV-CIN number

Increased ERK/MAPK signaling is the most common result of RASopathy-linked mutations (Tidyman and Rauen, 2016). We utilized a Cre-dependent, constitutively active *CAG-Loxp-Stop-Loxp-Mek1*$^{S217/221E}$ (*caMek1*) allele, which has been shown to hyperactivate MEK1/2-ERK1/2 signaling (Alessi et al., 1994; Bueno et al., 2000; Cowley et al., 1994; Klesse et al., 1999; Krenz et al., 2008; Lajiness et al., 2014; Li et al., 2012b). We generated *caMek1*, *Slc32A1:Cre* mice to hyperactivate MEK1 in a CIN-specific fashion during embryogenesis. Elevated MEK1 expression was clearly detectable in the E13.5 mantle zone of the ganglionic eminences, presumptive embryonic CINs migrating into the cortex, and adult CINs in primary somatosensory cortex (S1) (Figure S1A-H; J-O). *CaMek1*, *Slc32A1:Cre* mice were viable and phenotypically normal, though mutants exhibited larger body mass than controls in adulthood (Figure S1I).

Surprisingly, assessment of fluorescently-labeled CINs in *caMek1*, *Slc32A1:Cre*, *Ai9* sensory cortices revealed a significant reduction in total RFP$^+$ cell density (Figure 2A-I). In the adult cortex, approximately 40% of CINs express PV whereas 30% express SST, which serve as mostly non-overlapping markers of two distinct populations of CINs (Kelsom and Lu, 2013; Kessaris et al., 2014; Rudy et al., 2011). Strikingly, we observed a

significant reduction in the proportion of PV^+/RFP^+ CINs, but not in the proportion of SST^+/RFP^+ CINs (Figure 2K-Q). PV, but not SST, expressing CINs displayed a significant increase in somal area compared to control neurons (Figure 2R-U, V). A reduced density of PV-CINs was detected in a separate *caMek1, Dlx5/6:Cre* strain that also targets postmitotic CINs in the developing cortex (Figure S2A-D) (Monory et al., 2006).

Recombination within the entire GABAergic system left open the possibility that indirect changes in other neuroanatomical regions could alter global cortical activity and modulate PV-CIN number (Denaxa et al., 2018). To restrict Cre expression to primarily MGE-derived CINs, we generated *caMek1, Nkx2.1:Cre, Ai9* mice and assessed the proportion of PV^+/RFP^+ CINs. *CaMek1, Nkx2.1:Cre* mice exhibited generalized growth delay in the second-third postnatal week and were not viable past the first postnatal month (n=8). Nonetheless, consistent with our previous findings, P14 *caMek1, Nkx2.1:Cre, Ai9* mice displayed a reduction in PV^+/RFP^+-CIN density (Figure S2E-L, M). In summary, our data indicate that the establishment of PV-CIN number is cell-autonomously vulnerable to enhanced MEK1 signaling, while SST-CIN number is not altered.

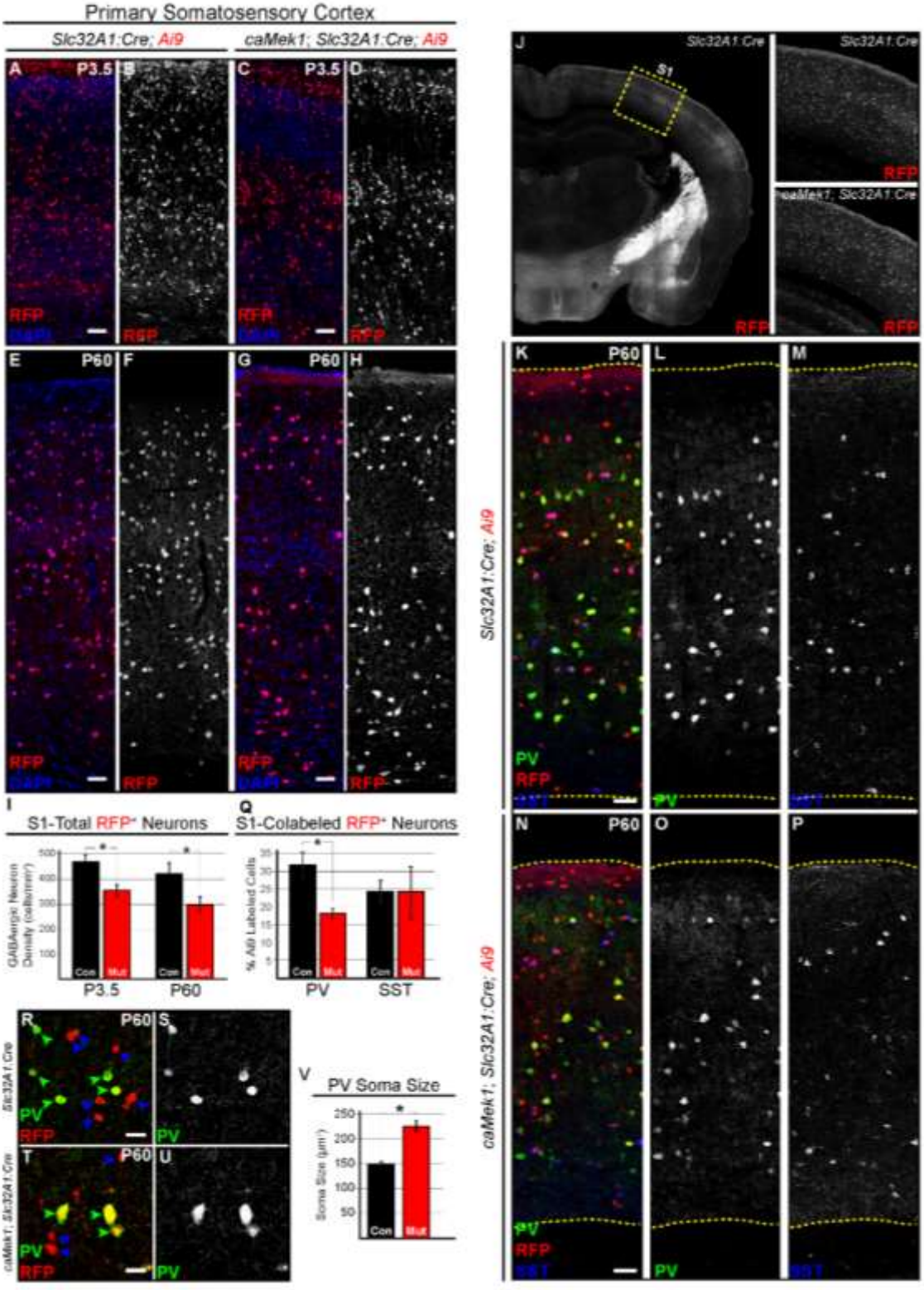
Primary Somatosensory Cortex
Slc32A1:Cre; Ai9
caMek1; Slc32A1:Cre; Ai9
A
P3.5
B
C
P3.5
D
RFP
DAPI
E
P60
F
G
P60
H
I
S1-Total RFP+ Neurons
GABAergic Neuron Density (cells/mm²)
Con
Mut
P3.5
P60
Q
S1-Colabeled RFP+ Neurons
% Ab Labeled Cells
PV
SST
J
S1
Slc32A1:Cre
caMek1; Slc32A1:Cre
K
L
M
N
O
P
PV
R
S
T
U
V
PV Soma Size
Soma Size (μm²)
Slc32A1:Cre; Ai9
caMek1; Slc32A1:Cre; Ai9

Figure 2. **MEK1 hyperactivation leads to a selective reduction in PV-expressing CINs in the postnatal cortex.** (**A-H**) caMek1, Slc32A1:Cre, Ai9 mutant P3.5 (**A-D**) and P60 (**E-H**) primary somatosensory cortices exhibit reduced numbers of Ai9-expressing CINs in comparison to Slc32A1:Cre, Ai9 controls (quantification in **I**, n=3, mean ± SEM, * = $p < 0.05$). (Scale bar = 100 μm) (**J-Q**) We quantified the proportion of fluorescently co-labeled PV/RFP or SST/RFP co-expressing CINs in the sensory cortex (**J**). Confocal micrographs of RFP-expressing CINs at P60 demonstrates that the proportion of PV+/RFP+ CINs, but not SST+/RFP+ CINs, was significantly decreased in mutants (**N-P**) in comparison to controls (**K-M**) (quantification in **Q**: n=3, mean ± SEM, * = $p < 0.05$). (Scale bar = 100 μm) (**R-V**) Mutant PV-CINs (**T-U**, green arrowheads in **T**) display increased soma size in comparison to control PV-CINs (**R-S**) (quantification in **V**, n = 21 control neurons, 42 mutant neurons, mean ± SEM, * = $p < 0.001$). PV-/RFP+ CINs displayed no qualitative change in soma size (blue arrowheads). (Scale bar = 25 μm).

Presumptive mutant PV-CINs in the embryonic subpallium undergo apoptosis

Our analyses of RFP^+ CINs in P3.5 *caMek1, Slc32A1:Cre* mice yielded a significant reduction in CIN density, thus, we hypothesized that gain-of-function MEK1 signaling disrupted embryonic processes necessary to establish CIN number. Indeed, examination of RFP^+ CIN density in the E17.5 cortical plate also revealed fewer CINs in *caMek1, Slc32A1:Cre* embryos (Figure S3A-D). We examined markers of neuronal death during mid-neurogenesis in the *caMek1, Slc32A1:Cre, Ai9* subpallium. Immunolabeling for the apoptotic marker cleaved caspase 3 (CC3) revealed colocalization of CC3 with some RFP^+ neurons within the mantle zone of the ganglionic eminences in E13.5 mutant, but not control, embryos (Figure 3A-E, F). $CC3^+/RFP^+$ neurons also presented with condensed, pyknotic nuclei (Figure 3G-N). We also observed $CC3^+/RFP^+$ cells with pyknotic nuclei in *caMek1, Nkx2.1:Cre, Ai9* mantle zone (Figure 3O-Q). No apoptotic cells were observed in the mutant ganglionic eminence VZ or the cortical migratory streams.

Analysis of recombined GABAergic neuron density in the dorsal striatum did not reveal a significant difference from controls, suggesting that the loss of PV-CINs is not due to altered CIN migratory trajectory. Together, our results suggest reduced PV-CIN density in the postnatal cortex is due to the death of a subset of migrating CINs in the ganglionic eminence.

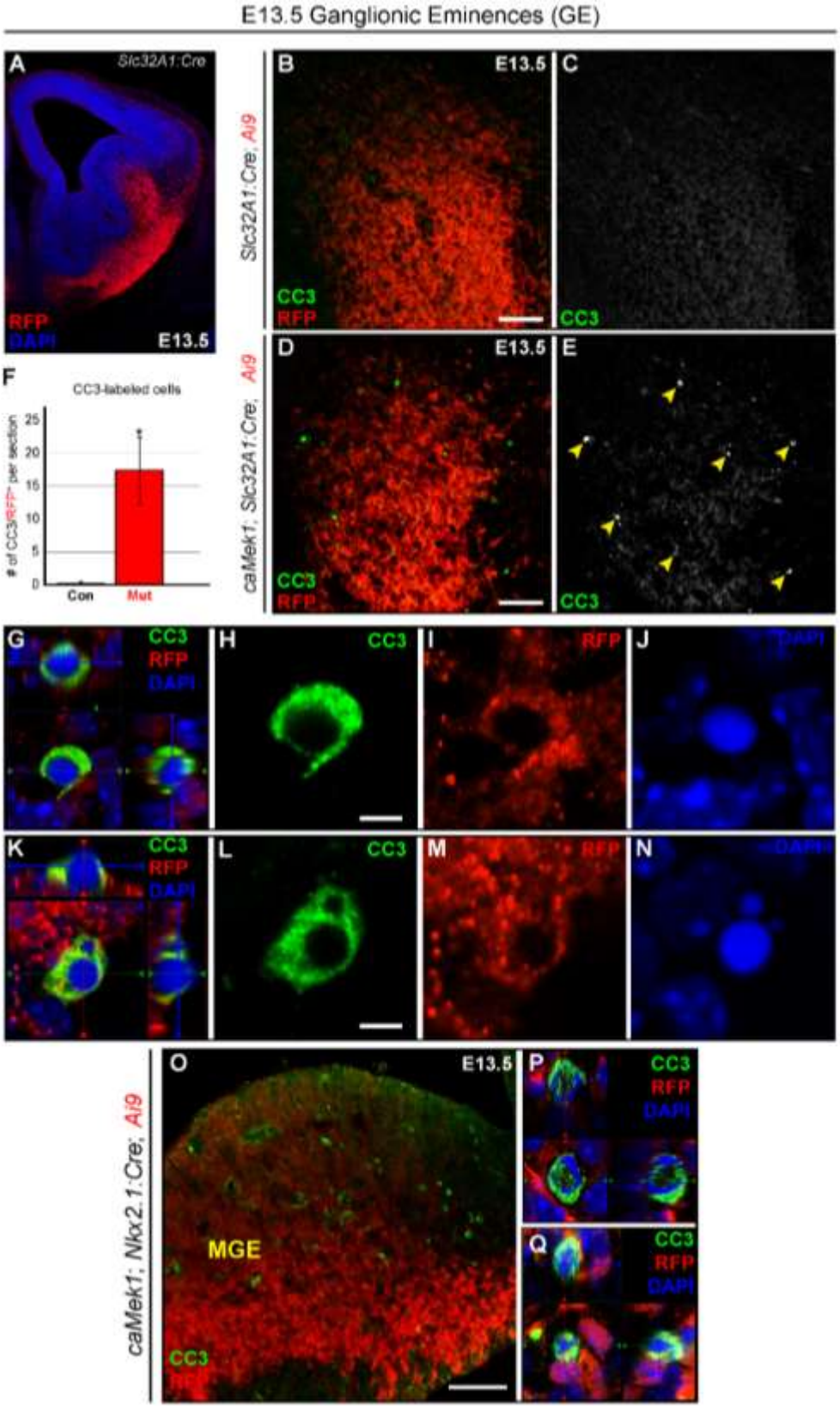
E13.5 Ganglionic Eminences (GE)
A
Slc32A1:Cre
RFP
DAPI
E13.5
B
E13.5
CC3
RFP
C
CC3
Slc32A1:Cre; Ai9
D
E13.5
CC3
RFP
E
CC3
caMek1; Slc32A1:Cre; Ai9
F
CC3-labeled cells
# of CC3/RFP+ per section
25
20
15
10
5
0
Con
Mut
G
CC3
RFP
DAPI
H
CC3
I
RFP
J
DAPI
K
CC3
RFP
DAPI
L
CC3
M
RFP
N
DAPI
O
E13.5
MGE
CC3
P
CC3
RFP
DAPI
Q
CC3
RFP
DAPI
caMek1; Nkx2.1:Cre; Ai9

Figure 3. **A subset of immature GABAergic neurons undergo cell death during mid-embryogenesis**. (**A**) E13.5 coronal section of RFP-labeled CINs in the mantle zones of the Slc32A1:Cre subpallium during mid-embryogenesis. (**B-F**) Immunolabeling for cleaved caspase 3 (CC3) showed a significant increase in the number of apoptotic profiles in caMek1, Slc32A1:Cre mutants (**D-E**) as compared to controls (**B-C**) (quantification in **F**; n=3, mean ± SEM, * = $p < 0.05$). (Scale bar = 100 µm) (**G-Q**) Representative confocal z-stacks of CC3 labeled cells from caMek1, Slc32A1:Cre embryos (**G-N**, Scale bar = 2 µm) and caMek1, Nkx2.1:Cre embryos (**O-Q**) show clear colocalization with RFP and a condensed, pyknotic nuclear morphology.

GABAergic-specific caMek1 promotes cortical hyperexcitability but does not significantly alter fast-spiking CIN electrophysiological properties

Nearly 40% of RASopathy individuals with mutations downstream of *RAS* experience seizures and epilepsy (Digilio et al., 2011; Rauen et al., 2013; Yoon et al., 2007). Whether MEK1 hyperactivation in GABAergic circuits mediates seizure activity in the RASopathies is unclear. We did not detect any signs of overt generalized tonic-clonic seizures in mutant mice while housed in home cages. We conducted a series of behavioral tests by first using the open field, then the elevated plus maze, and finally the social approach assay. No difference in global locomotor activity, anxiety-like behavior, or sociability could be detected with these tests (Figure S4). However, during the initial 60 sec of open field testing with 13 adult *caMek1, Slc32A1:Cre* mutants, two mutant mice exhibited increased head twitching, aberrant locomotor activity, and increased rearing. Three mutant mice displayed periods of overt sudden behavioral arrest and motionless staring. These behaviors were not observed in any of the control mice utilized in this study. Consistent with these subtle impairments, subsequent re-analysis of the first 10 sec of the

open field task revealed a significant reduction in distance traveled in *caMek1, Slc32A1:Cre* mutants, which was also observed in *caMek1, Dlx5/6:Cre* mutants.

We performed intracortical EEG recordings to directly assess cortical activity, which revealed spontaneous epileptiform-like discharges in three of six *caMek1, Slc32A1:Cre* adult mice, but not control mice (Figure 4A). These six mutants also exhibited a significantly reduced average threshold to seizure induction in response to pentylenetetrazol (PTZ) administration when compared to controls (Figure 4B). Seizures have been shown to increase the local expression of glial fibrillary acidic protein (GFAP) in astrocytes (STEWARD et al., 1992; Stringer, 1996). 3 of 3 newly generated and untreated *caMek1 Slc32A1:Cre* mice immunolabeled for GFAP exhibited clusters of GFAP-expressing astrocytes in the cortex consistent with local reactive astrogliosis near hyperexcitable regions (Figure 4C-F). Overall, some of the seizure-related phenotypes we observed were not completely penetrant, thus, these data indicate that MEK1 hyperactivation in CINs may be a potential risk factor for epilepsy in the RASopathies.

PV-CINs provide a powerful source of inhibition in the cortex, firing action potentials at frequencies greater than 200Hz (Okaty et al., 2009). Fast-spiking (FS) physiology is due in part to the unique expression of the fast-inactivating potassium channel Kv3.1, which begins in the second postnatal week (Goldberg et al., 2011; Rosato-Siri et al., 2015; Rudy and McBain, 2001). To determine if hyperactive MEK1 signaling was sufficient to alter basic physiological properties of FS CINs, we performed whole-cell patch clamp recordings on *caMek1, Nkx2.1:Cre* mice at the end of the third postnatal week. Current clamp recordings of fluorescently-labeled CINs revealed that both control and mutant neurons retained their distinctive electrophysiological fast-spiking phenotype

(Figure 4G, I) (Agmon & Connors, 2018; Anderson et al., 2010; McCormick et al., 1985). No significant differences were observed in resting membrane potential, adaptation index, rheobase, or action potential threshold, but a small increase in action potential amplitude was observed (Figure 4I). We did also detect a significant increase in FS CIN input resistance and a reduction in FI slope in *caMek1*, *Nkx2.1:Cre* mutant compared with *Nkx2.1:Cre* controls suggesting that mutants may have a reduction in the responsiveness and/or firing output of inhibitory neurons (Figure 4H-I). Overall, these data indicate that canonical electrophysiological features of fast-spiking CIN development were not altered by MEK1 hyperactivation. However, certain intrinsic properties exhibit subtle differences in mutant mice that might contribute to circuit-wide hyperexcitability.

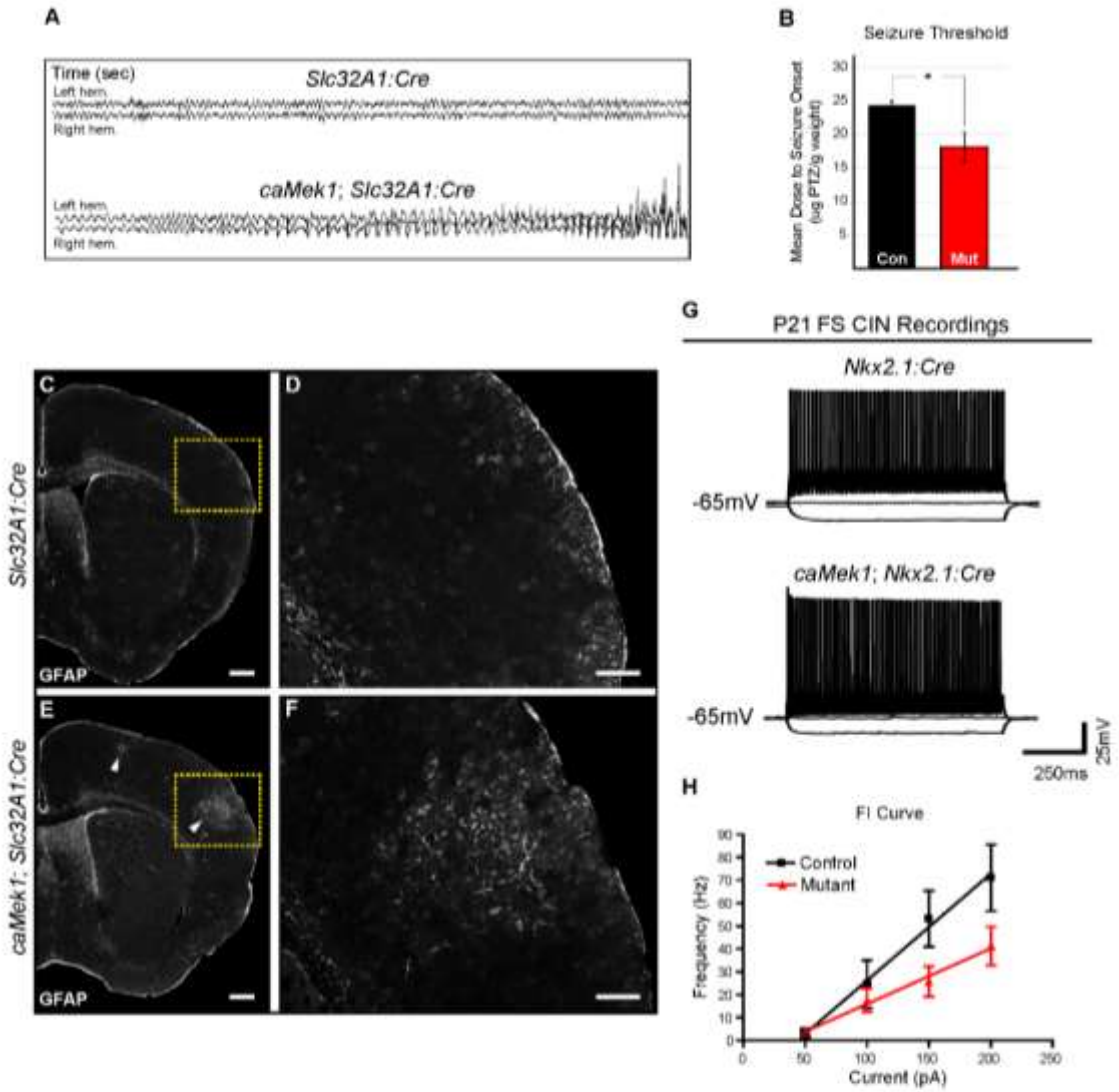

I

Parameter	Control (mean ± SEM)	Mutant (mean ± SEM)	p-value
Resting Membrane Potential (mV)	-67.08 ± 1.090	-66.78 ± 1.245	0.86
Input Resistance (MΩ)	203.3 ± 24.55	296.7 ± 33.47	0.03
FI Slope (Aps/pA)	0.570 ± 0.158	0.165 ± 0.050	0.03
Adaptation Index	0.959 ± 0.147	0.796 ± 0.072	0.39
Rheobase (pA)	117.9 ± 18.96	80.00 ± 13.79	0.14
Action Potential Threshold (mV)	22.33 ± 1.469	22.00 ± 1.106	0.87
Action Potential Amplitude (mV)	65.17 ± 2.229	74.33 ± 2.386	0.01

Figure 4. **CaMek1 CINs maintain typical fast-spiking properties, but a subset of mice exhibit seizure-like phenotypes.** (**A**) Representative traces from forebrain-penetrating EEG revealed epochs of synchronous firing in 3 of 6 *caMek1 Slc32A1:Cre*, but not control mice. (**B**) Tail vein PTZ injections revealed a significant reduction in mean dose to seizure onset of PTZ (n = 6, mean ± SEM, * = $p < 0.001$). (**C-F**) *caMek1 Slc32A1:Cre* cortices display aberrant clusters of GFAP-labeled astrocytes (**E**, arrowheads, insets in **F**) that were not observed in controls (**C-D**) (n=3). (Scale bar = 100 μm) (**G**) Representative current clamp recordings of FS CINs in P21 Nkx2.1:Cre Ai9 and *caMek1 Nkx2.1:Cre Ai9* mutant cortices. (**H**) Mutant CINs had a significantly reduced FI slope in comparison to controls (mean ± SEM, $p < 0.05$). (**K**) Summary table of FS CIN intrinsic properties.

Inhibitory synapse formation and perineuronal net accumulation are altered by MEK1 hyperactivity

PV-expressing CINs preferentially innervate pyramidal cells, often forming synapses on the perisomatic domain (Chattopadhyaya et al., 2004; Chattopadhyaya et al., 2007). We assessed whether perisomatic VGAT-labeled synapses surrounding layer 2/3 PNs were diminished in adult *caMek1, Slc32A1:Cre, Ai3* mice. We found the extent of VGAT-immunolabeling in the perisomatic space of $NEUN^{+}/GFP^{-}$ PN soma was significantly reduced in mutant cortices when compared to controls (Fig. 5A-F, M). Interestingly, the area of VGAT-labeling in the surrounding neuropil, typically innervated by SST-CINs, was unchanged (Fig. S5A-F). These data show that PV-CIN inhibitory output is selectively vulnerable to caMEK1 signaling while SST-CINs are less affected.

PV-CINs selectively accumulate an extracellular structure called the perineuronal net (PNN) derived primarily from glial chondroitin sulfate proteoglycans (CSPGs). PNNs are essential to cortical development, restricting plasticity during the closure of critical periods and protecting PV-CINs from oxidative stress associated with a high frequency firing rate (Cabungcal et al., 2013; Hensch, 2005b). Reductions in PNN formation have been noted in multiple models of neurodevelopmental disorders that exhibit loss of PV-

CINs (Bitanihirwe and Woo, 2014; Cabungcal et al., 2013; Krencik et al., 2015; Krishnan et al., 2015; Steullet et al., 2017). We utilized WFA-labeling to test whether PNN formation was reduced in adult *caMek1*, *Slc32A1:Cre, Ai3* mice (Figure 5H-M). Surprisingly, we found that surviving PV-CINs were WFA^+ in mutants (Figure 5G-L). PNNs were also not detected on *Ai3*-expressing neurons that lacked PV-expression. Consistent with the larger somal size of mutant PV-CINs, the cross-sectional area of WFA-labeled profiles was also significantly increased (Figure 5G-L, N). Analysis of the quantitative level of WFA-labeling in mutant PV-CINs revealed a robust increase in PNN accumulation as compared to controls (Figure 5G-L, O). Mutant WFA-labeled CINs exhibited normal expression of 8-oxo-2'-deoxyguanosine (8-oxo-dg), a marker of DNA oxidation often altered in neurons with reduced PNNs (Figure S5 F-I) (Steullet et al., 2017). Collectively, MEK1 hyperactivation clearly increases PNN accumulation, but does not trigger ectopic PNN formation on GABAergic neurons lacking PV.

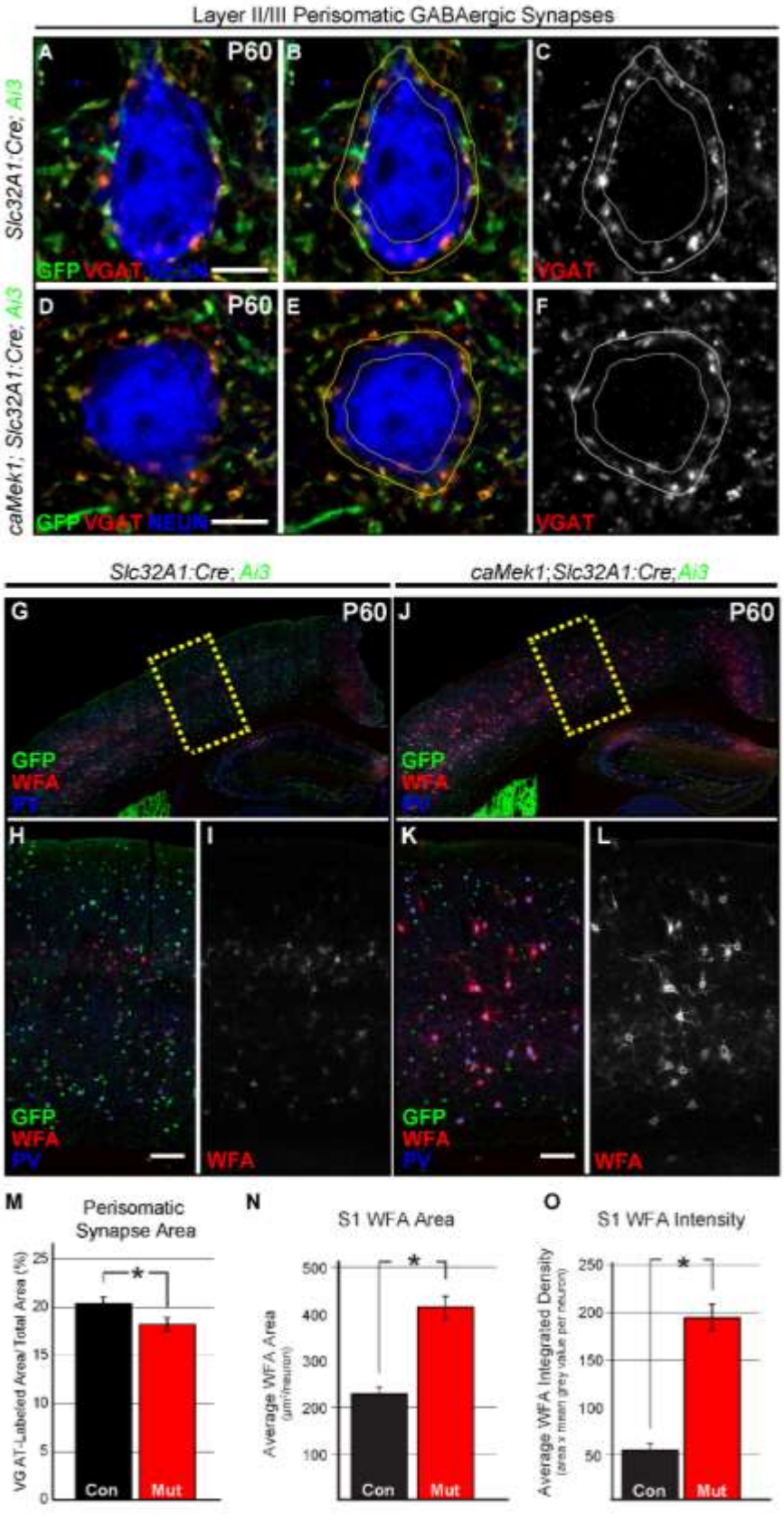
Layer II/III Perisomatic GABAergic Synapses
Slc32A1:Cre; Ai3
caMek1; Slc32A1:Cre; Ai3
A
P60
B
C
GFP VGAT NEUN
VGAT
D
P60
E
F
GFP VGAT NEUN
VGAT
Slc32A1:Cre; Ai3
caMek1;Slc32A1:Cre;Ai3
G
P60
J
P60
GFP
WFA
PV
H
I
K
L
GFP
WFA
PV
WFA
M
Perisomatic Synapse Area
VGAT-Labeled Area/Total Area (%)
Con
Mut
N
S1 WFA Area
Average WFA Area (μm²/neuron)
Con
Mut
O
S1 WFA Intensity
Average WFA Integrated Density (area x mean grey value per neuron)
Con
Mut

Figure 5. **Reduced perisomatic synapse labeling in mutant cortices coincide with a substantial increase in PNN formation on PV-CINs.** (**A-F**) Representative high-resolution confocal Airyscan images of triple immunolabeled cortical sections for Ai3/EYFP, VGAT, and NEUN. Excitatory neuron perisomatic domains were outlined and quantification of VGAT-labeled pixels revealed that mutants (**D-F**) have a significant reduction in the amount of perisomatic VGAT-labeling (Scale bar = 3 μm) in comparison to controls (**A-C**) (quantification in **M**; n = 48 control, 53 mutant neurons; mean ± SEM, * = $p < 0.05$). (**G-L**) P60 representative coronal sections of *Slc32A1:Cre Ai3* (**G-I**) and *caMek1 Slc32A1:Cre Ai3* (**J-L**) cortices immunolabeled for GFP, WFA, and PV. The WFA channel was imaged using the same acquisition settings for all samples. A significant increase in WFA-labeled area per neuron was detected in mutant cortices when compared to controls (quantification in **N**; n = 63 control, 54 mutant neurons, mean ± SEM, * = $p < 0.001$). Analysis of WFA-labeling intensity yielded a significant increase in integrated density in mutant CINs (quantification in **O**; n = 63 control, 54 mutant neurons, mean ± SEM, * = $p < 0.001$). (Scale bar = 100 μm).

caMek1, Slc32A1:Cre mice display delayed acquisition of FMI performance

Attention deficit hyperactivity disorder (ADHD) is associated with a significant proportion of RASopathy cases (Adviento et al., 2014; Garg et al., 2013; Green et al., 2017; Pierpont et al., 2018; Walsh et al., 2013). Altered prefrontal cortex (PFC) function has been implicated in ADHD (Gabay et al., 2018), and has been shown to contribute to cognitive deficits in a mouse model of Fragile X Syndrome (Krueger et al., 2011). Few studies have examined GABAergic contributions to PFC function in the context of RASopathies. As in sensory cortex, we noted a reduction in *Ai9*-expressing CINs in the PFC of mutant mice (Figure 6A-B, D-E). Interestingly, we found that PNs in the PFC exhibit reduced P-ERK1/2 expression in *caMek1, Slc32A1:Cre* mice (Figure 6A-F). These data indicate that MEK1 hyperactivation in developing CINs is sufficient to drive molecular abnormalities within specific cortical regions important for cognition.

Individuals with ADHD often exhibit structural changes in the PFC, which appear to be involved in the inhibition of reinforced responses (Seidman et al., 2006). To examine

response inhibition directly, we utilized a fixed minimum interval (FMI) test, a timing-based task that requires animals to withhold a response for a fixed period. This paradigm is perhaps more favorable than the five-choice serial reaction time task (5-CSRTT) and differential reinforcement of low rates task (DRL), because its self-paced design dissociates response inhibition capacity from motivational aspects of behavior (Bizarro et al., 2003; Doughty and Richards, 2002; Hill et al., 2012; Watterson et al., 2015). Here, adult control and *caMek1, Slc32A1:Cre* mice were trained to initiate trials via a nose-poke which resulted in the presentation of sweetened condensed milk in the reward receptacle. Mice were then placed on an FMI schedule, where a time delay between the initiating nose-poke and the availability of reinforcement in the reward receptacle was implemented (Figure 6G). Reward was delivered only if the time between the initiating nose-poke and attempt to obtain reward (inter-response time, or IRT) exceeded a pre-determined withholding period. If mice prematurely accessed the reward receptacle, no reward was delivered.

Following initial training on a FMI with a very short (0.5s) response-withholding period, we measured mouse performance when the withholding period was extended to 2s, 4s, and finally, 8s. We observed a main effect of FMI schedule irrespective of genotype, such that IRTs increased as the FMI withholding period increased ($F(2, 62) = 535.12$, $p < 0.01$). Importantly, mutants showed clear evidence of impaired acquisition of the FMI task. We found a main effect of genotype on the mean median IRT during the first 5 days of each FMI schedule (acquisition period), in which mutant mice had relatively lower IRTs compared to control mice ($F(1, 62) = 18.73$, $p < 0.01$) (Figure 6H). In further support of reduced response inhibition capacity, mutant mice exhibited increased variability in their

IRTs as measured by the coefficient of quartile variation (CQV) during acquisition ($F(1, 62) = 31.73$, $p < 0.01$) and asymptotic performance (defined as the last five days of the FMI) ($F(2, 62) = 5.055$, $p < 0.001$) across all schedules (Figure 6I). Median IRTs during the asymptotic phase in mutants and controls were not statistically different in any schedule (Figure 6H inset). Thus, these data suggest that mutant mice are capable of learning to inhibit reinforced responses for up to 4 s but show a significant delay in acquiring this capability.

Due to *Slc32A1:Cre*-mediated recombination within subcortical circuitry, it is possible that altered reward pathway activity influenced FMI performance. The latency to initiate (LTI) a trial provides a measure of motivation; for example, rats administered amphetamine show a reduction in LTI in a related task (Rojas-Leguizamón et al., 2018). However, we noted that mutants did not differ from controls in the median LTI at 2s and 4s, indicating that motivation to obtain rewards was not significantly altered between conditions (Tukey's b post-hoc test - 2s: $t(21) = 1.39$, $p=0.18$; 4s: $t(21) = -0.29$, $p=0.77$) (Figure 6J). We found that during the 8s FMI, mutant mice exhibited a statistically significant increase in LTI ($t(20) = 2.43$, $p < 0.05$). This apparent loss of motivation is likely due to the fact that the mean median asymptotic IRT did not reach the 8s criterion even after 32 days of testing (control: 8.45s ± 1.04; mutant: 7.26s ± 1.09) and is also consistent with the statistically significant reduction in mean obtained reinforcers at the 8s FMI (Figure 6K). Collectively, our data indicate that altered GABAergic circuitry regulates acquisition of response inhibition capacity in mice and may contribute to ADHD phenotypes associated with the RASopathies.

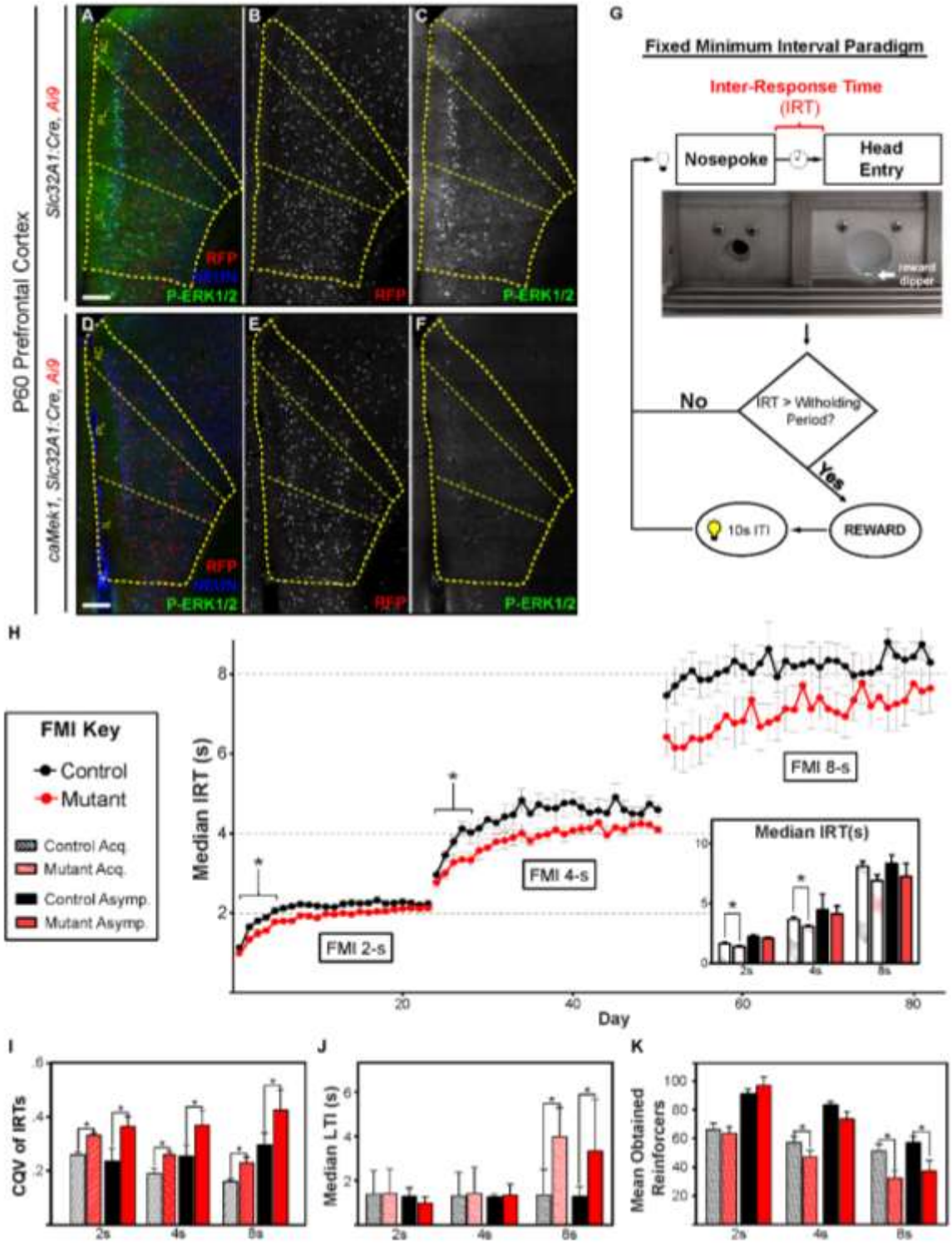
P60 Prefrontal Cortex
Slc32A1:Cre, A/9
caMek1, Slc32A1:Cre, A/9
A
B
C
D
E
F
RFP
NEUN
P-ERK1/2
G
Fixed Minimum Interval Paradigm
Inter-Response Time
(IRT)
Nosepoke
Head Entry
reward dipper
No
IRT > Witholding Period?
Yes
10s ITI
REWARD
H
FMI Key
Control
Mutant
Control Acq.
Mutant Acq.
Control Asymp.
Mutant Asymp.
Median IRT (s)
FMI 2-s
FMI 4-s
FMI 8-s
Median IRT(s)
Day
I
CQV of IRTs
J
Median LTI (s)
K
Mean Obtained Reinforcers
2s
4s
8s

Figure 6. ***caMek1 Slc32A1:Cre*** **mice exhibit reduced behavioral response inhibition capacity.** (**A-F**). P-ERK1/2 labeling in PFC PNs is significantly reduced in mutants as compared to controls. Note the decrease in RFP+ CINs in the mutant PFC (**E**) relative to control (**B**) (n=3). (Scale bar = 100 μm) (**G**) Schematic of the Fixed-minimum Interval (FMI) task. (**H**) Mutant mice had a significant reduction in mean median IRT during FMI acquisition in 2s and 4s schedules (n=12, mean ± SEM, * = $p < 0.05$). (**I**) Mutant mean CQV of IRTs during both acquisition and asymptotic phases was significantly increased in 2s, 4s, and 8s FMI schedules (mean ± SEM, * = $p < 0.05$). (**J**) Median acquisition and asymptotic LTI was significantly increased in the FMI 8s, but not in the 2s and 4s schedules (mean ± SEM, * = $p < 0.05$). (**K**) Mutant mice had a reduction in mean acquisition ORs at 4s and a significant reduction in both mean acquisition and asymptotic ORs during the 8s FMI (mean ± SEM, * = $p < 0.05$).

Discussion

Here, we show that GABAergic neuron-autonomous MEK1 hyperactivation causes the death of a subset of immature GABAergic neurons in the embryonic subpallium and is associated with a selective reduction in PV-CIN density, but not SST-CINs, in adulthood. We observed a significant reduction in perisomatic GABAergic synapses on layer 2/3 PNs and forebrain hyperexcitability, but a surprising increase in the extent of PNN accumulation in mutant PV-CINs. While mutants displayed relatively normal performance in assays of locomotion, sociability, and anxiety, we found notable defects in acquisition of behavioral response inhibition capacity, which has been linked to ADHD. These data suggest that GABAergic neuron-autonomous MEK1 hyperactivation selectively regulates embryonic PV-CIN survival and is an important contributor to seizure risk and cognitive deficits in the RASopathies.

While expression of ERK/MAPK pathway components is widespread, our findings reinforce the notion that expression levels are variable, and activation of this cascade is highly cell-type dependent. Cell-specific transcriptomic experiments have reported that RNA levels of *Mapk1*/*Erk2* and *Map2k1/Mek1*, but not *Mapk3/Erk1* or *Map2k2/Mek2*, are lower in CINs relative to PNs (Mardinly et al., 2016). We have extended these findings to show that protein levels of MAPK1/ERK2 and MAP2K1/MEK1 are typically lower in CINs than in surrounding PNs. Reduced expression of pan-ERK/MAPK components may contribute to the relatively low levels of phosphorylated ERK1/2 in CINs. Past work has shown that the experience-dependent transcriptional response in V1 PV-CINs is significantly smaller relative to PNs (Hrvatin et al., 2018). A more stringent degree of ERK/MAPK recruitment in CINs might contribute to reduced activity-dependent

transcription. Further analysis of activity-dependent responses in ERK/MAPK-mutant mice may assist in defining how CIN-specific functional properties are encoded (Tyssowski et al., 2018).

Defects in GABAergic circuitry have been implicated in the pathogenesis of Rett, Fragile X, schizophrenia and many other neurodevelopmental diseases (Chao et al., 2010; Cui et al., 2008; Steullet et al., 2017). Reduced PV-CIN number is often observed, however, the mechanism of loss is poorly understood. We show that MEK1 hyperactivation drives the GABAergic-neuron autonomous activation of caspase-3 and death of a subset of immature neurons in the embryonic ganglionic eminences. The selective reduction in PV-CIN density in the postnatal cortex suggests these early dying neurons were committed to the PV lineage. The death of this specific subset of GABAergic neurons occurs much earlier than the typical period of programmed cell death for CINs (Denaxa et al., 2018; Southwell et al., 2012) . Notably, *caMek1* expression in cortical excitatory neurons is not associated with significant neuronal loss during development (Nateri et al., 2007; Xing et al., 2016). Though ERK/MAPK typically acts as a promoter of cell survival, apoptotic death by sustained ERK/MAPK activity has been described in certain contexts (Cagnol and Chambard, 2010; Martin and Pognonec, 2010). It will be important to evaluate whether treatment with pharmacological MEK1/2 inhibitors or antioxidants during embryogenesis is capable of sustained restoration of CIN number in *caMek1*, *Slc32A1:Cre* mice. PV-CIN sensitivity to MEK1 hyperactivation may not only be an important factor in RASopathy neuropathology, but could be a relevant mechanism in other conditions that involve indirect activation of ERK/MAPK signaling during

embryogenesis, such as schizophrenia, Fragile X Syndrome, or prenatal stress (Fowke et al., 2018).

Recent scRNAseq analyses suggest the mature transcriptional signature of cardinal CIN subtypes is not fully specified until CINs migrate into the cortex (Mayer et al., 2018; Paul et al., 2017; Sandberg et al., 2018). MEF2C, a known substrate of ERK1/2 and p38 signaling, was identified as a transcription factor expressed early in the presumptive PV lineage, the deletion of which also leads to the selective reduction of PV-CINs (Mayer et al., 2018). Thus, regulation of MEF2C could mediate early effects of caMEK1 signaling on GABAergic neuron development. While further research is necessary, the selective vulnerability of presumptive PV-CINs to hyperactive MEK1 signaling may not be dependent upon a specific downstream transcriptional target. Compared to transcriptional networks, less is known regarding the function of many post-translational modifications during CIN specification. Our data hint at selective roles for kinase signaling networks at an early stage of CIN lineage differentiation.

Despite the effect of caMEK1 on early GABAergic neuron survival, the physiological maturation of mature *caMek1*-expressing PV-CINs was not significantly impeded. Surviving PV-CINs retained a characteristic fast-spiking signature with only minor differences in intrinsic electrophysiological parameters. We noted a modest, but statistically significant decrease in perisomatic inhibitory synapse number on cortical PNs in mutant mice. As might be expected, a subset of mutant animals exhibited forebrain hyperexcitability and sudden behavioral arrest similar to that reported in animal models of mild seizures. Overexpression of a similar *caMek1* mutation with *CamKII:Cre* has also been shown to cause seizure-like activity (Nateri et al., 2007). Overall, our findings indicate

that MEK1 hyperactivation in GABAergic neurons could increase the risk of epilepsy seen in RASopathies.

The PNN is a critically important structure involved in the maturation of cortical circuitry with an important role in protecting PV-CINs from oxidative stress and limiting synaptic plasticity (Cabungcal et al., 2013; Hensch, 2005a; Hensch, 2005b; Morishita et al., 2015). Mouse models of schizophrenia, Fragile X, and ASDs often exhibit reduced PV-CIN number and typically display a reduction in PNN formation (Steullet et al., 2017). In contrast to these disorders, PNNs appear to respond differently to RASopathy mutations. PV-CINs accumulate extracellular PNNs derived primarily from astrocyte-produced CSPGs (Galtrey and Fawcett, 2007; Sorg et al., 2016). RASopathic astrocytes upregulate secreted ECM-associated CSPGs and promote an increase in the extent of PNN accumulation around PV-CINs (Krencik et al., 2015). Our data is the first to indicate a PV-CIN autonomous role for enhanced PNN accumulation in response to MEK1 hyperactivation. It is thought that increased PNN accumulation on PV-CINs limits the plasticity of cortical regions (Pizzorusso et al., 2002). Modification of PNN levels may serve as a useful therapeutic strategy for the impaired cognitive function and intellectual disability frequently reported in RASopathy individuals (Tidyman and Rauen, 2016).

In addition to intellectual disability, ADHD is frequently diagnosed in Noonan Syndrome and NF1, two common RASopathies (Johnson et al., 2019; Miguel et al., 2015; Pierpont et al., 2015). Abnormal PFC function has been linked to ADHD (Seidman et al., 2006). Interestingly, we detected significantly reduced P-ERK1/2 levels in PFC PNs of mutant mice, suggesting that RASopathic CINs may alter the global development and function of this brain region. GABAergic signaling is known to be necessary for cortical

circuit maturation (Cancedda et al., 2007). We further examined ADHD-related behavioral phenotypes in *caMek1, Slc32A1:Cre* mice by assessing behavioral response inhibition capacity with a fixed-minimum interval (FMI) based task (Rojas-Leguizamón et al., 2018; Watterson et al., 2015). We detected significant deficits in the acquisition of response inhibition dependent behaviors in mutant mice relative to controls. It is plausible that FMI defects in caMEK1 mutants is due to the reduced plasticity of PFC GABAergic circuitry in response to heightened levels of PNN or GABAergic-dependent changes in PN development. These data show that GABAergic-directed MEK1 hyperactivation is sufficient to drive deficits in behavioral response inhibition possibly associated with ADHD.

Mutations in 'upstream' RASopathy genes modulate a much broader set of downstream cascades when compared to mutations in *Raf* or *Mek1/2*. *Nf1*, *Ptpn11/Shp2*, and *Syngap1* mutations result in a complex constellation of cellular changes, some of which depend upon ERK/MAPK modulation, whereas others involve different signaling cascades (Anastasaki and Gutmann, 2014; Brown et al., 2012). In combination with the findings of (Angara et al., 2019, co-submitted), it is clear that PV-CIN development is particularly sensitive to convergent signaling via NF1 and ERK/MAPK. Additional studies of human samples will be necessary to determine whether defective GABAergic circuits are a component of RASopathy pathogenesis. Collectively, our research suggests that hyperactivation of MEK1 in GABAergic neurons represents an important candidate mechanism for epilepsy and cognitive defects in RASopathic individuals.

Acknowledgements

We would like to thank Johan Martinez, Sam Lusk, Julia Pringle, Anna Kreuger, Sarah Sparks, Katie Riordan, Danielle Gonzalez, Elise Bouchal, and Kimberly Holter for their technical contributions to this work. All immunohistochemical experiments were conducted by Michael C. Holter in the laboratory of Jason Newbern. Electrophysiological experiments were performed under the guidance and expertise of Trent Anderson and were performed by Guohui Li. Fixed Minimum Interval testing was conducted in the laboratory of Federico Sanabria by Tanya Gupta and Kenji Nishimura. All figures were prepped for presentation by Michael C. Holter. This research is supported by National Institute of Health grants R00NS076661 and R01NS097537 awarded to JMN, R01NS087031 awarded to TRA, and R01NS031768 to WDS.

Supplemental Figures

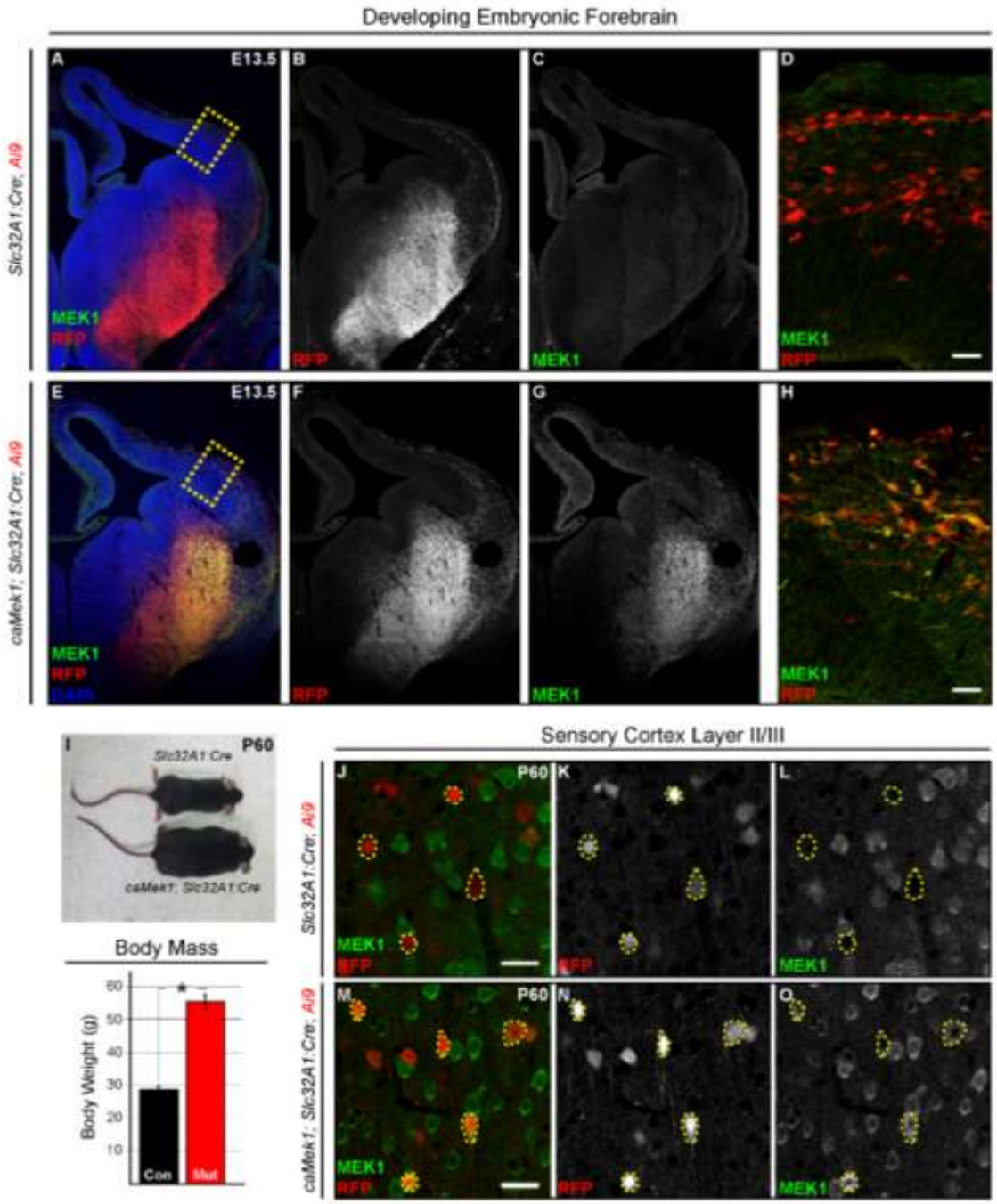

Figure S1. **Increased MEK1 expression in embryonic and postnatal mutant brains** (**A-H**) Representative coronal sections of E13.5 developing mouse forebrain immunolabeled for MEK1. High expression of MEK1 was detected in RFP-labeled cells in *caMek1 Slc32A1:Cre* ganglionic eminences and CIN migratory streams (compare **C** to **G**; **D** to **H**). (**I**) *CaMek1 Slc32A1:Cre* mice exhibited significantly increased body mass in adulthood as compared to controls (n = 12 controls, 12 mutants; mean ± SEM, * = $p < 0.05$). (**J-O**) Mutant CINs display increased MEK1 expression into adulthood (n=3). (Scale bar = 25 µm).

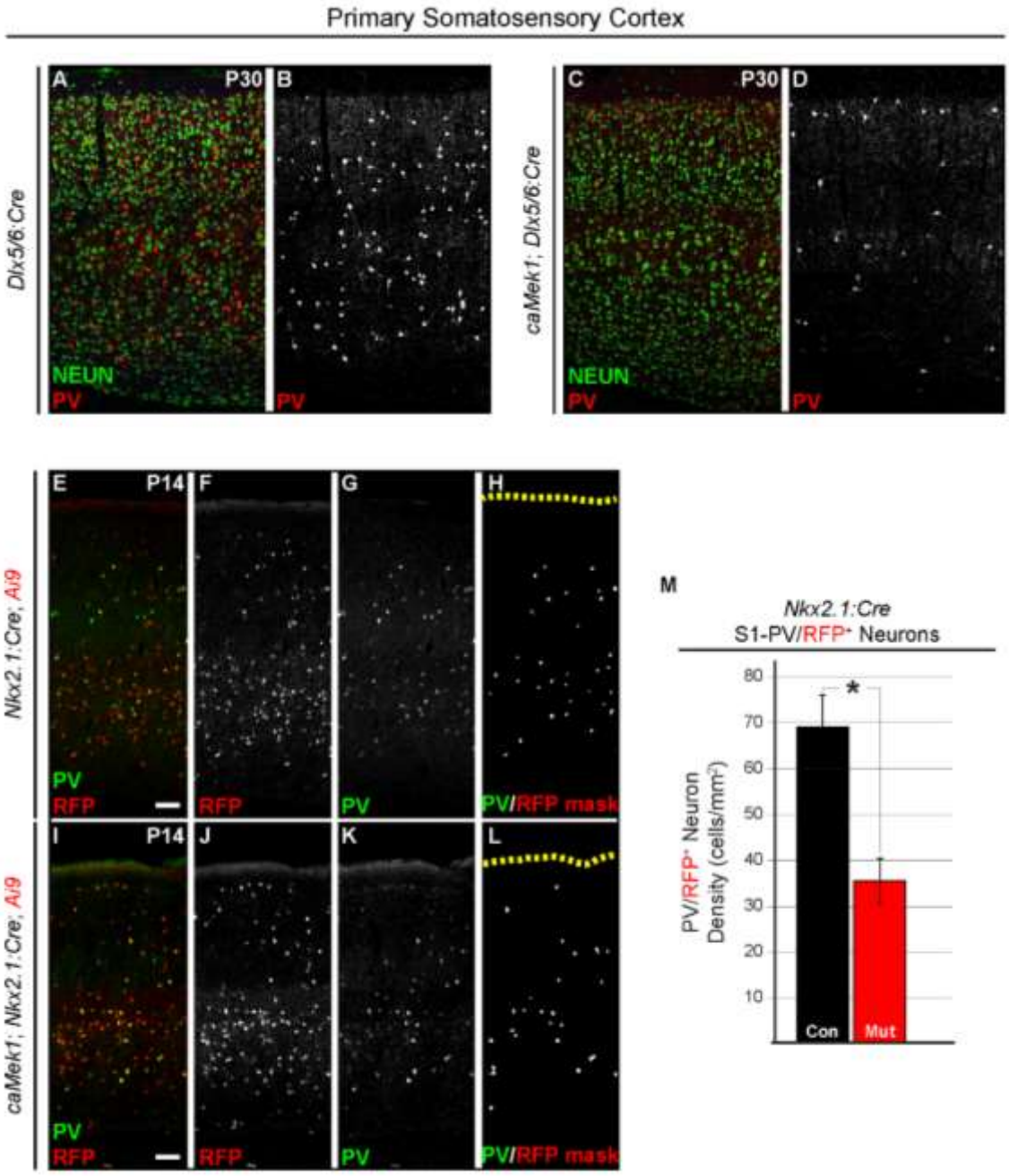

Figure S2. **Reduced PV-CINs in *caMek1, Dlx5/6:Cre* and *caMek1, Nkx2.1:Cre* brains.** (**A-D**) P30 coronal sections of *caMek1 Dlx5/6:Cre* primary sensory cortex revealed a substantial qualitative decrease in the number of PV-CINs relative to controls (n=3). (**E-M**) Representative confocal images of P14 *caMek1 Nkx2.1:Cre* sensory cortices immunolabeled for PV. The number of PV+/RFP+ co-expressing cells was significantly decreased in mutants as compared to littermate controls (quantification in **M**: n = 3; mean ± SEM, * = $p < 0.05$).

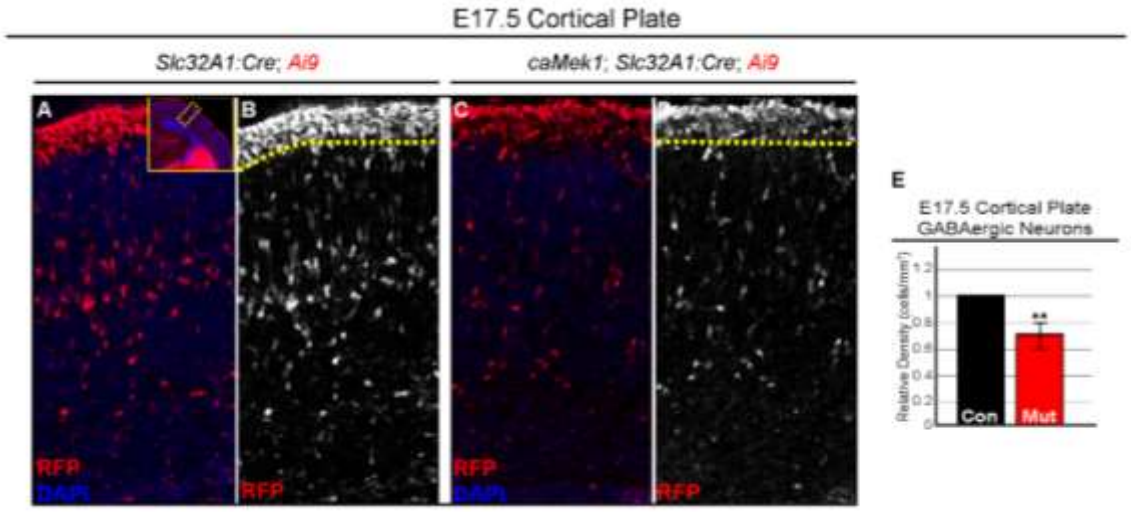

Figure S3. **Loss of CINs in late embryogenesis** (**A-D**) Representative confocal micrographs of the E17.5 developing cortical plate. A significant decrease in the number of RFP+ CINs was detected in *caMek1 Slc32A1:Cre* embryos (quantification in **E**: n = 3; mean ± SEM, * = $p < 0.05$).

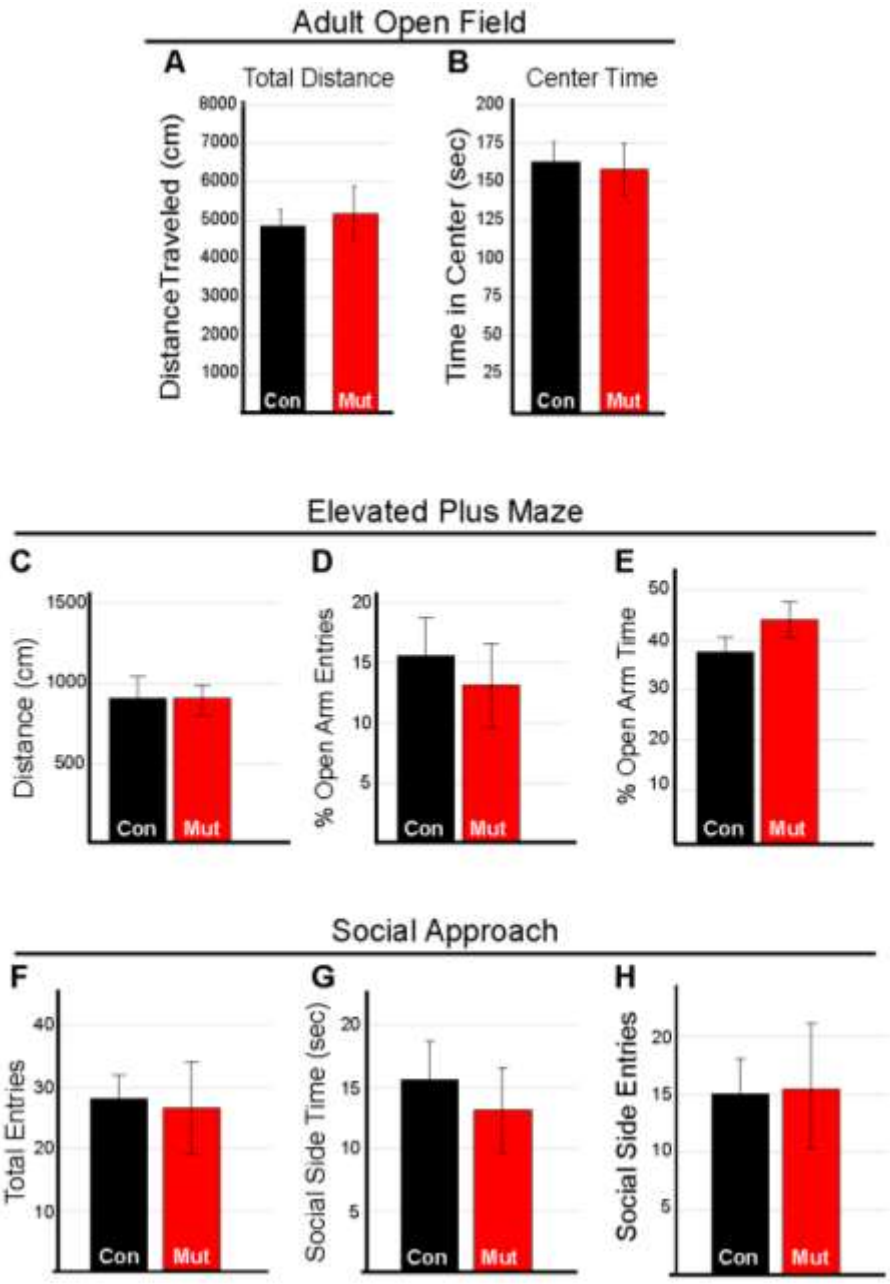

Figure S4. **Mutant mice exhibit normal locomotor and anxiety-like behaviors** (**A-B**) *CaMek1 Slc32A1:Cre* mice (n = 25 control, 13 mutant) were assessed for locomotor, anxiety-like behaviors, and sociability in the open field task. No significant differences in distance traveled or center time were observed throughout 10 min of open field testing. (**C-E**) Elevated plus maze testing did not detect a significant difference in % open arm entries or % time spent in open arms. (**F-H**) In the social approach assay mutants did not significantly differ from controls in total entries, time spent in the social side, or social side entries.

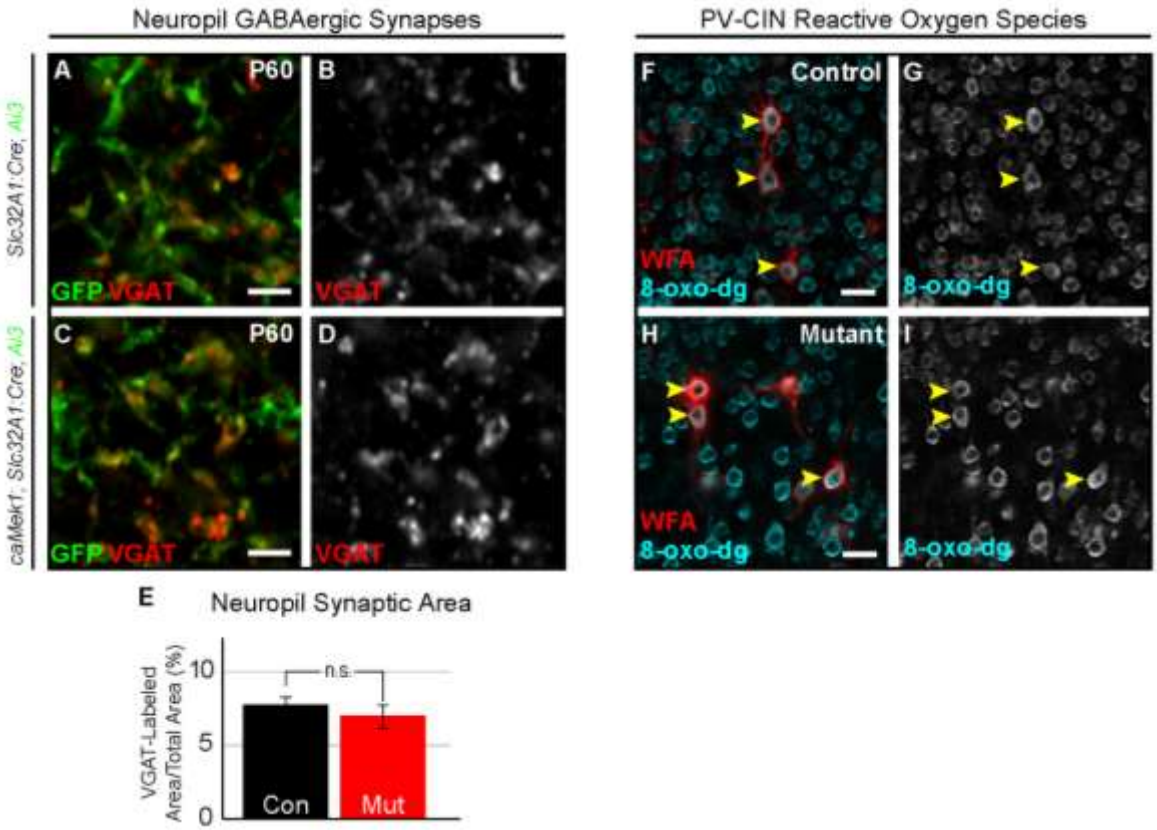

Figure S5. **Normal GABAergic synaptic area in cortical neuropil and PV-CIN oxidative stress** (**A-E**) Mutant mice exhibited normal VGAT-labeling in the layer 2/3 neuropil (quantification in **E**; n = 33 control, 30 mutant regions, mean ± SEM). (**F-I**) Expression of the DNA oxidation marker 8-oxo-dg expression in WFA+ *caMek1 Slc32A1:Cre* CINs was qualitatively unchanged when compared to control WFA+ CINs (control in **F-G**, mutant in **H-I**). (Scale bar = 25 μm).

CHAPTER 4

ERK1/2 is required for the normal specification and maturation of somatostatin-expressing interneurons

Authors: Michael C. Holter[1], Sara J. Knowles[1], George R. Bjorklund[1], Kenji J. Nishimura[1,#], Johan S. Martinez[1], and Jason M. Newbern[1]

Affiliations:

[1]School of Life Sciences, [2]Department of Psychology, Arizona State University; Tempe, AZ 85287, USA

[#]Present Address: Interdepartmental Neuroscience Graduate Program, University of Texas; Austin, TX, 78712, USA

Abstract

Aberrant ERK/MAPK pathway activity is commonly observed in a family of neurodevelopmental syndromes called the "RASopathies." Though many mutations in upstream regulators of RAS signaling and the core kinases of the ERK/MAPK pathway result in increased activity of the principal ERK1/2 proteins, some mutations may also reduce cascade activity. In addition, disorders such as 16p11.2 microdeletion syndrome and distal 22q11 microdeletion may also result in reduced ERK/MAPK activity. Cortical GABAergic interneurons (CINs) are an important, heterogeneous subgroup of neurons necessary for excitatory/inhibitory balance in the brain and processes such as learning and memory. The basic functions of ERK1/2 in CIN development and function have not been well studied. Here, we show that the initial establishment of CIN number does not require ERK1/2. No differences in the number parvalbumin-expressing (PV) CIN number were detected; however, we observed a striking reduction in the density of somatostatin-expressing (SST) CINs by P14. Reduced SST-expression persisted into adulthood, suggesting SST-CINs require ERK1/2 for their specification. In addition, we have developed a unique CIN-specific chemogenetic tool to modulate GABAergic circuit activity. Our results suggest a CIN subtype-specific requirement for ERK1/2 during development and may inform future therapeutic studies aiming to repair defective GABAergic circuitry.

Introduction

The canonical ERK/MAPK cascade is a ubiquitously utilized intracellular kinase pathway that is dynamically expressed during brain development. Mutations within the ERK/MAPK cascade, typically resulting in increased pathway activity, drive the pathogenesis of a family of neurodevelopmental syndromes collectively termed the "RASopathies" (Rauen et al., 2013). However, copy number variants of core kinases in the ERK/MAPK cascade can reduce pathway activity. Loss of ERK/MAPK activity has been observed in 16p11.2 microdeletion syndrome, which accounts for 1% of all ASD cases, a locus of 11 genes that includes *MAPK3/ERK1* (Pucilowska et al., 2012; Pucilowska et al., 2008; Pucilowska et al., 2018; Pucilowska et al., 2015; Vithayathil et al., 2018). Distal 22q11 microdeletion, a chromosomal abnormality often associated with DiGeorge Syndrome, results in copy number variants of *MAPK1/ERK2* (Newbern et al., 2008; Saitta et al., 2004; Samuels et al., 2009). Recently, loss-of-function mutations within *MAP2K2/MEK2* was implicated in rare cases of the RASopathies (Nowaczyk et al., 2014). Collectively, individuals with these disorders experience neurological symptoms including intellectual disability, developmental delay, autistic behaviors, and epilepsy (Rauen et al., 2013). A holistic understanding of how alterations in ERK/MAPK signaling during brain development give rise to neurological dysfunction will be important in future therapeutic design.

The normal development and maturation of the cerebral cortex broadly requires ERK1/2 signaling. However, the complexity of neural circuit composition poses challenges in understanding the basic functions of ERK/MAPK signaling in cortical development, and importantly, how aberrant ERK/MAPK activity results in neurological dysfunction. In

particular, differential expression of ERK/MAPK pathway components in cortical cell types suggests that individual groups of cells may be more susceptible to specific mutations than others. Indeed, pallial cell types such as radial glia, glutamatergic projection neurons (PNs), and astrocytes differentially express regulators of RAS activity such as *Syngap1* and *Nf1*, and RAS downstream kinases *Map2k1* and *Erk2* (Loo et al., 2019; Mardinly et al., 2016). Dysfunctional PN circuits appear to be the primary driver of neurological dysfunction in *Syngap1* mutant mice, whereas neurological phenotypes in *Nf1* mutants appear to be mediated primarily by abnormal GABAergic circuits (Cui et al., 2008; Ozkan et al., 2014). Thus, specific disease-causing gene mutations in regulators and canonical kinases of the ERK/MAPK pathway differentially affect unique cortical cell populations.

Furthermore, it is unclear how downstream intracellular kinase cascades mediate the development individual cell types and how changes in their activity drive neuropathogenesis. During pallial development, loss of ERK1/2 from radial glia leads to the complete lack of gliogenesis and cortical thinning, which can be rescued by re-expression of the Ets family transcription factor, Erm (Li et al., 2012b; Pucilowska et al., 2008; Pucilowska et al., 2015). Long-range PNs populating layer 5 of the cortex require ERK1/2 for sustained survival, though layer 2/3 neurons are minimally affected (Xing et al., 2016). While the roles of ERK1/2 have been well studied in pallial cell types, it is currently unclear how cortical cell populations originating in the subpallium are affected by loss of ERK1/2.

Cortical GABAergic interneurons (CINs) comprise 20% of all cortical neurons and provide the inhibitory balance to excitation (Wonders and Anderson, 2006). CINs are functionally diverse and exhibit differential gene expression, morphological

characteristics, patterns of connectivity, and electrophysiological signatures (DeFelipe et al., 2013; Fino et al., 2013; Rudy et al., 2011). In particular, parvalbumin (PV) and somatostatin (SST) -expressing CINs constitute the most populous subtypes. PV- and SST-CINs originate in spatiotemporal fashion primarily from the medial ganglionic eminence (MGE) and migrate tangentially to the cortical plate (Rudy et al., 2011). Tangential migration requires extensive chemotaxic regulation, and recruits ERK/MAPK-independent kinase pathways (Flames et al., 2004; Marin, 2013; Marin and Rubenstein, 2001; Polleux et al., 2002; Stanco et al., 2009). Once in the cortical plate, neuregulin-3 signaling mediates the transition to radial migration and is subsequently important for laminar allocation of CINs (Bartolini et al., 2017). Despite a significant transcriptomic basis for CIN identity (Lim et al., 2018; Mi et al., 2018), recent evidence suggests differential activation of intracellular signaling cascades may be essential for certain aspects of CIN development (McKenzie et al., 2019). Interestingly, Ryk-dependent Wnt signaling controls the balance between PV- and SST-CIN generation in the MGE (McKenzie et al., 2019). Furthermore, abnormal receptor tyrosine kinase (RTK) signaling disrupts GABAergic interneuron maturation in the postnatal cortex (Fazzari et al., 2010). Hyperactive MEK1 downstream of RTKs in the developing subpallium disrupts early postmitotic PV-CIN maturation and drives the death of a subset of these cells (Holter et al., 2019; unpublished). The basic roles of principal ERK1/2 isoforms in CIN development have not been explored.

Here we examined the functions of ERK1/2 signaling in CIN development. We show that ERK1/2 is dispensable for the initial establishment of CIN number. Interestingly, we observed a significant reduction in the expression of SST in the postnatal cortex, but normal densities of PV-expressing CINs. Consistent with these observations, we found

qualitatively normal perineuronal net (PNN) accumulation, a major extracellular matrix (ECM) structure necessary for the functional maturation of PV-CINs and cortical circuits. Adult mutant mice exhibited a significant reduction in total distance travelled in the Open Field task. Additionally, we observed a global reduction in the cortical projection neuron (PN) expression of the activity-dependent gene, Arc. To determine whether major ERK1/2 related phenotypes could be rescued through ERK/MAPK independent means, we generated mice expressing an HM3Dq chemogenetic construct selectively in CINs to mimic glutamatergic input in inhibitory circuits in adulthood. Collectively, our results suggest a critically important role for ERK1/2 in the maturation of GABAergic circuits that may underlie some aspects of ERK/MAPK-linked neuropathology.

Materials and Methods

Mice

All mice were handled and housed in accordance with the guidelines of the Institutional Animal Care and Use Committee at Arizona State University. Mice were free to feed *ad libitum* and were housed under a daily 12-hour light-dark cycle. To generate ERK1/2 loss-of-function mutants, mice expressing *Slc32A1:Cre*$^{+/+}$, *Dlx5/6:Cre*$^{+/-}$, or *Nkx2.1:Cre*$^{+/-}$ to mice possessing a neo-insertion in exons 1-7 in the *Mapk3/Erk1* gene (herein referred to as *Mapk3/Erk1*$^{-/-}$). Transgenic mice were then bred with another strain containing a loxp flanked exon 2 in the *Mapk1/Erk2* gene (referred to as *Mapk1/Erk2*$^{fl/fl}$). Littermates expressing Cre-Recombinase containing one functional copy of *Mapk1/Erk2* in CINs were used as controls. Either a cre-dependent tdTomato (*Ai9*) or eYFP (*Ai3*) strain was used to visualize fluorescently-labeled cre-expressing cells. We extracted genomic DNA from tail or toe samples for genotyping by PCR. The primers used for genotyping were as follows: (listed 5'-3'): Cre – TTCGCAAGAACCTGATGGAC and CATTGCTGTCACTTGGTCGT to amplify a 266 bp fragment; *Mapk3/Erk1* – AAGGTTAACATCCGGTCCAGCA, AAGCAAGGCTAAGCCGTACC, and CATGCTCCAGACTGCCTTGG to amplify a 571 bp segment wild type and a 250 bp segment KO allele; *Mapk1/Erk2* – AGCCAACAATCCCAAACCTG, and GGCTGCAACCATCTCACAAT amplify 275 bp wild-type and 350 bp floxed alleles; *Ai3/Ai9* – four primers were used - AAGGGAGCTGCAGTGGAGTA, CCGAAAATCTGTGGGAAGTC, ACATGGTCCTGCTGGAGTTC, and GGCATTAAAGCAGCGTATCC amplify a 297 bp wt Rosa26 segment and a 212 bp

Ai3/*Ai9* allele; and *hM3Dq* – CGCCACCATGTACCCATAC and GTGGTACCGTCTGGAGAGGA to amplify a 204 bp fragment.

Tissue Preparation and Immunostaining

Mice of the specified age were anesthetized and perfused with cold 1X PBS followed by a 4% PFA in 1X PBS solution. Brains were then removed and post-fixed overnight at 4C. Brains were then sliced with a vibratome or were cryoprotected for preparation on a cryostat. Sectioned brain tissue was then incubated overnight at 4C in a primary antibody solution diluted in 0.05 – 0.2% Triton in 1X PBS with 5% Normal Donkey Serum (NDS). Primary antibodies were: rabbit anti-Somatostatin (Peninsula, 1:1000), Parvalbumin (Swant, 1:1000), rabbit anti-Arc (Synaptic Systems, 1:1000), chick anti-GFP (Aves, 1:1000), chick anti-RFP (Rockland, 1:1000), biotin-conjugated WFA (Vector, 60ug/mL), rabbit anti-Erk2 (Abcam, 1:1000), mouse anti-NeuN (Millipore, 1:1000), and anti-HA (Biolegend, 1:1000). Tissue incubated in primary solution was then washed three times 1X PBS 0.05% Triton and incubated in a solution containing Alexa-Fluor 488, 568, and 647 conjugated anti-rabbit, anti-goat, and anti-chick secondary antibodies. Secondaries were diluted to 1:1000 in 1X PBS 0.05 – 0.2% Triton and 5% NDS. A separate streptavidin-conjugated fluorophore was used specifically for WFA-labeled tissue. A Zeiss (LSM710 & LSM800) laser scanning confocal microscope was to collect representative images which were optimized for brightness and contrast in Adobe Photoshop and prepared for presentation purposes in Adobe Illustrator.

Image Analysis

Images from no fewer than three regions of interest per mouse were quantified for cell density by an observer blinded to genotype. In order to estimate cortical cell density, a cortical column was defined in Photoshop, the area was acquired, and labeled cells were quantified. For some experiments, cell densities were performed on endogenously-labeled cells by examination of the cre-dependent fluorescent protein. The mean cell density from three or more regions of interest was calculated for each mouse. A minimum of three mice were collected for each genotype and results were statistically analyzed by Student's t-test.

Results

Loss of ERK1/2 signaling does not alter CIN number

ERK/MAPK activity is necessary for the survival and physiological maturation of select dorsal-derived PNs (Li et al., 2012b; Xing et al., 2016), but it is unclear if ERK/MAPK regulates CIN number *in vivo*. We therefore generated quadruple transgenic mice with germline deletion of *Mapk3/Erk1* (*Erk1*$^{-/-}$), CKO of *Mapk1*/*Erk2* alleles (*Erk2*$^{fl/fl}$) and *Ai9* with *Slc32A1:Cre* expressing strain. *Erk1*$^{-/-}$, *Erk2*$^{fl/fl}$, *Ai9*, *Slc32A1:Cre* mice were obtained at normal Mendelian ratios, but exhibited profound growth delay by the end of the first postnatal week and lethality in the second to third postnatal week (n=10). No gross neuroanatomical abnormalities between mutant and control brains were observed in the first postnatal week (Figure 1A, B). ERK2 immunolabeling confirmed a reduction of ERK2 protein in mutant CINs in comparison to controls (Figure 1C-H). We then examined the relative density of RFP^{+} CINs in mutant cortices to controls. No significant difference in the relative density of CINs was observed between mutant and control cortices (Figure 1I-L, M). Similar results were obtained in the S1 of *Erk1*$^{-/-}$, *Erk2*$^{fl/fl}$, *Dlx5/6:Cre*, *Ai3* mice, which also restricts recombination to post-mitotic CINs in the ventral telencephalon (Supplemental Figure 1A-D). Early growth delay and lethality limited further assessment of GABAergic maturation and subtype specification in both *Erk1*$^{-/-}$, *Erk2*$^{fl/fl}$, *Dlx5/6:Cre* and *Slc32A1:Cre* brains. Nonetheless, these data suggest that ERK/MAPK signaling is dispensable for the initial establishment of CIN number.

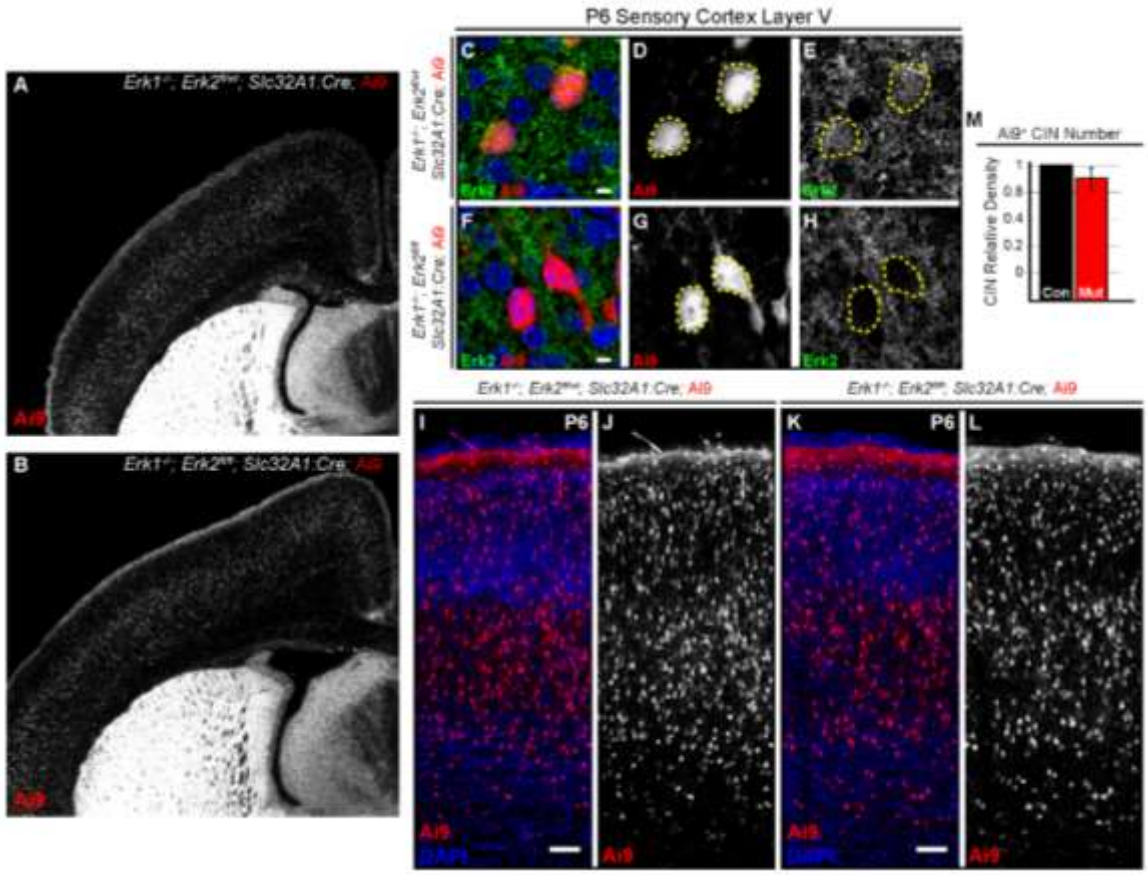

Figure 1. **Loss of ERK1/2 does not alter CIN number**. **(A-B)** Representative images of P6 coronal brain slices show no gross anatomical defects between *Erk1*$^{-/-}$, *Erk2*$^{fl/fl}$, *Slc32A1:Cre*, *Ai9* mutants and *Erk1*$^{-/-}$, *Erk2*$^{fl/wt}$, *Slc32A1:Cre*, *Ai9* controls. **(C-H)** Reduced ERK2 protein was observed in layer V *Ai9*-expressing CINs in mutant primary somatosensory cortices in comparison to controls. (Scale bar = 3 µm) **(I-L)** No difference in the density of *Ai9*-expressing CINs was observed between mutants and controls (quantification in **M;** n=3, mean ± SEM, $p > 0.05$). (Scale bar = 100 µm).

ERK1/2 is required for the specification of SST-expressing CINs but not PV-CINs

PV-CINs are sensitive to RASopathy-linked mutations (Holter et al., 2019 unpublished; Krenick et al., 2015). The onset of the expression PV occurs within the second postnatal week (del Río et al., 1994; Huang et al., 1999; Soriano et al., 1992). Neonatal death of *Erk1*$^{-/-}$, *Erk2*$^{fl/fl}$, *Ai9, Slc32A1:Cre* mice therefore barred further assessment of *Erk1/2* loss on maturing PV- and SST-CINs. To further assess subtype-specific effects of ERK1/2 CKO on CINs, we generated *Erk1*$^{-/-}$, *Erk2*$^{fl/fl}$, *Nkx2.1:Cre, Ai3* mice to restrict Cre-mediated recombination to forebrain cells derived from the MGE. Mutant mice were fully viable with mild growth abnormalities, and adult brains were normal in appearance with no apparent differences in size. Consistent with our findings from *Erk1*$^{-/-}$, *Erk2*$^{fl/fl}$, *Ai9, Slc32A1:Cre* mice, quantitative assessment of fluorescently-labeled CINs in *Erk1*$^{-/-}$, *Erk2*$^{fl/fl}$, *Nkx2.1:Cre, Ai3* P14 mutant sensory cortices revealed no change in EYFP-cell density as compared to *Erk1*$^{-/-}$, *Erk2*$^{fl/wt}$, *Nkx2.1:Cre, Ai3* controls (Figure 2A-H, Q). Immunolabeling for PV revealed no change in PV-CIN density (Figure 2C, G, R), however, we observed a significant reduction in the density of SST immunoreactive CINs at the end of the second postnatal week (Figure 2D, H, R). Furthermore, the density of EYFP-expressing cells was unchanged in the adult sensory cortex (Figure 2I-P, Q). Reduced SST-immunoreactivity persisted into the adult cortex (Figure 2L, P, Q). Taken together, loss of ERK1/2 signaling is sufficient to disrupt specific aspects of SST-CIN identity but does not appear to alter PV-CIN specification.

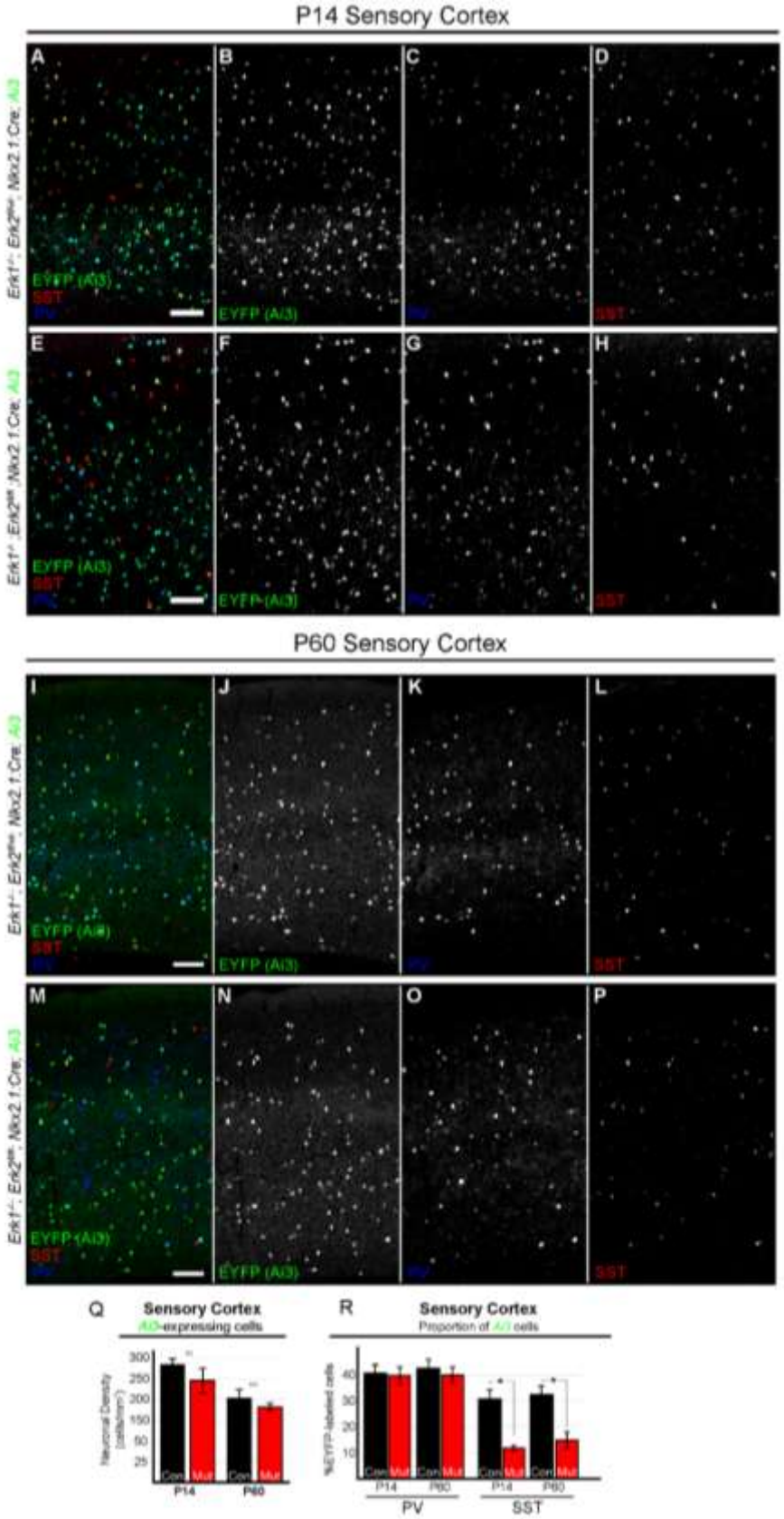
P14 Sensory Cortex
P60 Sensory Cortex
A
B
C
D
E
F
G
H
I
J
K
L
M
N
O
P
EYFP (Ai3)
SST
Q
Sensory Cortex
Ai3-expressing cells
R
Sensory Cortex
Proportion of Ai3 cells
Con
Mut
P14
P60
PV
SST

Figure 2. SST-CINs are selectively vulnerable to reduced ERK1/2 signaling. (**A-H**) Representative confocal images of P14 *Erk1*$^{-/-}$, *Erk2*$^{fl/wt}$, *Nkx2.1:Cre*, *Ai3* and *Erk1*$^{-/-}$, *Erk2*$^{fl/fl}$, *Nkx2.1:Cre*, *Ai3* mouse sensory cortices. No difference in the density of EYFP-expressing cells was detected (**B, F**, quantification in **Q**; mean ± SEM, $p > 0.05$). No difference in PV-CINs was detected between mutants and controls (**C, G**, quantification in **R**; mean ± SEM, $p > 0.05$). A significant decrease in the density of SST/EYFP cells was detected in the mutant sensory cortex (**D, H**, quantification in **R**; mean ± SEM, $p < 0.05$). (**I-P**) Confocal micrographs of P60 *Erk1*$^{-/-}$, *Erk2*$^{fl/wt}$, *Nkx2.1:Cre*, *Ai3* and *Erk1*$^{-/-}$, *Erk2*$^{fl/fl}$, *Nkx2.1:Cre*, *Ai3* mature sensory cortices. We detected no change in the density of EYFP^{+} CINs (**J, N**, quantification in **Q**; mean ± SEM, $p > 0.05$). PV-CIN density was unchanged in the sensory cortex (**K, O**, quantification in **R**; mean ± SEM, $p > 0.05$). Reduced SST-expression persisted into adulthood (**L, P**, quantification in **Q**; mean ± SEM, $p < 0.05$). *Images and graphs generated by Johan Martinez and prepped for presentation by Michael Holter.*

PV-CINs do not require ERK1/2 for perineuronal net formation

Extracellular matrix (ECM) remodeling constitutes the end of critical period plasticity and is a fundamental process in the maturation of cortical circuits (Hensch, 2005a; Hensch, 2005b). PV-CINs preferentially sequester members of the chondroitin sulfate proteoglycan (CSPG) family derived primarily from protoplasmic astrocytes. Aberrant PNN formation has been observed in numerous neurodevelopmental disease states (Steullet et al., 2017) and may be a primary contributor to the pathology of the RASopathies (Krencik et al., 2015). Gain-of-function ERK/MAPK signaling in CINs or astrocytes is sufficient to increase accumulation of PNN components (Holter et al., 2019, unpublished; Krencik et al., 2015), though reduced PNN accumulation has been observed in other models of neurodevelopmental disease (Bitanihirwe and Woo, 2014; Cabungcal et al., 2013; Krishnan et al., 2015; Steullet et al., 2017). We therefore asked whether loss of ERK1/2 in CINs was sufficient to disrupt PNN formation.

To assess the extent of PNN sequestering around PV-CINs, we stained *Erk1*$^{-/-}$, *Erk2*$^{fl/fl}$, *Nkx2.1:Cre*, *Ai3* mutant and *Erk1*$^{-/-}$, *Erk2*$^{fl/wt}$, *Nkx2.1:Cre*, *Ai3* control brain

sections with the lectin *wisteria floribunda agglutinin* (WFA) (Figure 3A-D). We observed no change in the pattern of cortical WFA-labeling, and all PV-expressing CINs in the adult mutant sensory cortex co-labeled with WFA (Figure 3, compare A to C). The extent of PNN accumulation around PV-CINs appeared qualitatively normal between mutant and control cortices (Figure 3B, D). We did not observe aberrant accumulation of PNNs around PV^- CINs. Collectively, these findings suggest that loss of ERK1/2 in developing GABAergic circuits was not sufficient to alter PV-CIN maturation and critical ECM remodeling processes.

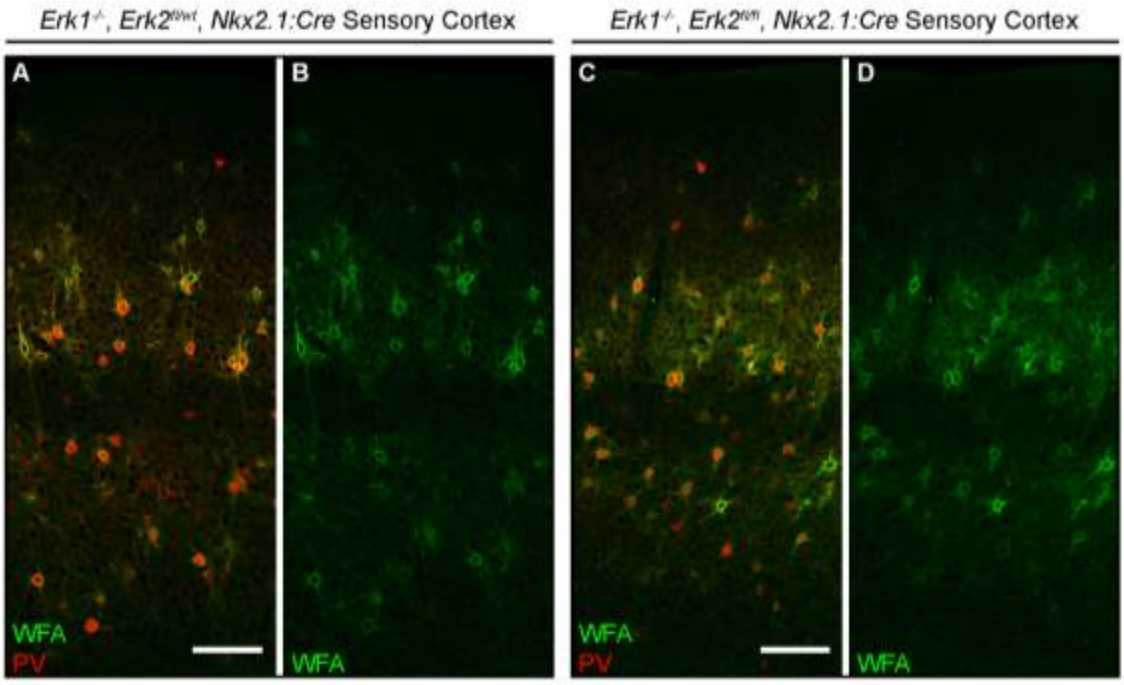

Figure 3. The extent of PNN accumulation around PV-CINs is unchanged in ERK1/2 CKO mice. (**A-D**) Representative confocal micrographs of adult *Erk1*$^{-/-}$, *Erk2*$^{fl/wt}$, *Nkx2.1:Cre* and *Erk1*$^{-/-}$, *Erk2*$^{fl/fl}$, *Nkx2.1:Cre* sensory cortices. The pattern of WFA labeling did not appear to differ between controls and mutants. All PV-CINs in the mutant sensory cortex accumulated a PNN (compare **A** to **C**). Qualitative assessment suggests that PNN formation is unaltered in response to ERK1/2 deletion from MGE-derived CINs.

Reduction of activity-dependent gene expression in cortical projection neurons

During the first postnatal week, GABA binding exerts trophic effects in cortical circuits that are essential for normal maturation of PNs (Ben-Ari, 2002; Cancedda et al., 2007; Pan et al., 2019). GABA signaling becomes inhibitory near the end of the first postnatal week after cortical expression of KCC2, which reverses the Cl^- gradient. Early PN neurite outgrowth and subsequent dendritic arborization requires inotropic and metabotropic GABAergic stimulation (Cancedda et al., 2007). SST-expressing CINs form synaptic contacts primarily in the dendrites of PNs and participate broadly in neural computation. We therefore hypothesized that abnormalities in SST-CIN development in *Erk1*$^{-/-}$, *Erk2*$^{fl/fl}$, *Nkx2.1:Cre* mice may therefore alter specific processes in PN development and drive changes in PN excitability. To understand cortical circuit-wide ramifications of abnormal SST-CIN development, we examined global levels of activity-dependent gene expression in adult mice (Figure 4). Interestingly, we found that *Erk1*$^{-/-}$, *Erk2*$^{fl/fl}$, *Nkx2.1:Cre, Ai3* mutant brains had a significant reduction in cortical layer 2/3 expression of Activity-regulated cytoskeletal (Arc) protein than *Erk1*$^{-/-}$, *Erk2*$^{fl/wt}$, *Nkx2.1:Cre, Ai3* controls (Figure 4A, B). Taken together, loss of ERK1/2 from CINs is sufficient to disrupt broad cortical circuit activity in adulthood.

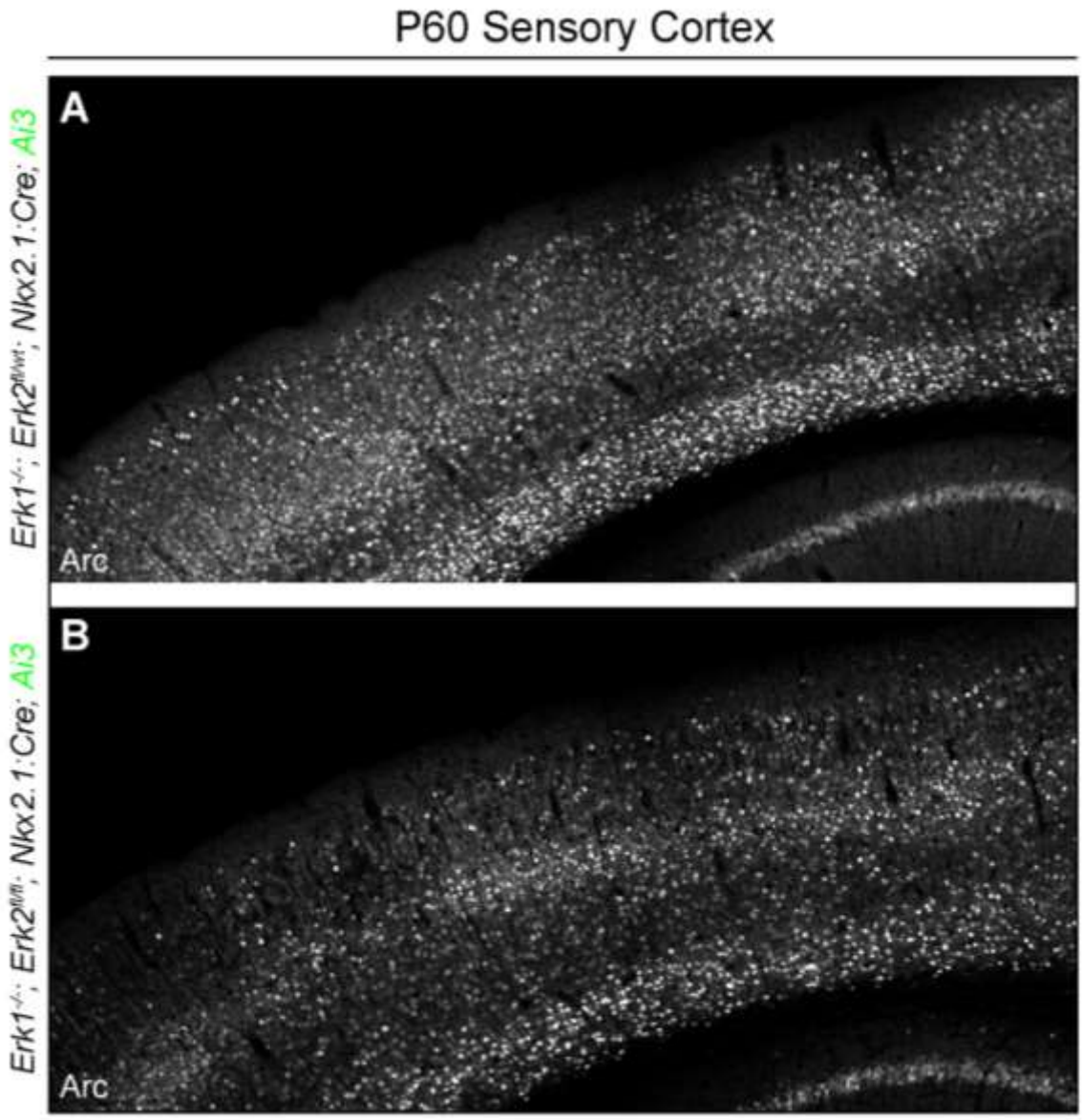

Figure 4. Disrupted Arc expression in layer 2/3 cortical PNs. (**A, B**) Representative regions of adult *Erk1*$^{-/-}$, *Erk2*$^{fl/wt}$, *Nkx2.1:Cre* and *Erk1*$^{-/-}$, *Erk2*$^{fl/fl}$, *Nkx2.1:Cre* cortices. We observed a significant decrease in the expression of Arc in PNs populating layer 2/3 of the mutant cortex in comparison to controls. No qualitative changes in deep layer 5/6 Arc expression was observed in mutant cortices. *Images generated by Johan Martinez.*

Generation of Erk1$^{-/-}$, Erk2$^{fl/fl}$, hM3Dq, Nkx2.1:Cre mice

Neural activity through cortical circuits is imperative for the normal maturation of specific groups of neurons, including both excitatory and inhibitory neurons (Bartolini et al., 2013; Chattopadhyaya et al., 2004; Close et al., 2012; Le Magueresse and Monyer, 2013; Mardinly et al., 2016; Pan et al., 2019; Wamsley and Fishell, 2017). Recent developments of chemogenetic tools termed Designer Receptors Exclusively Activated by Designer Drugs (DREADDs) have made possible the non-invasive modulation of neural circuit activity (Armbruster et al., 2007; Dimidschstein et al., 2016; Roth, 2016). We hypothesized that increased activation of ERK/MAPK-deleted CINs in adulthood is sufficient to rescue global cortical hypoexcitability. We therefore generated *Erk1$^{-/-}$, Erk2$^{fl/fl}$, hM3Dq, Nkx2.1:Cre* mice, which express a genetically encoded human muscarinic receptor to activate neural circuits in response to clozapine N-oxide (CNO) administration (Figure 5) (Armbruster et al., 2007; Roth, 2016). CNO binding increases levels of intracellular calcium, allowing for temporal control over neural circuit activity (Roth, 2016).

Expression of the hemagglutinin (HA)-tagged hM3Dq localized to the membrane of MGE-derived CIN subtypes, including some PV-CINs (Figure 5A-C). Expression of HA was observed throughout the cortical layers and localized to CIN soma, dendrites, and axonal projections (Figure 5C). Consistent with previous reports of some PV-CINs generated by non-*Nkx2.1* expressing progenitors (Miyoshi et al., 2010), we detected PV-CINs that did not express the HA-tag populating the superficial cortical layers (Figure 5D-F, yellow inset). Furthermore, we observed co-labeling of HA with PV in deeper cortical layers, consistent with migration tendencies of PV-CINs derived from the MGE (Bartolini

et al., 2017) (Figure 5G-I). The specificity of hM3Dq for CINs in this model may provide a powerful tool for modulating GABAergic circuit activity and exploration of repairing cortical circuit abnormalities in response to CIN-specific ERK1/2 CKO.

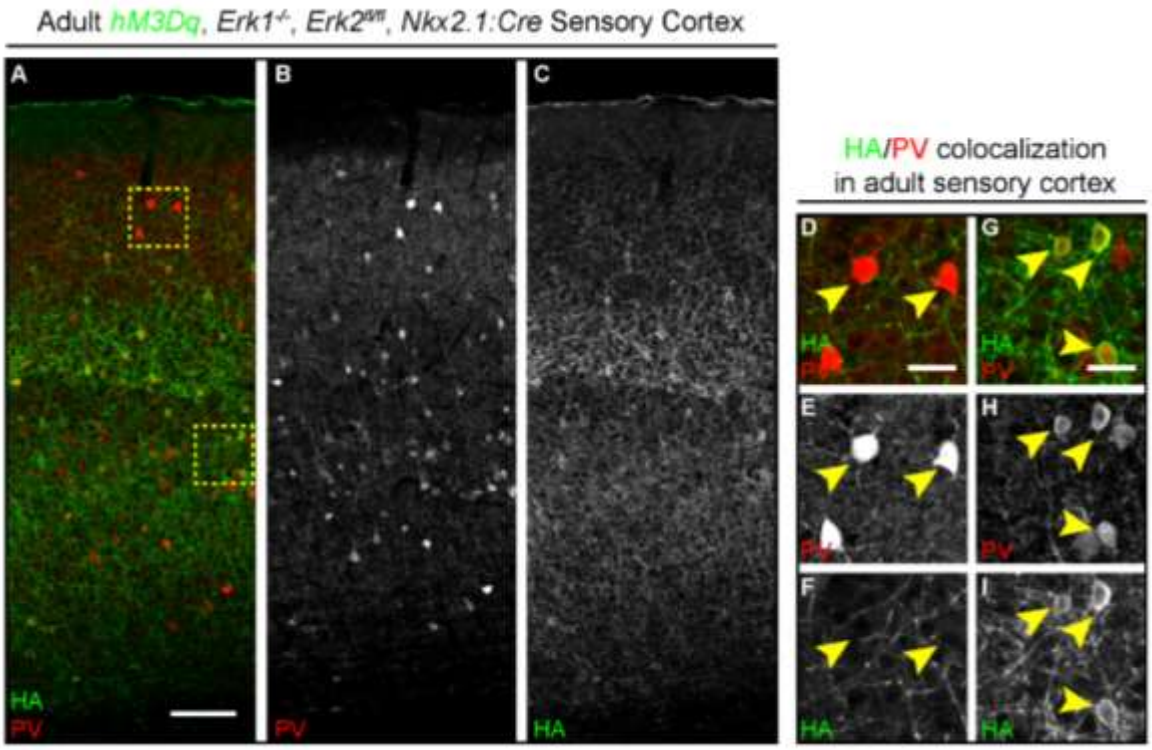

Figure 5. hM3Dq expression is detectable in ERK1/2-deleted CINs. (**A-C**) Representative confocal micrographs of HA and PV immunolabeling in *Erk1*$^{-/-}$, *Erk2*$^{fl/fl}$, *hM3Dq, Nkx2.1:Cre* mutant mice. (**A**) Colocalization of the HA-tagged hM3Dq receptor was observed in PV-expressing CINs throughout the cortex. (**B**) PV-CIN distribution within the CIN-specific ERK1/2 CKO sensory cortex. (**C**) HA immunolabeling shows extensive dendritic and axonal distribution of hM3Dq in CINs. (**D-F**) Some PV^{+} CINs located in layer 2/3 did not express HA (yellow arrows). (**G-I**) Deep layer PV-CINs expressed high levels of HA. (Cortical bar: *scale bar = 100μm*; insets: *scale bar = 25μm*).

Discussion

Here, we show that loss of ERK1/2 signaling during CIN development disrupts the specification of SST-CINs. Interestingly, reduced ERK1/2 signaling in developing GABAergic circuits did not regulate the number of mature CINs. We observed no significant differences in the density or distribution of PV-expressing CINs at the end of the second postnatal week and into adulthood. All PV-CINs developed a PNN and exhibited a normal extent of PNN labeling. We did not detect aberrant formation of PNNs around PV^- interneurons. Interestingly, we detected a significant decrease in the cortical expression of SST, suggesting that ERK1/2 is required for the specification and maturation of SST-CINs. These data suggest that canonical ERK/MAPK signaling has differential roles in the development of specific CIN subtypes and may be particularly impactful for future therapeutic design.

Aberrant GABAergic circuit function is observed in a number of neurodevelopment syndromes (Chao et al., 2010; Cui et al., 2008; Pizzarelli and Cherubini, 2011). How changes in intracellular signaling pathways translate to changes in CIN development have only begun to be elucidated. We show that the principal kinases of the canonical ERK/MAPK pathway, ERK1/2, are required for the specification of SST-expressing CINs. Consistent with past studies, we show that loss of ERK1/2 does not regulate CIN migration from subpallial ganglionic eminences (Polleux et al., 2002). Interestingly, we detected a significant decrease in the amount of cortical SST-labeling but no change in the number of endogenously-labeled CINs. This selective loss of SST-expression suggests that ERK/MAPK signaling regulates crucial steps of SST-CIN development. During neurogenesis, SST transcripts can be detected in postmitotic GABAergic neurons as early

as E13.5 (Batista-Brito et al., 2008), and cortical expression of SST persists into adulthood. The events governing the loss of SST expression in the adult cortex are incompletely understood. SST expression is thought to be regulated in part by binding of the CRE response element in its promoter by P-CREB (Cha-Molstad et al., 2004; Gonzalez et al., 1989). Thus, loss of SST expression may be driven by reduced phosphorylation of CREB in the absence of the ERK1/2 kinases. Moreover, it will be important to determine the temporal dynamics of SST expression loss. Recent work has shown that modulation of Ryk signaling during embryogenesis establishes the rostro-caudal axis of the MGE and biases progenitor divisions to specific CIN subtype fates (McKenzie et al., 2019). It is possible that SST-specification is altered at the progenitor stage in *Erk1*$^{-/-}$, *Erk2*$^{fl/fl}$, *Nkx2.1:Cre* embryos though unlikely due to the normal densities of PV-CINs in the adult cortex. Further work assessing the temporal dynamics of SST expression will be necessary to address this possibility and will be informative in understanding the basic functions of ERK1/2 in CIN generation and post-mitotic differentiation.

Perturbation of GABA excitatory action during the first week of postnatal life leads to significant morphological defects of cortical PNs and may lead to abnormal behaviors (Cancedda et al., 2007). Here, we show that ERK1/2 deletion from a subset of CINs drives global changes in cortical expression of *Arc*, an immediate early gene highly expressed by PNs. Disruption of key PN dendritic arborization processes linked to aberrant GABA signaling may be an underlying cause of cortical hypoexcitability. Due to high affinity for SST synaptogenesis in the cortical neuropil (Fino et al., 2013), it is likely that abnormal SST development in the absence of ERK1/2 led to changes in PN morphological complexity. Furthermore, we have generated a CIN-specific hM3Dq chemogenetic mouse

line to examine the reversibility of SST expression loss and rescue of broad cortical circuit level abnormalities. It will be important to examine multiple temporal windows for prevention of these phenotypes, in particular due to drastic changes of GABA action in early postnatal cortical development (Ben-Ari, 2002). Reversibility of these phenotypes by modulation of neural activity would provide unprecedented insight into treating neurodevelopmental syndromes.

Canonical ERK/MAPK signaling is a known regulator of morphological and electrophysiological maturation of cortical PNs (Xing et al., 2016). However, it is unclear if ERK/MAPK regulates these processes in CIN populations. In contrast to PNs, ERK/MAPK pathway activity is not required for the survival of CIN populations. We therefore suggest that loss of ERK1/2 signaling during CIN development may also regulate dendritic arborization and intrinsic electrophysiological properties. In support of this hypothesis, the receptor tyrosine kinase ERBB4, which lies upstream of the canonical ERK/MAPK cascade, is highly enriched in PV-expressing CINs and is important for GABAergic synaptic transmission (Fazzari et al., 2010). We suggest that loss of ERK1/2 may drive similar alterations in CIN physiology.

A number of neurological disorders implicate abnormal PV-CIN development and function in neuropathogenesis (Bitanihirwe and Woo, 2014; Cabungcal et al., 2013; Fazzari et al., 2010; Selby et al., 2007; Steullet et al., 2017; Xu et al., 2018). However, we did not detect overt PV-CIN developmental abnormalities in *Erk1*$^{-/-}$, *Erk2*$^{fl/fl}$, *Nkx2.1:Cre* cortices. In contrast to increased ERK/MAPK pathway activity during CIN development (Holter et al., 2019; unpublished), loss of ERK1/2 signaling did not disrupt the number of PV-expressing CINs in the adult cortex. Moreover, we did not observe differences in the

extent of cortical PNN-labeling, suggesting that PV-CIN maturation in ERK1/2 CKO mutants is intact. Thus, there appear to be distinct requirements of ERK1/2 for specific CIN subtypes. The most common pathogenic mechanism driving RASopathy neuropathogenesis is an increase in canonical ERK/MAPK pathway activity. Our data suggest that therapies aimed at normalizing ERK/MAPK activity during CIN development may significantly impair processes necessary for normal SST-CIN maturation. Together, this work provides insight into the basic biological functions of ERK1/2 in CIN development and highlights subtype-specific requirements for ERK1/2 in GABAergic circuits.

Supplemental Figures

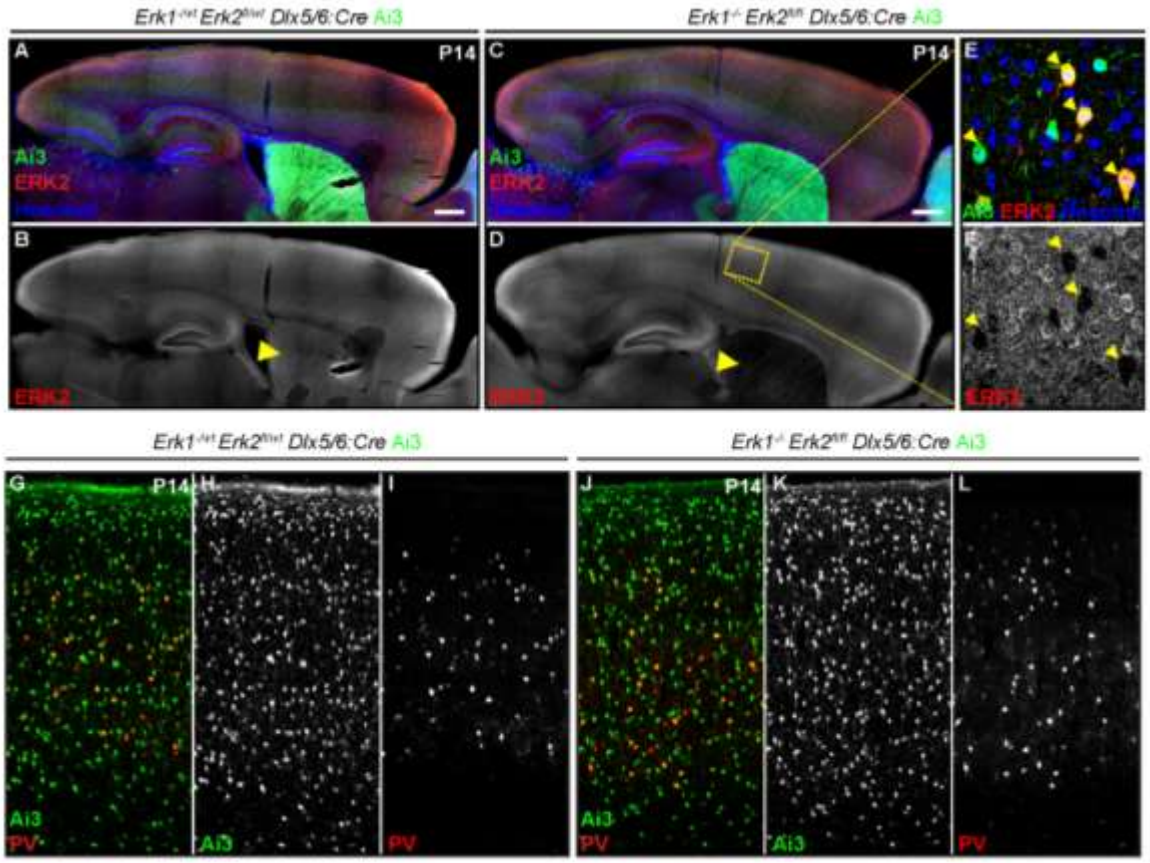

Supplemental Figure 1. PV-CIN density is unaltered in *Erk1*$^{-/-}$ *Erk2*$^{fl/fl,}$ *Dlx5/6:cre* mutant cortices (A-D) Representative saggital sections of P14 *Erk1*$^{-/-}$, *Erk2*$^{fl/fl}$, *Dlx5/6:Cre*, Ai3 mutants and *Erk1*$^{-/-}$, *Erk2*$^{fl/wt}$, *Dlx5/6:Cre*, Ai3 controls labeled for ERK2. **(E-F)** Reduced ERK2 protein was detected in mutant CINs as compared to controls (yellow arrowheads). **(G-L)** P14 coronal sections of *Erk1*$^{-/-}$, *Erk2*$^{fl/fl}$, *Slc32A1:Cre*, Ai3 and *Erk1*$^{-/-}$, *Erk2*$^{fl/wt}$, *Slc32A1:Cre*, Ai3 primary S1 immunolabeled for PV showed no qualitative decrease in the number of Ai3^{+} CINs (n=3).

CHAPTER 5

CONCLUSION

The canonical ERK/MAPK cascade is important for the construction of the brain, including complex structures such as the cerebral cortex. Perturbations to ERK/MAPK signaling during development give rise to a family of neurodevelopmental syndromes collectively termed the "RASopathies." Here, I aimed to further the understanding of how specific mutations that drive changes in ERK/MAPK pathway activity affect the development and function of cortical circuits. My data argues for the generation of patient-specific molecular therapeutics and suggests that modulation of GABAergic circuits may be a particularly effective treatment option for some RASopathy individuals.

Differential neurocognitive outcomes in the RASopathies

RASopathy individuals present with a variety of neurological phenotypes that include intellectual disability, ADHD, developmental delay, and seizures (Adviento et al., 2014; Rauen et al., 2013; Tidyman and Rauen, 2016). Individuals with unique RASopathy-associated mutations often display overlapping neurological phenotypes, though many are incompletely penetrant and of varying severity (Pierpont et al., 2018; Pierpont et al., 2009; Pierpont et al., 2010b; Pierpont et al., 2013). Due to the heterogeneity of neurological outcomes of RASopathy mutations, continued study of individual genes will be necessary to treat patients effectively and efficiently. For example, a Polish family consisting of several individuals with the Noonan Syndrome-associated $RAF1^{L613V}$ mutation display diversity in intellectual functioning (Pandit et al., 2007; Razzaque et al., 2007). While $RAF1^{L613V}$ did result in intellectual disability in two family members, a third had

considerably better than average performance on an IQ test (E. Ciara et al., 2009, ASHG, abstract). Other studies of adaptive behavior in RASopathy individuals have shown that people with mutations in *BRAF*, *SOS1*, and *PTPN11* have heterogeneous capabilities and therefore require different levels of care (Pierpont et al., 2009; Pierpont et al., 2010a; Pierpont et al., 2013). Furthermore, individuals with the same mutation do not necessarily experience the same neurological outcomes. Individuals with point mutations in upstream regulators of ERK/MAPK signaling, which typically comprise the majority of RASopathy cases, have heterogenous neurocognitive outcomes (Pierpont et al., 2018; Pierpont et al., 2009; Rauen et al., 2015; Tidyman and Rauen, 2016).

Interestingly, individuals with mutations in kinases downstream of RAS, such as *BRAF* and *MEK* isoforms, tend to have increased severity of neurocognitive dysfunction (Pierpont et al., 2010b). It is therefore likely that aberrant ERK/MAPK activity is a central regulator of RASopathy neurological phenotypes, though the mechanisms by which ERK/MAPK mediates neurocognitive phenotypes in patients is still under investigation. Furthermore, it is unclear how unique mutations in different regulators and core kinases of the ERK/MAPK pathway affect the development of specific cell types and subsequent formation and function of neurobiological circuits. Thus, broad characterization of individual patient mutations and requirements of RASopathy-linked genes in the development of neural cell types will be necessary to understand the molecular and cellular events that give rise to the RASopathies. This work will be beneficial to our collective efforts in the basic understanding of canonical ERK/MAPK pathway activity in neurodevelopment as well as the design of new therapeutics for RASopathic individuals.

$Raf1^{L613V}$ drives changes in glial development

Here, I have provided the first data to characterize neurological phenotypes in a germline *$Raf1^{L613V}$* mouse model of Noonan Syndrome. Mutations in core kinases of the ERK/MAPK pathway downstream of RAS are associated with profound deficits in intellectual ability (Pierpont et al., 2010b). However, we report the first germline RASopathy mouse model to drive enhanced spatial reference and working memory, and improved fear learning. Improvements in learning coincided with modest yet significant increases in the density of cortical and hippocampal astrocytes, and a significant increase in the density of cortical OPCs.

Abnormal development of glial cells such as astrocytes and oligodendrocytes is thought to contribute to neurodevelopmental disease (Koini et al., 2017; Molofsky et al., 2012). Previous work had identified essential trophic stimuli, such as cardiotrophin-1, ciliary neurotrophic factor (CNTF), and leukemia inhibitory factor (LIF), that were necessary to shift radial glia into a gliogenic state (Miller and Gauthier, 2007; Nakashima et al., 2001; Nakashima et al., 1999; Ware et al., 1995). However, knowledge of intracellular molecular events mediating this process downstream of receptor activation were relatively unresolved. The gp130/JAK-STAT pathway was revealed as the major molecular cascade necessary for the switch to astrogenesis during embryonic brain development, and mouse cortices lacking the gp130 receptor did not produce astrocytes (Nakashima et al., 1999). During corticogenesis, the ERK/MAPK cascade is a key instructor in the neuro- to gliogenic switch (Li et al., 2012b). Furthermore, both loss- and gain-of-function MEK mutations have profound effects on the number of astrocytes generated during gliogenesis (Li et al., 2012b). These phenotypes arise due to an abnormal

temporal shift in radial glial production of astrocytes during mouse corticogenesis and suggests that ERK/MAPK regulation of gliogenic genes is the key to the initial generation of astrocytes. In comparison, the gain-of-function *Raf1*^{L613V} mutation drove modest increases in glial number in the mouse sensory cortex and hippocampus. *Raf1*^{L613V} mutant mice had significantly increased densities of GFAP^{+} astrocytes and PDGFRα^{+} OPCs in the adult cortex. These data are consistent with previous reports of abnormal glial development in response to changes in ERK/MAPK signaling (Breunig et al., 2015; Gauthier et al., 2007; Krencik et al., 2015; Li et al., 2012b; Rizvi et al., 1999; Tien et al., 2012; Zhu et al., 2005).

Interestingly, we detected no differences in the density of astrocytes and OPCs during the second postnatal week. These findings contrast with previous RASopathy literature showing that hyperactive ERK/MAPK mutations drive changes in early gliogenic processes and subsequent astrocyte and oligodendrocyte overproduction (Ehrman et al., 2014; Li et al., 2012b). Our data suggests that the *Raf1*^{L613V} mutation works through an independent mechanism, by which a postnatal proliferative event may be responsible for increased glial density in *Raf1*^{L613V} cortices. Consistent with this hypothesis, we detected an increased density of PDGFRα^{+} non-myelinating OPCs in the mouse sensory cortex. OPCs remain quiescent but maintain proliferative capabilities in adulthood (Dawson et al., 2003; Fernandez-Castaneda and Gaultier, 2016; Wang et al., 2006). Whether or not OPC proliferation, increased astrocytic divisions, or invasion of glia from other brain regions is responsible for increased glial cell density in the *Raf1*^{L613V} cortex remains open for exploration. Conditional studies utilizing a Cre-dependent *Raf1*^{L613V} mutation will be necessary for a comprehensive understanding of gliobiological events in *Raf1*^{L613V} mutant

mice. Study of these events will be particularly impactful for therapeutic design due to the late temporal onset of this phenotype.

Despite modest changes in glial number, we detected no overt signs of glial dysfunction in *Raf1*^{L613V} mice. Diffusion tensor imaging (DTI) of RASopathy and ASD patient brains often show changes in white matter structure, which may be driven by specific changes in oligodendrocyte development (Filges et al., 2014; Koini et al., 2017; Owen et al., 2014). Interestingly, assessment of myelination in the *Raf1*^{L613V} corpus callosum revealed no change in the extent of myelin sheath thickness around individual PN axons, suggesting that processes linked to myelinogenesis are relatively intact. We also observed no changes in the initiation of myelination in *Raf1*^{L613V} cortices. Furthermore, key extracellular matrix remodeling processes mediated by astrocytes were unaltered in *Raf1*^{L613V} mutants. We observed no significant differences in the extent of PNN accumulation around PV CINs in the hippocampus.

The unique biochemical properties of distinct RASopathy mutations result in differential activation of the principal ERK1/2 kinases (Rodriguez-Viciana et al., 2008). Differences in RASopathy biochemical dynamics may therefore underlie contrasting cellular phenotypes in RASopathy disease states. For instance, the *Raf1*^{L613V} mutation induces qualitatively weak phosphorylation of ERK1/2 when compared to other RASopathy mutations (Holter et al., 2019; Rodriguez-Viciana et al., 2008). In *Raf1*^{L613V} cortices, we detected subtle increases in the number of high P-ERK1/2-expressing PNs in layer 2/3 in adulthood. We observed no differences in the protein levels of P-ERK1/2 across all cortical layers during the third postnatal week at the peak level of ERK/MAPK pathway activity. Due to *Raf1*^{L613V} driving only subtle changes in RAF1 biochemical

activity in non-neuronal cell types (Wu et al., 2011), it is likely that slight increases in ERK/MAPK activity are not sufficient to broadly alter cortical architecture. However, glial cells appear to be sensitive to changes in ERK/MAPK activity, potentially due to heightened expression of canonical ERK/MAPK pathway components. It will be important to understand how changes in the *Raf1*^{L613V} mouse brain translate to human neuropathology. To date, few individuals with the *RAF1*^{L613V} mutation have been documented and none have been extensively characterized (E. Ciara et al., 2009, ASHG, abstract; Pandit et al., 2007; Razzaque et al., 2007). Cell-specific studies and neuroimaging of individuals with the *RAF1*^{L613V} mutation will reinforce our understanding of neurocognitive heterogeneity in the RASopathies and provide further insight into the neuropathology of other RASopathy disorders.

Effects of RASopathy mutations on cognition

The cellular underpinnings of neurocognitive disability in the RASopathies remains unclear. Germline and cell-specific studies of RASopathy-linked mutations yielded mixed results in determining the origins of neurocognitive dysfunction (Clement et al., 2012; Costa et al., 2002; Cui et al., 2008; Holter et al., 2019; Kushner et al., 2005; Lee et al., 2014; Lee and Silva, 2009; Ozkan et al., 2014; Schreiber et al., 2017). In the germline, the Costello Syndrome-linked *Hras*^{G12V} mutation drove impaired hippocampal-dependent memory (Schreiber et al., 2017); however, mutant mice expressing *Hras*^{G12V} specifically in glutamatergic circuits exhibited significant improvements in spatial reference memory (Kushner et al., 2005). These results therefore suggest that glutamatergic circuits in *Hras*^{G12V} mice do not significantly contribute to the neurocognitive impairments observed

in germline mutants. Moreover, neurocognitive dysfunction in germline *Hras*^{G12V} mice is either mediated by other neurotransmitter systems, complex cell-cell interactions, or combinatorial effects of multiple defective neural circuits.

These data contrast with other related mutations in regulators of RAS activity. *Syngap1* mutant mice exhibit significant neurological deficits that are primarily driven by defective glutamatergic circuitry (Ozkan et al., 2014). Surprisingly, glutamatergic-directed mutations in *Nf1* lead to no change in spatial reference memory (Cui et al., 2008). Deletion of *Nf1* from GABAergic circuits was sufficient to drive impairments in hippocampal-dependent memory, which therefore suggests that contributions of individual neuron subtypes may be dependent on gene mutation and differential expression patterns of RASopathy-linked genes. Further cell-specific studies of a broad array of RASopathy-linked mutations will be informative for understanding the cellular underpinnings of RASopathy neuropathogenesis and elucidate potential targets for molecular therapeutics.

The circuit mechanisms driving enhanced spatial reference, working, and fear memory in *Raf1*^{L613V} mice remain unclear. We hypothesized that significant increases in hippocampal GFAP^{+} astrocyte density may contribute to improved spatial reference and working memory. Importantly, previous studies have shown that modest increases in the release of inflammatory cytokines, such as TNFα, from hippocampal astrocytes is correlated with improved memory (Camara et al., 2015; Camara et al., 2013; Han et al., 2013). We detected no significant differences in the amount of TNFα labeling, suggesting that other molecular mechanisms underlie enhanced behavioral performance in these mice. Whether a single neurotransmitter system is responsible for memory improvements in these *Raf1*^{L613V} mutants is unclear, though this may be mediated by glutamatergic-driven

improvements in LTP within the hippocampal microcircuit (Kushner et al., 2005). LTP assays in conjunction with local field potentials in *Raf1*^{L613V} Schaffer collaterals will be instructive in understanding the circuit mechanisms responsible for enhanced cognitive performance in these mice. Further cell-specific studies of the *Raf1*^{L613V} mutation will definitively determine the circuit origins of improved learning.

Dysfunctional GABAergic circuits in the RASopathies

Previous studies have had mixed results concerning GABAergic circuit involvement in RASopathy neuropathogenesis (Cui et al., 2008; Krencik et al., 2015; Kushner et al., 2005; Ozkan et al., 2014). It is likely that heterogeneity in GABAergic circuit dysfunction is mediated by a combination of factors such as 1) low expression of some RASopathy-related genes and 2) differential activation of downstream kinase cascades. In support of these hypotheses, CINs express low levels of *Syngap1* in comparison to PNs, which may render them less susceptible to specific mutations within this gene (Mardinly et al., 2016). Furthermore, expression of canonical ERK/MAPK components *Map2k1/Mek1* and *Mapk1/Erk2* is substantially lower in CINs as compared to other neuron subtypes and glia (Loo et al., 2019; Mardinly et al., 2016). Thus, the naturally low levels of these kinases may render CIN populations more susceptible to gain-of-function RASopathy mutations within the canonical ERK/MAPK pathway.

Here I've shown that increased MEK1 signaling during embryogenesis disrupts the establishment of PV-CIN number by cleaved-caspase 3 (CC3) mediated apoptosis. Surprisingly, SST-CIN number remained intact in adult mutant cortices. Reduced PV-CIN number was correlated with increased seizure susceptibility and defects in prefrontal cortex

function. The mature mutant cortex had a significant reduction in PN perisomatic GABAergic synapses, likely driven by the loss of PV-CIN basket cells (Fino et al., 2013). Interestingly, surviving PV-CINs exhibited a significant increase in somal area, but did not display significant alterations in intrinsic electrophysiological properties. Developmental disease mutations that affect PV-CIN number typically result in increased oxidative stress and a coinciding reduction in the extent of PNN labeling. However, gain-of-function MEK1 signaling within GABAergic circuits led to a significant increase in the sequestering of CSPGs around surviving PV-CINs as assessed by *WFA* labeling. Collectively, abnormal PV-CIN development may mediate aspects of neuropathogenesis in some disorders of the RASopathy family.

The mechanism by which caMek1 drives the death of embryonic PV-CINs is yet to be determined. Due to a small proportion of dying cells in the mantle zone of the MGE, it is difficult to pinpoint the precise cause of death by standard biochemical and transcriptomic methods. *In vitro* methods such as MGE cultures may be particularly informative in identifying molecular pathways associated with PV-CIN death. This method can be further optimized by adding antagonists of Wnt signaling, which has recently been shown to bias MGE progenitors toward PV-CIN generation at the expense of SST-CINs (McKenzie et al., 2019). Interestingly, upregulation of death cascades by sustained ERK/MAPK activation has been reported in numerous cancer and developmental models (Cagnol and Chambard, 2010). Adult PV-CINs have markedly high densities of mitochondria, therefore implicating mitochondrial-regulated death pathways as attractive candidate mediators of PV-CIN apoptosis.

We have established a role for aberrant GABAergic circuit development in RASopathy-linked ADHD, a co-morbid condition that affects approximately 40% of RASopathy individuals (Boyd et al., 2009; Green et al., 2017; Johnson et al., 2019; Miguel et al., 2015; Pierpont et al., 2018; Pierpont et al., 2015; Walsh et al., 2013). Previous studies of neurodevelopmental disease have suggested that defective glutamatergic circuitry mediates prefrontal cortex (PFC) dysfunction (Krueger et al., 2011). We show that abnormal GABAergic circuit development in response to gain-of-function ERK/MAPK pathway activity disrupts FMI performance. However, it is not clear if FMI deficits in *caMek1 Slc32A1:Cre* mice are mediated solely by cortical circuit dysfunction. The interface of the PFC to regions of the basal ganglia, such as the striatum, is essential to timing-related behaviors (Kim et al., 2018). The GABA-expressing D1 medium spiny neurons (MSNs) of the striatum have been previously shown to mediate aspects of temporal control (Narayanan et al., 2012). It will therefore be interesting to examine whether changes in D1-MSN development coincide with FMI performance deficits in *caMek1 Slc32A1:Cre* mice (Hutton et al., 2017).

While altered GABAergic output may disrupt the function of the PFC, it is also likely that GABA-mediated disruption of layer 2/3 PFC glutamatergic neurons drives deficits in behavioral response inhibition. PNs in the mutant PFC expressed significantly lower levels of P-ERK1/2 than controls, which may be due to changes in inhibition during perinatal development. Aberrant GABA signaling during the first postnatal week is sufficient to disrupt morphological features of PNs in the developing cortex (Cancedda et al., 2007). SST-CINs primarily form synaptic contacts in the cortical neuropil, and though SST-CIN density remained unchanged, reduced P-ERK1/2 in PNs may be mediated by

improper activity-dependent maturation in response to abnormal SST-CIN input. However, our data provides evidence that dysfunctional GABA signaling by PV-CINs drives cortical circuit-wide abnormalities that may underlie significant changes in behavioral response inhibition.

In contrast to gain-of-function MEK1 signaling, we show that loss of ERK1/2 in developing CINs had little effect on PV-CIN development and postnatal maturation. Furthermore, PV-CINs were present in normal densities and distributions within the cortex. We observed normal sequestering of PNN components in *Erk1*$^{-/-}$, *Erk2*$^{fl/fl}$, *Nkx2.1:Cre* mutant mice, suggesting that the specific expression of the principal ERK1/2 proteins by CINs is non-essential to the formation of the PNN. Unlike cortical PNs, we show that canonical ERK/MAPK signaling does not regulate CIN number (Xing et al., 2016). However, immunolabeling for the major CIN subtypes, PV and SST, revealed a significant decrease in the density of SST-immunoreactive cells in the adult cortex. We further show that loss of SST expression is detectable by the end of the second postnatal week. It is therefore likely that this phenotype is due to either aberrant specification of SST-CINs during embryonic development or potentially due to the disruption of activity-dependent maturation during perinatal development. Assessment of SST expression patterns at birth and in the embryo will be necessary to inform these possibilities.

The *Somatostatin* gene contains a CRE sequence that can be bound by the phosphorylated form of cAMP Response Element-binding Protein (CREB) (Cha-Molstad et al., 2004; Gonzalez et al., 1989). CREB activation lies downstream of canonical ERK1/2 signaling, and in the nervous system, can be stimulated by calcium currents during neural activity (Wu et al., 2001). Regulation of P-CREB is primarily mediated by Calmodulin

Kinase (CaMK) stimulation and is activated slowly by ERK/MAPK pathway activity (Wu et al., 2001). Furthermore, dominant negative RAS is sufficient to disrupt phosphorylation of CREB by both ERK1/2 and CaMK-dependent pathways (Wu et al., 2001). Loss of SST expression in response to reduced ERK1/2 in the postnatal cortex may therefore be due to aberrant activity-dependent maturation of SST-CINs. Enhanced excitation of SST-CINs in critical windows of CIN development may be sufficient to restore SST expression in this population of CINs. We thus hypothesized that chemogenetic activation of SST-CINs is sufficient to increase SST expression. Stimulation of the hM3Dq receptor by its ligand CNO has previously been shown to increase intracellular calcium release (Roth, 2016). Whether it is possible to treat an ERK1/2-linked phenotype by modulation of cellular activity is currently unknown. Successful reversal of an ERK1/2-linked phenotype by independent molecular pathways will provide unprecedented insight into RASopathy therapeutics. Collectively, our work highlights specific roles of ERK1/2 signaling in the development of CIN subpopulations and suggests that modulation of GABAergic signaling may be an effective treatment option for RASopathic individuals.

Pharmacological intervention in the RASopathies

Excitingly, pharmacological intervention with ERK/MAPK pathway inhibitors has shown promise in the treatment of RASopathy phenotypes. Administration of the second-generation inhibitor of MEK1, PD0325901 (PD), was sufficient to rescue cardiac and skeletal defects in $Raf1^{L613V}$ mice (Wu et al., 2011). Importantly, IP administration of PD from 4-10 weeks of age once daily was sufficient to reverse phenotypes related to the $Raf1^{L613V}$ mutation. These data provide critical evidence that specific RASopathy

phenotypes may be able to be reversed in humans in late embryonic and early postnatal development. Furthermore, it is unclear if modulation of ERK/MAPK signaling in the *Raf1*^{L613V} mouse model would result in phenotypically normal spatial reference and working memory, potentially minimizing the benefits of this mutation in mice. In addition, PD treatment in a separate *Ptpn11*^{D61G} mouse model of Noonan Syndrome provided evidence that Mek1 inhibitors can normalize neurological dysfunction in adulthood, a promising finding for RASopathy individuals (Lee et al., 2014). Moreover, these findings also suggest that neurocognitive impairments in individuals with mutations in upstream regulators of RAS signaling may be due to altered canonical ERK/MAPK signaling.

The majority of RASopathy-causing mutations lie in upstream regulators of RAS signaling (Rauen et al., 2013). Therefore, it will be important to explore how modulation of ERK/MAPK-independent parallel cascades affect neurocognition. Indeed, pharmacological normalization of ROCK, NOTCH, PKC, and cAMP/PKA pathways downstream of RAS are sufficient to reverse cellular deficits driven by mutations in *NF1* (Anastasaki and Gutmann, 2014; Brown et al., 2012; Kaul et al., 2015). These data suggest that these signaling cascades may have important contributions to behavioral deficits observed in the RASopathies. Further study of how normalization of these pathways in the RASopathies influences behavioral outcome will be necessary to understand broad contributions of cell signaling to defects in neurocognition.

Clinical trials assessing the therapeutic benefits of RAS activity modulation have yielded mixed results. Individuals with Neurofibromatosis Type 1 treated with the 3-hydroxy-3-methylglutamyl coenzyme A reductase inhibitor, simvastatin, had no improvement in cognitive function at the end of a twelve-week administration period (Krab

et al., 2008). Interestingly, separate clinical trials examining the efficacy of lovastatin treatment, a small molecule with a similar mechanism of action to simvastatin, yielded exciting results. Individuals with Neurofibromatosis Type 1 treated with lovastatin for three months exhibited significant improvements in both verbal and non-verbal memory (Acosta et al., 2011; Bearden et al., 2016). However, other neurocognitive phenotypes associated with NF1, including visuospatial memory and attention, do not appear to improve in response to lovastatin treatment (Payne et al., 2016). Recently, a small clinical trial consisting of two Noonan Syndrome patients examined the effects of trametinib, a MEK1/2 inhibitor, on cardiac hypertrophy (Andelfinger et al., 2019). Trametinib was administered to the affected infants beginning at 13 and 14 weeks of age, and treatment lasted for three months. Upon completion of treatment, both Noonan Syndrome infants had dramatic improvements in cardiac structure and function (Andelfinger et al., 2019). The study provides promising results of MEK1/2 modulation for the treatment of Noonan Syndrome symptoms. The successes of these treatments lays the foundation for widespread examination of canonical ERK/MAPK pathway modulation for neurocognitive therapies in humans. Importantly, the reversal of some neurocognitive abnormalities in NF1 individuals in conjunction with extensive mouse studies provides essential information that some phenotypes may be able to be resolved after the onset of symptoms in the early years of life.

RASopathy individuals experience neurological symptoms that often include intellectual disability, ADHD, motor delay, and seizures. Importantly, an increased interest in the genetic origin of the RASopathies has led to the characterization of many unique point mutations and disease-causing genes. Within individual genes, multiple distinct point

mutations have been discovered that can give rise to RASopathy neuropathogenesis. Though the cellular origins underlying neurobehavioral phenotypes in RASopathy individuals is still under investigation, promising results from Phase II clinical trials have suggested that normalization of ERK/MAPK signaling may be effective for many RASopathy individuals. Here, we show that characterization of RASopathy mutations is important in understanding how unique genes influence cellular pathology and affect behavior. We find that subpopulations of neural cell types, including neurons and glia, are differentially affected by specific RASopathy point-mutations. Furthermore, we have shown that aberrant ERK/MAPK pathway activity disrupts the early formation of GABAergic circuits and drives impairments in cognition. Collectively, our data suggest that normalization of GABAergic signaling may be a particularly effective treatment option in some instances of the RASopathies and ultimately lead to a better quality of life for affected individuals.

REFERENCES

Acosta, M., Kardel, P., Walsh, K., Rosenbaum, K., Gioia, G., and Packer, R. (2011). Lovastatin as Treatment for Neurocognitive Deficits Type 1: Phase I Study. Pediatric Neurology *45*, 241-245.

Adviento, B., Corbin, I.L., Widjaja, F., Desachy, G., Enrique, N., Rosser, T., Risi, S., Marco, E.J., Hendren, R.L., Bearden, C.E., *et al.* (2014). Autism traits in the RASopathies. J Med Genet *51*, 10-20.

Alessi, D.R., Saito, Y., Campbell, D.G., Cohen, P., Sithanandam, G., Rapp, U., Ashworth, A., Marshall, C.J., and Cowley, S. (1994). Identification of the sites in MAP kinase kinase-1 phosphorylated by p74raf-1. EMBO J *13*, 1610-1619.

Alfieri, P., Cesarini, L., Mallardi, M., Gambardella, M., Piccini, G., Caciolo, C., Pantaleoni, F., Petrangeli, V., Leoni, C., Selicorni, A., *et al.* (2010). Long term memory profile of disorders associated with dysregulation of RAS-MAPK signaling cascade. Journal of Applied Research in Intellectual Disabilities *23*, 512-512.

Anastasaki, C., and Gutmann, D. (2014). Neuronal NF1/RAS regulation of cyclic AMP requires atypical PKC activation. Human Molecular Genetics *23*, 6712-6721.

Andelfinger, G., Marquis, C., Raboisson, M.J., Théoret, Y., Waldmüller, S., Wiegand, G., Gelb, B.D., Zenker, M., Delrue, M.A., and Hofbeck, M. (2019). Hypertrophic Cardiomyopathy in Noonan Syndrome Treated by MEK-Inhibition. J Am Coll Cardiol *73*, 2237-2239.

Andreadi, C., Cheung, L.K., Giblett, S., Patel, B., Jin, H., Mercer, K., Kamata, T., Lee, P., Williams, A., McMahon, M., *et al.* (2012). The intermediate-activity (L597V)BRAF mutant acts as an epistatic modifier of oncogenic RAS by enhancing signaling through the RAF/MEK/ERK pathway. Genes Dev *26*, 1945-1958.

Aoidi, R., Houde, N., Landry-Truchon, K., Holter, M., Jacquet, K., Charron, L., Krishnaswami, S., Yu, B., Rauen, K., Bisson, N., *et al.* (2018). Mek1(Y130C) mice recapitulate aspects of human cardio-facio-cutaneous syndrome. Disease Models & Mechanisms *11*.

Armbruster, B.N., Li, X., Pausch, M.H., Herlitze, S., and Roth, B.L. (2007). Evolving the lock to fit the key to create a family of G protein-coupled receptors potently activated by an inert ligand. Proc Natl Acad Sci U S A *104*, 5163-5168.

Bae, M.H., Bissonette, G.B., Mars, W.M., Michalopoulos, G.K., Achim, C.L., Depireux, D.A., and Powell, E.M. (2010). Hepatocyte growth factor (HGF) modulates GABAergic inhibition and seizure susceptibility. Exp Neurol *221*, 129-135.

Barnabé-Heider, F., Wasylnka, J.A., Fernandes, K.J., Porsche, C., Sendtner, M., Kaplan, D.R., and Miller, F.D. (2005). Evidence that embryonic neurons regulate the onset of cortical gliogenesis via cardiotrophin-1. Neuron *48*, 253-265.

Bartolini, G., Ciceri, G., and Marin, O. (2013). Integration of GABAergic Interneurons into Cortical Cell Assemblies: Lessons from Embryos and Adults. Neuron *79*, 849-864.

Bartolini, G., Sánchez-Alcañiz, J.A., Osório, C., Valiente, M., García-Frigola, C., and Marín, O. (2017). Neuregulin 3 Mediates Cortical Plate Invasion and Laminar Allocation of GABAergic Interneurons. Cell Rep *18*, 1157-1170.

Batista-Brito, R., Machold, R., Klein, C., and Fishell, G. (2008). Gene expression in cortical interneuron precursors is prescient of their mature function. Cereb Cortex *18*, 2306-2317.

Bearden, C.E., Hellemann, G.S., Rosser, T., Montojo, C., Jonas, R., Enrique, N., Pacheco, L., Hussain, S.A., Wu, J.Y., Ho, J.S., *et al.* (2016). A randomized placebo-controlled lovastatin trial for neurobehavioral function in neurofibromatosis I. Ann Clin Transl Neurol *3*, 266-279.

Ben-Ari, Y. (2002). Excitatory actions of gaba during development: the nature of the nurture. Nat Rev Neurosci *3*, 728-739.

Bennett, M., Rizvi, T., Karyala, S., McKinnon, R., and Ratner, N. (2003). Aberrant growth and differentiation of oligodendrocyte progenitors in neurofibromatosis type 1 mutants. Journal of Neuroscience *23*, 7207-7217.

Berryer, M.H., Chattopadhyaya, B., Xing, P., Riebe, I., Bosoi, C., Sanon, N., Antoine-Bertrand, J., Lévesque, M., Avoli, M., Hamdan, F.F., *et al.* (2016). Decrease of SYNGAP1 in GABAergic cells impairs inhibitory synapse connectivity, synaptic inhibition and cognitive function. Nat Commun *7*, 13340.

Bimonte-Nelson, H.A. (2015). The maze book : theories, practice, and protocols for testing rodent cognition (New York, NY: Humana Press ; Springer).

Bitanihirwe, B.K., and Woo, T.U. (2014). Perineuronal nets and schizophrenia: the importance of neuronal coatings. Neurosci Biobehav Rev *45*, 85-99.

Bizarro, L., Murtagh, C., and Stolerman, I. (2003). Differing effects of nicotine, amphetamine and caffeine on performance of a 5-choice serial reaction time task. Journal of Psychopharmacology *17*, A31-A31.

Boyd, K.P., Korf, B.R., and Theos, A. (2009). Neurofibromatosis type 1. J Am Acad Dermatol *61*, 1-14; quiz 15-16.

Breunig, J.J., Levy, R., Antonuk, C.D., Molina, J., Dutra-Clarke, M., Park, H., Akhtar, A.A., Kim, G.B., Hu, X., Bannykh, S.I., *et al.* (2015). Ets Factors Regulate Neural Stem Cell Depletion and Gliogenesis in Ras Pathway Glioma. Cell Rep *12*, 258-271.

Brown, J., Diggs-Andrews, K., Gianino, S., and Gutmann, D. (2012). Neurofibromatosis-1 heterozygosity impairs CNS neuronal morphology in a cAMP/PKA/ROCK-dependent manner. Molecular and Cellular Neuroscience *49*, 13-22.

Bueno, O.F., De Windt, L.J., Tymitz, K.M., Witt, S.A., Kimball, T.R., Klevitsky, R., Hewett, T.E., Jones, S.P., Lefer, D.J., Peng, C.F., *et al.* (2000). The MEK1-ERK1/2 signaling pathway promotes compensated cardiac hypertrophy in transgenic mice. EMBO J *19*, 6341-6350.

Butt, S., Fuccillo, M., Nery, S., Noctor, S., Kriegstein, A., Corbin, J., and Fishell, G. (2005). The temporal and spatial origins of cortical interneurons predict their physiological subtype. Neuron *48*, 591-604.

Cabungcal, J.H., Steullet, P., Morishita, H., Kraftsik, R., Cuenod, M., Hensch, T.K., and Do, K.Q. (2013). Perineuronal nets protect fast-spiking interneurons against oxidative stress. Proc Natl Acad Sci U S A *110*, 9130-9135.

Cagnol, S., and Chambard, J.C. (2010). ERK and cell death: mechanisms of ERK-induced cell death--apoptosis, autophagy and senescence. FEBS J *277*, 2-21.

Cahoy, J.D., Emery, B., Kaushal, A., Foo, L.C., Zamanian, J.L., Christopherson, K.S., Xing, Y., Lubischer, J.L., Krieg, P.A., Krupenko, S.A., *et al.* (2008). A transcriptome database for astrocytes, neurons, and oligodendrocytes: a new resource for understanding brain development and function. J Neurosci *28*, 264-278.

Cai, J., Chen, Y., Cai, W.H., Hurlock, E.C., Wu, H., Kernie, S.G., Parada, L.F., and Lu, Q.R. (2007). A crucial role for Olig2 in white matter astrocyte development. Development *134*, 1887-1899.

Camara, M.L., Corrigan, F., Jaehne, E.J., Jawahar, M.C., Anscomb, H., and Baune, B.T. (2015). Tumor necrosis factor alpha and its receptors in behaviour and neurobiology of adult mice, in the absence of an immune challenge. Behav Brain Res *290*, 51-60.

Camara, M.L., Corrigan, F., Jaehne, E.J., Jawahar, M.C., Anscomb, H., Koerner, H., and Baune, B.T. (2013). TNF-α and its receptors modulate complex behaviours and neurotrophins in transgenic mice. Psychoneuroendocrinology *38*, 3102-3114.

Cancedda, L., Fiumelli, H., Chen, K., and Poo, M. (2007). Excitatory GABA action is essential for morphological maturation of cortical neurons in vivo. Journal of Neuroscience *27*, 5224-5235.

Cancedda, L., Putignano, E., Impey, S., Maffei, L., Ratto, G.M., and Pizzorusso, T. (2003). Patterned vision causes CRE-mediated gene expression in the visual cortex through PKA and ERK. J Neurosci *23*, 7012-7020.

Castellano, E., and Downward, J. (2011). RAS Interaction with PI3K: More Than Just Another Effector Pathway. Genes Cancer *2*, 261-274.

Castrén, E., Zafra, F., Thoenen, H., and Lindholm, D. (1992). Light regulates expression of brain-derived neurotrophic factor mRNA in rat visual cortex. Proc Natl Acad Sci U S A *89*, 9444-9448.

Cesarini, L., Alfieri, P., Pantaleoni, F., Vasta, I., Cerutti, M., Petrangeli, V., Mariotti, P., Leoni, C., Ricci, D., Vicari, S., *et al.* (2009). Cognitive Profile of Disorders Associated With Dysregulation of the RAS/MAPK Signaling Cascade. American Journal of Medical Genetics Part a *149A*, 140-146.

Cha-Molstad, H., Keller, D.M., Yochum, G.S., Impey, S., and Goodman, R.H. (2004). Cell-type-specific binding of the transcription factor CREB to the cAMP-response element. Proc Natl Acad Sci U S A *101*, 13572-13577.

Chao, H.T., Chen, H., Samaco, R.C., Xue, M., Chahrour, M., Yoo, J., Neul, J.L., Gong, S., Lu, H.C., Heintz, N., *et al.* (2010). Dysfunction in GABA signalling mediates autism-like stereotypies and Rett syndrome phenotypes. Nature *468*, 263-269.

Chattopadhyaya, B., Di Cristo, G., Higashiyama, H., Knott, G.W., Kuhlman, S.J., Welker, E., and Huang, Z.J. (2004). Experience and activity-dependent maturation of perisomatic GABAergic innervation in primary visual cortex during a postnatal critical period. J Neurosci *24*, 9598-9611.

Chattopadhyaya, B., Di Cristo, G., Wu, C.Z., Knott, G., Kuhlman, S., Fu, Y., Palmiter, R.D., and Huang, Z.J. (2007). GAD67-mediated GABA synthesis and signaling regulate inhibitory synaptic innervation in the visual cortex. Neuron *54*, 889-903.

Chen, P.C., Yin, J., Yu, H.W., Yuan, T., Fernandez, M., Yung, C.K., Trinh, Q.M., Peltekova, V.D., Reid, J.G., Tworog-Dube, E., *et al.* (2014). Next-generation sequencing identifies rare variants associated with Noonan syndrome. Proc Natl Acad Sci U S A *111*, 11473-11478.

Clement, J.P., Aceti, M., Creson, T.K., Ozkan, E.D., Shi, Y., Reish, N.J., Almonte, A.G., Miller, B.H., Wiltgen, B.J., Miller, C.A., *et al.* (2012). Pathogenic SYNGAP1 mutations impair cognitive development by disrupting maturation of dendritic spine synapses. Cell *151*, 709-723.

Close, J., Xu, H., Garcia, N., Batista-Brito, R., Rossignol, E., Rudy, B., and Fishell, G. (2012). Satb1 Is an Activity-Modulated Transcription Factor Required for the Terminal Differentiation and Connectivity of Medial Ganglionic Eminence-Derived Cortical Interneurons. Journal of Neuroscience *32*, 17690-17705.

Cobos, I., Calcagnotto, M., Vilaythong, A., Thwin, M., Noebels, J., Baraban, S., and Rubenstein, J. (2005). Mice lacking Dlx1 show subtype-specific loss of interneurons, reduced inhibition and epilepsy. Nature Neuroscience *8*, 1059-1068.

Cooper, J.A. (2008). A mechanism for inside-out lamination in the neocortex. Trends Neurosci *31*, 113-119.

Costa, R., Federov, N., Kogan, J., Murphy, G., Stern, J., Ohno, M., Kucherlapati, R., Jacks, T., and Silva, A. (2002). Mechanism for the learning deficits in a mouse model of neurofibromatosis type 1. Nature *415*, 526-530.

Cowley, S., Paterson, H., Kemp, P., and Marshall, C.J. (1994). Activation of MAP kinase kinase is necessary and sufficient for PC12 differentiation and for transformation of NIH 3T3 cells. Cell *77*, 841-852.

Crawley, J.N. (1999). Behavioral phenotyping of transgenic and knockout mice: experimental design and evaluation of general health, sensory functions, motor abilities, and specific behavioral tests. Brain Res *835*, 18-26.

Cui, Y., Costa, R., Murphy, G., Elgersma, Y., Zhu, Y., Gutmann, D., Parada, L., Mody, I., and Silva, A. (2008). Neurofibromin Regulation of ERK Signaling Modulates GABA Release and Learning. Cell *135*, 549-560.

Dawson, M.R., Polito, A., Levine, J.M., and Reynolds, R. (2003). NG2-expressing glial progenitor cells: an abundant and widespread population of cycling cells in the adult rat CNS. Mol Cell Neurosci *24*, 476-488.

DeFelipe, J., Lopez-Cruz, P., Benavides-Piccione, R., Bielza, C., Larranaga, P., Anderson, S., Burkhalter, A., Cauli, B., Fairen, A., Feldmeyer, D., *et al.* (2013). New insights into the classification and nomenclature of cortical GABAergic interneurons. Nature Reviews Neuroscience *14*, 202-216.

del Río, J.A., de Lecea, L., Ferrer, I., and Soriano, E. (1994). The development of parvalbumin-immunoreactivity in the neocortex of the mouse. Brain Res Dev Brain Res *81*, 247-259.

Denaxa, M., Neves, G., Rabinowitz, A., Kemlo, S., Liodis, P., Burrone, J., and Pachnis, V. (2018). Modulation of Apoptosis Controls Inhibitory Interneuron Number in the Cortex. Cell Rep *22*, 1710-1721.

Denayer, E., Devriendt, K., de Ravel, T., Van Buggenhout, G., Smeets, E., Francois, I., Sznajer, Y., Craen, M., Leventopoulos, G., Mutesa, L., *et al.* (2010). Tumor Spectrum in Children With Noonan Syndrome and SOS1 or RAF1 Mutations. Genes Chromosomes & Cancer *49*, 242-252.

Digilio, M.C., Lepri, F., Baban, A., Dentici, M.L., Versacci, P., Capolino, R., Ferese, R., De Luca, A., Tartaglia, M., Marino, B., *et al.* (2011). RASopathies: Clinical Diagnosis in the First Year of Life. Mol Syndromol *1*, 282-289.

Dileone, M., Profice, P., Pilato, F., Alfieri, P., Cesarini, L., Mercuri, E., Leoni, C., Tartaglia, M., Di Iorio, R., Zampino, G., *et al.* (2010). Enhanced human brain associative plasticity in Costello syndrome. J Physiol *588*, 3445-3456.

Dimidschstein, J., Chen, Q., Tremblay, R., Rogers, S., Saldi, G., Guo, L., Xu, Q., Liu, R., Lu, C., Chu, J., *et al.* (2016). A viral strategy for targeting and manipulating interneurons across vertebrate species. Nature Neuroscience *19*, 1743-1749.

Doughty, A.H., and Richards, J.B. (2002). Effects of reinforcer magnitude on responding under differential-reinforcement-of-low-rate schedules of rats and pigeons. J Exp Anal Behav *78*, 17-30.

Ehrman, L., Nardini, D., Ehrman, S., Rizvi, T., Gulick, J., Krenz, M., Dasgupta, B., Robbins, J., Ratner, N., Nakafuku, M., *et al.* (2014). The Protein Tyrosine Phosphatase Shp2 Is Required for the Generation of Oligodendrocyte Progenitor Cells and Myelination in the Mouse Telencephalon. Journal of Neuroscience *34*, 3767-3778.

Elias, L., Wang, D., and Kriegstein, A. (2007). Gap junction adhesion is necessary for radial migration in the neocortex. Nature *448*, 901-U903.

Fancy, S.P., Baranzini, S.E., Zhao, C., Yuk, D.I., Irvine, K.A., Kaing, S., Sanai, N., Franklin, R.J., and Rowitch, D.H. (2009). Dysregulation of the Wnt pathway inhibits timely myelination and remyelination in the mammalian CNS. Genes Dev *23*, 1571-1585.

Fazzari, P., Paternain, A.V., Valiente, M., Pla, R., Luján, R., Lloyd, K., Lerma, J., Marín, O., and Rico, B. (2010). Control of cortical GABA circuitry development by Nrg1 and ErbB4 signalling. Nature *464*, 1376-1380.

Fernandez-Castaneda, A., and Gaultier, A. (2016). Adult oligodendrocyte progenitor cells - Multifaceted regulators of the CNS in health and disease. Brain Behav Immun *57*, 1-7.

Filges, I., Sparagana, S., Sargent, M., Selby, K., Schlade-Bartusiak, K., Lueder, G., Robichaux-Viehoever, A., Schlaggar, B., Shimony, J., and Shinawi, M. (2014). Brain MRI Abnormalities and Spectrum of Neurological and Clinical Findings in Three Patients With Proximal 16p11.2 Microduplication. American Journal of Medical Genetics Part a *164*, 2003-2012.

Filonova, I., Trotter, J.H., Banko, J.L., and Weeber, E.J. (2014). Activity-dependent changes in MAPK activation in the Angelman Syndrome mouse model. Learn Mem *21*, 98-104.

Fino, E., Packer, A.M., and Yuste, R. (2013). The logic of inhibitory connectivity in the neocortex. Neuroscientist *19*, 228-237.

Flames, N., Long, J., Garratt, A., Fischer, T., Gassmann, M., Birchmeier, C., Lai, C., Rubenstein, J., and Marin, O. (2004). Short- and long-range attraction of cortical GABAergic interneurons by Neuregulin-1. Neuron *44*, 251-261.

Fowke, T.M., Galinsky, R., Davidson, J.O., Wassink, G., Karunasinghe, R.N., Prasad, J.D., Bennet, L., Gunn, A.J., and Dean, J.M. (2018). Loss of interneurons and disruption of perineuronal nets in the cerebral cortex following hypoxia-ischaemia in near-term fetal sheep. Sci Rep *8*, 17686.

Fremin, C., Saba-El-Leil, M., Levesque, K., Ang, S., and Meloche, S. (2015). Functional Redundancy of ERK1 and ERK2 MAP Kinases during Development. Cell Reports *12*, 913-921.

Gabay, Y., Shahbari-Khateb, E., and Mendelsohn, A. (2018). Feedback Timing Modulates Probabilistic Learning in Adults with ADHD. Sci Rep *8*, 15524.

Galtrey, C.M., and Fawcett, J.W. (2007). The role of chondroitin sulfate proteoglycans in regeneration and plasticity in the central nervous system. Brain Res Rev *54*, 1-18.

Garg, S., Lehtonen, A., Huson, S.M., Emsley, R., Trump, D., Evans, D.G., and Green, J. (2013). Autism and other psychiatric comorbidity in neurofibromatosis type 1: evidence from a population-based study. Dev Med Child Neurol *55*, 139-145.

Gauthier, A., Furstoss, O., Araki, T., Chan, R., Neel, B., Kaplan, D., and Miller, F. (2007). Control of CNS cell-fate decisions by SHP-2 and its dysregulation in Noonan syndrome. Neuron *54*, 245-262.

Gelman, D., Martini, F., Nobrega-Pereira, S., Pierani, A., Kessaris, N., and Marin, O. (2009). The Embryonic Preoptic Area Is a Novel Source of Cortical GABAergic Interneurons. Journal of Neuroscience *29*, 9380-9389.

Gelman, D.M., and Marín, O. (2010). Generation of interneuron diversity in the mouse cerebral cortex. Eur J Neurosci *31*, 2136-2141.

Gibson, E.M., Purger, D., Mount, C.W., Goldstein, A.K., Lin, G.L., Wood, L.S., Inema, I., Miller, S.E., Bieri, G., Zuchero, J.B., *et al.* (2014). Neuronal activity promotes oligodendrogenesis and adaptive myelination in the mammalian brain. Science *344*, 1252304.

Goldberg, E., Jeong, H., Kruglikov, I., Tremblay, R., Lazarenko, R., and Rudy, B. (2011). Rapid Developmental Maturation of Neocortical FS Cell Intrinsic Excitability. Cerebral Cortex *21*, 666-682.

Gomes, W.A., Mehler, M.F., and Kessler, J.A. (2003). Transgenic overexpression of BMP4 increases astroglial and decreases oligodendroglial lineage commitment. Dev Biol *255*, 164-177.

Gonzalez, G.A., Yamamoto, K.K., Fischer, W.H., Karr, D., Menzel, P., Biggs, W., Vale, W.W., and Montminy, M.R. (1989). A cluster of phosphorylation sites on the cyclic AMP-regulated nuclear factor CREB predicted by its sequence. Nature *337*, 749-752.

Goyal, Y., Jindal, G.A., Pelliccia, J.L., Yamaya, K., Yeung, E., Futran, A.S., Burdine, R.D., Schüpbach, T., and Shvartsman, S.Y. (2017). Divergent effects of intrinsically active MEK variants on developmental Ras signaling. Nat Genet *49*, 465-469.

Green, T., Naylor, P.E., and Davies, W. (2017). Attention deficit hyperactivity disorder (ADHD) in phenotypically similar neurogenetic conditions: Turner syndrome and the RASopathies. J Neurodev Disord *9*, 25.

Greer, P.L., Hanayama, R., Bloodgood, B.L., Mardinly, A.R., Lipton, D.M., Flavell, S.W., Kim, T.K., Griffith, E.C., Waldon, Z., Maehr, R., *et al.* (2010). The Angelman Syndrome protein Ube3A regulates synapse development by ubiquitinating arc. Cell *140*, 704-716.

Greig, L.C., Woodworth, M.B., Galazo, M.J., Padmanabhan, H., and Macklis, J.D. (2013). Molecular logic of neocortical projection neuron specification, development and diversity. Nat Rev Neurosci *14*, 755-769.

Gutmann, D., Loehr, A., Zhang, Y., Kim, J., Henkemeyer, M., and Cashen, A. (1999). Haploinsufficiency for the neurofibromatosis 1 (NF1) tumor suppressor results in increased astrocyte proliferation. Oncogene *18*, 4450-4459.

Gutmann, D., Wu, Y., Hedrick, N., Zhu, Y., Guha, A., and Parada, L. (2001). Heterozygosity for the neurofibromatosis 1 (NF1) tumor suppressor results in abnormalities in cell attachment, spreading and motility in astrocytes. Human Molecular Genetics *10*, 3009-3016.

Han, X., Chen, M., Wang, F., Windrem, M., Wang, S., Shanz, S., Xu, Q., Oberheim, N., Bekar, L., Betstadt, S., *et al.* (2013). Forebrain Engraftment by Human Glial Progenitor Cells Enhances Synaptic Plasticity and Learning in Adult Mice. Cell Stem Cell *12*, 342-353.

Hatzivassiliou, G., Song, K., Yen, I., Brandhuber, B.J., Anderson, D.J., Alvarado, R., Ludlam, M.J., Stokoe, D., Gloor, S.L., Vigers, G., *et al.* (2010). RAF inhibitors prime wild-type RAF to activate the MAPK pathway and enhance growth. Nature *464*, 431-435.

Haueis, P. (2016). The life of the cortical column: opening the domain of functional architecture of the cortex (1955-1981). Hist Philos Life Sci *38*, 2.

Haydon, P.G., and Nedergaard, M. (2014). How do astrocytes participate in neural plasticity? Cold Spring Harb Perspect Biol *7*, a020438.

Hegedus, B., Dasgupta, B., Shin, J., Emnett, R., Hart-Mahon, E., Elghazi, L., Bernal-Mizrachi, E., and Gutmann, D. (2007). Neurofibromatosis-1 regulates neuronal and glial cell differentiation from neuroglial progenitors in vivo by both cAMP- and ras-dependent mechanisms. Cell Stem Cell *1*, 443-457.

Heidorn, S.J., Milagre, C., Whittaker, S., Nourry, A., Niculescu-Duvas, I., Dhomen, N., Hussain, J., Reis-Filho, J.S., Springer, C.J., Pritchard, C., *et al.* (2010). Kinase-dead BRAF and oncogenic RAS cooperate to drive tumor progression through CRAF. Cell *140*, 209-221.

Hensch, T. (2005a). Critical period mechanisms in developing visual cortex. Current Topics in Developmental Biology, Vol 69 *69*, 215-+.

Hensch, T.K. (2005b). Critical period plasticity in local cortical circuits. Nat Rev Neurosci *6*, 877-888.

Hernandez-Miranda, L., Parnavelas, J., and Chiara, F. (2010). Molecules and mechanisms involved in the generation and migration of cortical interneurons. Asn Neuro *2*.

Hill, J.C., Herbst, K., and Sanabria, F. (2012). Characterizing operant hyperactivity in the Spontaneously Hypertensive Rat. Behav Brain Funct *8*, 5.

Holter, M.C., Hewitt, L.T., Koebele, S.V., Judd, J.M., Xing, L., Bimonte-Nelson, H.A., Conrad, C.D., Araki, T., Neel, B.G., Snider, W.D., *et al.* (2019). The Noonan Syndrome-linked Raf1L613V mutation drives increased glial number in the mouse cortex and enhanced learning. PLoS Genet *15*, e1008108.

Hrvatin, S., Hochbaum, D.R., Nagy, M.A., Cicconet, M., Robertson, K., Cheadle, L., Zilionis, R., Ratner, A., Borges-Monroy, R., Klein, A.M., *et al.* (2018). Single-cell analysis of experience-dependent transcriptomic states in the mouse visual cortex. Nat Neurosci *21*, 120-129.

Huang, Z. (2009). Molecular regulation of neuronal migration during neocortical development. Molecular and Cellular Neuroscience *42*, 11-22.

Huang, Z., Di Cristo, G., and Ango, F. (2007). Development of GABA innervation in the cerebral and cerebellar cortices. Nature Reviews Neuroscience *8*, 673-686.

Huang, Z.J., Kirkwood, A., Pizzorusso, T., Porciatti, V., Morales, B., Bear, M.F., Maffei, L., and Tonegawa, S. (1999). BDNF regulates the maturation of inhibition and the critical period of plasticity in mouse visual cortex. Cell *98*, 739-755.

Hutton, S.R., Otis, J.M., Kim, E.M., Lamsal, Y., Stuber, G.D., and Snider, W.D. (2017). ERK/MAPK Signaling Is Required for Pathway-Specific Striatal Motor Functions. J Neurosci *37*, 8102-8115.

Hyde, L.A., Sherman, G.F., Hoplight, B.J., and Denenberg, V.H. (2000). Working memory deficits in BXSB mice with neocortical ectopias. Physiol Behav *70*, 1-5.

Ishii, A., Furusho, M., and Bansal, R. (2013). Sustained Activation of ERK1/2 MAPK in Oligodendrocytes and Schwann Cells Enhances Myelin Growth and Stimulates Oligodendrocyte Progenitor Expansion. Journal of Neuroscience *33*, 175-186.

Jindal, G.A., Goyal, Y., Burdine, R.D., Rauen, K.A., and Shvartsman, S.Y. (2015). RASopathies: unraveling mechanisms with animal models. Dis Model Mech *8*, 769-782.

Johnson, E.M., Ishak, A.D., Naylor, P.E., Stevenson, D.A., Reiss, A.L., and Green, T. (2019). PTPN11 Gain-of-Function Mutations Affect the Developing Human Brain, Memory, and Attention. Cereb Cortex *29*, 2915-2923.

Kann, O., Papageorgiou, I.E., and Draguhn, A. (2014). Highly energized inhibitory interneurons are a central element for information processing in cortical networks. J Cereb Blood Flow Metab *34*, 1270-1282.

Kaul, A., Toonen, J.A., Cimino, P.J., Gianino, S.M., and Gutmann, D.H. (2015). Akt- or MEK-mediated mTOR inhibition suppresses Nf1 optic glioma growth. Neuro Oncol *17*, 843-853.

Kawauchi, T. (2015). Cellullar insights into cerebral cortical development: focusing on the locomotion mode of neuronal migration. Frontiers in Cellular Neuroscience *9*.

Kelsom, C., and Lu, W. (2013). Development and specification of GABAergic cortical interneurons. Cell Biosci *3*, 19.

Kessaris, N., Magno, L., Rubin, A.N., and Oliveira, M.G. (2014). Genetic programs controlling cortical interneuron fate. Curr Opin Neurobiol *26*, 79-87.

Kim, J., Kim, D., and Jung, M.W. (2018). Distinct Dynamics of Striatal and Prefrontal Neural Activity During Temporal Discrimination. Front Integr Neurosci *12*, 34.

Klesse, L.J., Meyers, K.A., Marshall, C.J., and Parada, L.F. (1999). Nerve growth factor induces survival and differentiation through two distinct signaling cascades in PC12 cells. Oncogene *18*, 2055-2068.

Kobayashi, T., Aoki, Y., Niihori, T., Cavé, H., Verloes, A., Okamoto, N., Kawame, H., Fujiwara, I., Takada, F., Ohata, T., *et al.* (2010). Molecular and clinical analysis of RAF1 in Noonan syndrome and related disorders: dephosphorylation of serine 259 as the essential mechanism for mutant activation. Hum Mutat *31*, 284-294.

Koini, M., Rombouts, S.A.R.B., Veer, I.M., Van Buchem, M.A., and Huijbregts, S.C.J. (2017). White matter microstructure of patients with neurofibromatosis type 1 and its relation to inhibitory control. Brain Imaging Behav *11*, 1731-1740.

Komada, M., Takao, K., and Miyakawa, T. (2008). Elevated plus maze for mice. J Vis Exp.

Krab, L.C., de Goede-Bolder, A., Aarsen, F.K., Pluijm, S.M., Bouman, M.J., van der Geest, J.N., Lequin, M., Catsman, C.E., Arts, W.F., Kushner, S.A., *et al.* (2008). Effect of simvastatin on cognitive functioning in children with neurofibromatosis type 1: a randomized controlled trial. JAMA *300*, 287-294.

Krencik, R., Hokanson, K.C., Narayan, A.R., Dvornik, J., Rooney, G.E., Rauen, K.A., Weiss, L.A., Rowitch, D.H., and Ullian, E.M. (2015). Dysregulation of astrocyte extracellular signaling in Costello syndrome. Sci Transl Med *7*, 286ra266.

Krens, S.F., Spaink, H.P., and Snaar-Jagalska, B.E. (2006). Functions of the MAPK family in vertebrate-development. FEBS Lett *580*, 4984-4990.

Krenz, M., Gulick, J., Osinska, H.E., Colbert, M.C., Molkentin, J.D., and Robbins, J. (2008). Role of ERK1/2 signaling in congenital valve malformations in Noonan syndrome. Proc Natl Acad Sci U S A *105*, 18930-18935.

Krishnan, K., Wang, B.S., Lu, J., Wang, L., Maffei, A., Cang, J., and Huang, Z.J. (2015). MeCP2 regulates the timing of critical period plasticity that shapes functional connectivity in primary visual cortex. Proc Natl Acad Sci U S A *112*, E4782-4791.

Krueger, D.D., Osterweil, E.K., Chen, S.P., Tye, L.D., and Bear, M.F. (2011). Cognitive dysfunction and prefrontal synaptic abnormalities in a mouse model of fragile X syndrome. Proc Natl Acad Sci U S A *108*, 2587-2592.

Kumar, R.A., KaraMohamed, S., Sudi, J., Conrad, D.F., Brune, C., Badner, J.A., Gilliam, T.C., Nowak, N.J., Cook, E.H., Dobyns, W.B., *et al.* (2008). Recurrent 16p11.2 microdeletions in autism. Hum Mol Genet *17*, 628-638.

Kushner, S., Elgersma, Y., Murphy, G., Jaarsma, D., Hojjati, M., Cui, Y., LeBoutillier, J., Marrone, D., Choi, E., De Zeeuw, C., *et al.* (2005). Modulation of presynaptic plasticity and learning by the H-ras/extracellular signal-regulated kinase/synapsin I signaling pathway. Journal of Neuroscience *25*, 9721-9734.

Lajiness, J.D., Snider, P., Wang, J., Feng, G.S., Krenz, M., and Conway, S.J. (2014). SHP-2 deletion in postmigratory neural crest cells results in impaired cardiac sympathetic innervation. Proc Natl Acad Sci U S A *111*, E1374-1382.

Langdon, Y., Tandon, P., Paden, E., Duddy, J., Taylor, J.M., and Conlon, F.L. (2012). SHP-2 acts via ROCK to regulate the cardiac actin cytoskeleton. Development *139*, 948-957.

Lavdas, A.A., Grigoriou, M., Pachnis, V., and Parnavelas, J.G. (1999). The medial ganglionic eminence gives rise to a population of early neurons in the developing cerebral cortex. J Neurosci *19*, 7881-7888.

Lavoie, H., and Therrien, M. (2015). Regulation of RAF protein kinases in ERK signalling. Nat Rev Mol Cell Biol *16*, 281-298.

Le Magueresse, C., and Monyer, H. (2013). GABAergic Interneurons Shape the Functional Maturation of the Cortex. Neuron *77*, 388-405.

Le, T., Du, G., Fonseca, M., Zhou, Q., Wigle, J., and Eisenstat, D. (2007). Dlx homeobox genes promote cortical interneuron migration from the basal forebrain by direct repression of the semaphorin receptor Neuropilin-2. Journal of Biological Chemistry *282*, 19071-19081.

Lee, Y., Ehninger, D., Zhou, M., Oh, J., Kang, M., Kwak, C., Ryu, H., Butz, D., Araki, T., Cai, Y., *et al.* (2014). Mechanism and treatment for learning and memory deficits in mouse models of Noonan syndrome. Nature Neuroscience *17*, 1736-1743.

Lee, Y., and Silva, A. (2009). The molecular and cellular biology of enhanced cognition. Nature Reviews Neuroscience *10*, 126-140.

Legius, E., Descheemaeker, M.J., Steyaert, J., Spaepen, A., Vlietinck, R., Casaer, P., Demaerel, P., and Fryns, J.P. (1995). Neurofibromatosis type 1 in childhood: correlation of MRI findings with intelligence. J Neurol Neurosurg Psychiatry *59*, 638-640.

Lehmann, K., Steinecke, A., and Bolz, J. (2012). GABA through the Ages: Regulation of Cortical Function and Plasticity by Inhibitory Interneurons. Neural Plasticity.

Li, H., Chou, S., Hamasaki, T., Perez-Garcia, C., and O'Leary, D. (2012a). Neuregulin repellent signaling via ErbB4 restricts GABAergic interneurons to migratory paths from ganglionic eminence to cortical destinations. Neural Development *7*.

Li, X., Newbern, J., Wu, Y., Morgan-Smith, M., Zhong, J., Charron, J., and Snider, W. (2012b). MEK Is a Key Regulator of Gliogenesis in the Developing Brain. Neuron *75*, 1035-1050.

Li, Y., McKay, R.M., Riethmacher, D., and Parada, L.F. (2012c). Neurofibromin modulates adult hippocampal neurogenesis and behavioral effects of antidepressants. J Neurosci *32*, 3529-3539.

Liddelow, S.A., and Barres, B.A. (2017). Reactive Astrocytes: Production, Function, and Therapeutic Potential. Immunity *46*, 957-967.

Lim, L., Mi, D., Llorca, A., and Marín, O. (2018). Development and Functional Diversification of Cortical Interneurons. Neuron *100*, 294-313.

Loitfelder, M., Huijbregts, S.C., Veer, I.M., Swaab, H.S., Van Buchem, M.A., Schmidt, R., and Rombouts, S.A. (2015). Functional Connectivity Changes and Executive and Social Problems in Neurofibromatosis Type I. Brain Connect *5*, 312-320.

Long, J., Swan, C., Liang, W., Cobos, I., Potter, G., and Rubenstein, J. (2009). Dlx1&2 and Mash1 Transcription Factors Control Striatal Patterning and Differentiation Through Parallel and Overlapping Pathways. Journal of Comparative Neurology *512*, 556-572.

Loo, L., Simon, J.M., Xing, L., McCoy, E.S., Niehaus, J.K., Guo, J., Anton, E.S., and Zylka, M.J. (2019). Single-cell transcriptomic analysis of mouse neocortical development. Nat Commun *10*, 134.

Lush, M., Li, Y., Kwon, C., Chen, J., and Parada, L. (2008). Neurofibromin is required for barrel formation in the mouse somatosensory cortex. Journal of Neuroscience *28*, 1580-1587.

López-Juárez, A., Titus, H.E., Silbak, S.H., Pressler, J.W., Rizvi, T.A., Bogard, M., Bennett, M.R., Ciraolo, G., Williams, M.T., Vorhees, C.V., *et al.* (2017). Oligodendrocyte Nf1 Controls Aberrant Notch Activation and Regulates Myelin Structure and Behavior. Cell Rep *19*, 545-557.

Madisen, L., Zwingman, T.A., Sunkin, S.M., Oh, S.W., Zariwala, H.A., Gu, H., Ng, L.L., Palmiter, R.D., Hawrylycz, M.J., Jones, A.R., *et al.* (2010). A robust and high-throughput Cre reporting and characterization system for the whole mouse brain. Nat Neurosci *13*, 133-140.

Mainberger, F., Jung, N.H., Zenker, M., Wahlländer, U., Freudenberg, L., Langer, S., Berweck, S., Winkler, T., Straube, A., Heinen, F., *et al.* (2013). Lovastatin improves impaired synaptic plasticity and phasic alertness in patients with neurofibromatosis type 1. BMC Neurol *13*, 131.

Mardinly, A.R., Spiegel, I., Patrizi, A., Centofante, E., Bazinet, J.E., Tzeng, C.P., Mandel-Brehm, C., Harmin, D.A., Adesnik, H., Fagiolini, M., *et al.* (2016). Sensory experience regulates cortical inhibition by inducing IGF1 in VIP neurons. Nature *531*, 371-375.

Marin, O. (2013). Cellular and molecular mechanisms controlling the migration of neocortical interneurons. European Journal of Neuroscience *38*, 2019-2029.

Marin, O., and Rubenstein, J. (2001). A long, remarkable journey: Tangential migration in the telencephalon. Nature Reviews Neuroscience *2*, 780-790.

Marin, O., and Rubenstein, J. (2003). Cell migration in the forebrain. Annual Review of Neuroscience *26*, 441-483.

Marin, O., Valiente, M., Ge, X., and Tsai, L. (2010). Guiding Neuronal Cell Migrations. Cold Spring Harbor Perspectives in Biology *2*.

Markram, H., Toledo-Rodriguez, M., Wang, Y., Gupta, A., Silberberg, G., and Wu, C. (2004). Interneurons of the neocortical inhibitory system. Nature Reviews Neuroscience *5*, 793-807.

Martin, P., and Pognonec, P. (2010). ERK and cell death: cadmium toxicity, sustained ERK activation and cell death. FEBS J *277*, 39-46.

Mayer, C., Hafemeister, C., Bandler, R.C., Machold, R., Batista Brito, R., Jaglin, X., Allaway, K., Butler, A., Fishell, G., and Satija, R. (2018). Developmental diversification of cortical inhibitory interneurons. Nature *555*, 457-462.

Mayes, D.A., Rizvi, T.A., Titus-Mitchell, H., Oberst, R., Ciraolo, G.M., Vorhees, C.V., Robinson, A.P., Miller, S.D., Cancelas, J.A., Stemmer-Rachamimov, A.O., *et al.* (2013). Nf1 loss and Ras hyperactivation in oligodendrocytes induce NOS-driven defects in myelin and vasculature. Cell Rep *4*, 1197-1212.

McKenzie, I.A., Ohayon, D., Li, H., de Faria, J.P., Emery, B., Tohyama, K., and Richardson, W.D. (2014). Motor skill learning requires active central myelination. Science *346*, 318-322.

McKenzie, M.G., Cobbs, L.V., Dummer, P.D., Petros, T.J., Halford, M.M., Stacker, S.A., Zou, Y., Fishell, G.J., and Au, E. (2019). Non-canonical Wnt Signaling through Ryk Regulates the Generation of Somatostatin- and Parvalbumin-Expressing Cortical Interneurons. Neuron *103*, 853-864.e854.

McMillan, E.L., Kamps, A.L., Lake, S.S., Svendsen, C.N., and Bhattacharyya, A. (2012). Gene expression changes in the MAPK pathway in both Fragile X and Down syndrome human neural progenitor cells. Am J Stem Cells *1*, 154-162.

Metin, C., Baudoin, J., Rakic, S., and Parnavelas, J. (2006). Cell and molecular mechanisms involved in the migration of cortical interneurons. European Journal of Neuroscience *23*, 894-900.

Mi, D., Li, Z., Lim, L., Li, M., Moissidis, M., Yang, Y., Gao, T., Hu, T.X., Pratt, T., Price, D.J., *et al.* (2018). Early emergence of cortical interneuron diversity in the mouse embryo. Science *360*, 81-85.

Michalon, A., Sidorov, M., Ballard, T.M., Ozmen, L., Spooren, W., Wettstein, J.G., Jaeschke, G., Bear, M.F., and Lindemann, L. (2012). Chronic pharmacological mGlu5 inhibition corrects fragile X in adult mice. Neuron *74*, 49-56.

Miguel, C.S., Chaim-Avancini, T.M., Silva, M.A., and Louzã, M.R. (2015). Neurofibromatosis type 1 and attention deficit hyperactivity disorder: a case study and literature review. Neuropsychiatr Dis Treat *11*, 815-821.

Miller, F.D., and Gauthier, A.S. (2007). Timing is everything: making neurons versus glia in the developing cortex. Neuron *54*, 357-369.

Mitra, I., Lavillaureix, A., Yeh, E., Traglia, M., Tsang, K., Bearden, C.E., Rauen, K.A., and Weiss, L.A. (2017). Reverse Pathway Genetic Approach Identifies Epistasis in Autism Spectrum Disorders. PLoS Genet *13*, e1006516.

Miyoshi, G., and Fishell, G. (2011). GABAergic Interneuron Lineages Selectively Sort into Specific Cortical Layers during Early Postnatal Development. Cerebral Cortex *21*, 845-852.

Miyoshi, G., Hjerling-Leffler, J., Karayannis, T., Sousa, V., Butt, S., Battiste, J., Johnson, J., Machold, R., and Fishell, G. (2010). Genetic Fate Mapping Reveals That the Caudal Ganglionic Eminence Produces a Large and Diverse Population of Superficial Cortical Interneurons. Journal of Neuroscience *30*, 1582-1594.

Miyoshi, G., Young, A., Petros, T., Karayannis, T., Chang, M., Lavado, A., Iwano, T., Nakajima, M., Taniguchi, H., Huang, Z., *et al.* (2015). Prox1 Regulates the Subtype-Specific Development of Caudal Ganglionic Eminence-Derived GABAergic Cortical Interneurons. Journal of Neuroscience *35*, 12869-12889.

Molofsky, A., Krenick, R., Ullian, E., Tsai, H., Deneen, B., Richardson, W., Barres, B., and Rowitch, D. (2012). Astrocytes and disease: a neurodevelopmental perspective. Genes & Development *26*, 891-907.

Monory, K., Massa, F., Egertová, M., Eder, M., Blaudzun, H., Westenbroek, R., Kelsch, W., Jacob, W., Marsch, R., Ekker, M., *et al.* (2006). The endocannabinoid system controls key epileptogenic circuits in the hippocampus. Neuron *51*, 455-466.

Morishita, H., Cabungcal, J., Chen, Y., Do, K., and Hensch, T. (2015). Prolonged Period of Cortical Plasticity upon Redox Dysregulation in Fast-Spiking Interneurons. Biological Psychiatry *78*, 396-402.

Mountcastle, V.B. (1997). The columnar organization of the neocortex. Brain *120 (Pt 4)*, 701-722.

Nakashima, K., Takizawa, T., Ochiai, W., Yanagisawa, M., Hisatsune, T., Nakafuku, M., Miyazono, K., Kishimoto, T., Kageyama, R., and Taga, T. (2001). BMP2-mediated alteration in the developmental pathway of fetal mouse brain cells from neurogenesis to astrocytogenesis. Proc Natl Acad Sci U S A *98*, 5868-5873.

Nakashima, K., Wiese, S., Yanagisawa, M., Arakawa, H., Kimura, N., Hisatsune, T., Yoshida, K., Kishimoto, T., Sendtner, M., and Taga, T. (1999). Developmental requirement of gp130 signaling in neuronal survival and astrocyte differentiation. J Neurosci *19*, 5429-5434.

Narayanan, N.S., Land, B.B., Solder, J.E., Deisseroth, K., and DiLeone, R.J. (2012). Prefrontal D1 dopamine signaling is required for temporal control. Proc Natl Acad Sci U S A *109*, 20726-20731.

Nateri, A.S., Raivich, G., Gebhardt, C., Da Costa, C., Naumann, H., Vreugdenhil, M., Makwana, M., Brandner, S., Adams, R.H., Jefferys, J.G., *et al.* (2007). ERK activation causes epilepsy by stimulating NMDA receptor activity. EMBO J *26*, 4891-4901.

Newbern, J., Zhong, J., Wickramasinghe, S., Li, X., Wu, Y., Samuels, I., Cherosky, N., Karlo, J., O'Loughlin, B., Wikenheiser, J., *et al.* (2008). Mouse and human phenotypes indicate a critical conserved role for ERK2 signaling in neural crest development. Proceedings of the National Academy of Sciences of the United States of America *105*, 17115-17120.

Newbern, J.M., Li, X., Shoemaker, S.E., Zhou, J., Zhong, J., Wu, Y., Bonder, D., Hollenback, S., Coppola, G., Geschwind, D.H., *et al.* (2011). Specific functions for ERK/MAPK signaling during PNS development. Neuron *69*, 91-105.

Nordlund, M.L., Rizvi, T.A., Brannan, C.I., and Ratner, N. (1995). Neurofibromin expression and astrogliosis in neurofibromatosis (type 1) brains. J Neuropathol Exp Neurol *54*, 588-600.

North, K., Joy, P., Yuille, D., Cocks, N., Mobbs, E., Hutchins, P., McHugh, K., and de Silva, M. (1994). Specific learning disability in children with neurofibromatosis type 1: significance of MRI abnormalities. Neurology *44*, 878-883.

Nowaczyk, M.J., Thompson, B.A., Zeesman, S., Moog, U., Sanchez-Lara, P.A., Magoulas, P.L., Falk, R.E., Hoover-Fong, J.E., Batista, D.A., Amudhavalli, S.M., *et al.* (2014). Deletion of MAP2K2/MEK2: a novel mechanism for a RASopathy? Clin Genet *85*, 138-146.

Okaty, B., Miller, M., Sugino, K., Hempel, C., and Nelson, S. (2009). Transcriptional and Electrophysiological Maturation of Neocortical Fast-Spiking GABAergic Interneurons. Journal of Neuroscience *29*, 7040-7052.

Owen, J.P., Chang, Y.S., Pojman, N.J., Bukshpun, P., Wakahiro, M.L., Marco, E.J., Berman, J.I., Spiro, J.E., Chung, W.K., Buckner, R.L., *et al.* (2014). Aberrant white matter microstructure in children with 16p11.2 deletions. J Neurosci *34*, 6214-6223.

Ozkan, E.D., Creson, T.K., Kramár, E.A., Rojas, C., Seese, R.R., Babyan, A.H., Shi, Y., Lucero, R., Xu, X., Noebels, J.L., *et al.* (2014). Reduced cognition in Syngap1 mutants is caused by isolated damage within developing forebrain excitatory neurons. Neuron *82*, 1317-1333.

Paluszkiewicz, S.M., Martin, B.S., and Huntsman, M.M. (2011). Fragile X syndrome: the GABAergic system and circuit dysfunction. Dev Neurosci *33*, 349-364.

Pan, N.C., Fang, A., Shen, C., Sun, L., Wu, Q., and Wang, X. (2019). Early Excitatory Activity-Dependent Maturation of Somatostatin Interneurons in Cortical Layer 2/3 of Mice. Cereb Cortex *29*, 4107-4118.

Pandit, B., Sarkozy, A., Pennacchio, L.A., Carta, C., Oishi, K., Martinelli, S., Pogna, E.A., Schackwitz, W., Ustaszewska, A., Landstrom, A., *et al.* (2007). Gain-of-function RAF1 mutations cause Noonan and LEOPARD syndromes with hypertrophic cardiomyopathy. Nat Genet *39*, 1007-1012.

Paquin, A., Hordo, C., Kaplan, D., and Miller, F. (2009). Costello syndrome H-Ras alleles regulate cortical development. Developmental Biology *330*, 440-451.

Parnavelas, J.G. (2000). The origin and migration of cortical neurones: new vistas. Trends Neurosci *23*, 126-131.

Paul, A., Crow, M., Raudales, R., He, M., Gillis, J., and Huang, Z.J. (2017). Transcriptional Architecture of Synaptic Communication Delineates GABAergic Neuron Identity. Cell *171*, 522-539.e520.

Payne, J.M., Barton, B., Ullrich, N.J., Cantor, A., Hearps, S.J., Cutter, G., Rosser, T., Walsh, K.S., Gioia, G.A., Wolters, P.L., *et al.* (2016). Randomized placebo-controlled study of lovastatin in children with neurofibromatosis type 1. Neurology *87*, 2575-2584.

Perrinjaquet, M., Sjostrand, D., Moliner, A., Zechel, S., Lamballe, F., Maina, F., and Ibanez, C. (2011). MET signaling in GABAergic neuronal precursors of the medial ganglionic eminence restricts GDNF activity in cells that express GFR alpha 1 and a new transmembrane receptor partner. Journal of Cell Science *124*, 2797-2805.

Petros, T.J., Bultje, R.S., Ross, M.E., Fishell, G., and Anderson, S.A. (2015). Apical versus Basal Neurogenesis Directs Cortical Interneuron Subclass Fate. Cell Rep *13*, 1090-1095.

Pham, T.A., Graham, S.J., Suzuki, S., Barco, A., Kandel, E.R., Gordon, B., and Lickey, M.E. (2004). A semi-persistent adult ocular dominance plasticity in visual cortex is stabilized by activated CREB. Learn Mem *11*, 738-747.

Pierpont, E., Hudock, R., Foy, A., Semrud-Clikeman, M., Pierpont, M., Berry, S., Shanley, R., Rubin, N., Sommer, K., and Moertel, C. (2018). Social skills in children with RASopathies: a comparison of Noonan syndrome and neurofibromatosis type 1. Journal of Neurodevelopmental Disorders *10*.

Pierpont, E., Pierpont, M., Mendelsohn, N., Roberts, A., Tworog-Dube, E., and Seidenberg, M. (2009). Genotype differences in cognitive functioning in Noonan syndrome. Genes Brain and Behavior *8*, 275-282.

Pierpont, E., Tworog-Dube, E., and Roberts, A. (2015). Attention skills and executive functioning in children with Noonan syndrome and their unaffected siblings. Developmental Medicine and Child Neurology *57*, 385-392.

Pierpont, E.I., Ellis Weismer, S., Roberts, A.E., Tworog-Dube, E., Pierpont, M.E., Mendelsohn, N.J., and Seidenberg, M.S. (2010a). The language phenotype of children and adolescents with Noonan syndrome. J Speech Lang Hear Res *53*, 917-932.

Pierpont, E.I., Pierpont, M.E., Mendelsohn, N.J., Roberts, A.E., Tworog-Dube, E., Rauen, K.A., and Seidenberg, M.S. (2010b). Effects of germline mutations in the

Ras/MAPK signaling pathway on adaptive behavior: cardiofaciocutaneous syndrome and Noonan syndrome. Am J Med Genet A *152A*, 591-600.

Pierpont, E.I., Tworog-Dube, E., and Roberts, A.E. (2013). Learning and memory in children with Noonan syndrome. Am J Med Genet A *161A*, 2250-2257.

Pizzarelli, R., and Cherubini, E. (2011). Alterations of GABAergic Signaling in Autism Spectrum Disorders. Neural Plasticity.

Pizzorusso, T., Medini, P., Berardi, N., Chierzi, S., Fawcett, J.W., and Maffei, L. (2002). Reactivation of ocular dominance plasticity in the adult visual cortex. Science *298*, 1248-1251.

Polleux, F., Whitford, K., Dijkhuizen, P., Vitalis, T., and Ghosh, A. (2002). Control of cortical interneuron migration by neurotrophins and PI3-kinase signaling. Development *129*, 3147-3160.

Poulikakos, P.I., Zhang, C., Bollag, G., Shokat, K.M., and Rosen, N. (2010). RAF inhibitors transactivate RAF dimers and ERK signalling in cells with wild-type BRAF. Nature *464*, 427-430.

Pozas, E., and Ibanez, C. (2005). GDNF and GFR alpha 1 promote differentiation and tangential migration of cortical GABAergic neurons. Neuron *45*, 701-713.

Pucilowska, J., Puzerey, P., Karlo, J., Galan, R., and Landreth, G. (2012). Disrupted ERK Signaling during Cortical Development Leads to Abnormal Progenitor Proliferation, Neuronal and Network Excitability and Behavior, Modeling Human Neuro-Cardio-Facial-Cutaneous and Related Syndromes. Journal of Neuroscience *32*, 8663-8677.

Pucilowska, J., Samuels, I., Karlo, C., and Landreth, G. (2008). Simultaneous inactivation of Erk1 and Erk2 leads to perturbations in the control of the cell cycle during neurogenesis. International Journal of Developmental Neuroscience *26*, 877-878.

Pucilowska, J., Vithayathil, J., Pagani, M., Kelly, C., Karlo, J.C., Robol, C., Morella, I., Gozzi, A., Brambilla, R., and Landreth, G.E. (2018). Pharmacological Inhibition of ERK Signaling Rescues Pathophysiology and Behavioral Phenotype Associated with 16p11.2 Chromosomal Deletion in Mice. J Neurosci *38*, 6640-6652.

Pucilowska, J., Vithayathil, J., Tavares, E., Kelly, C., Karlo, J., and Landreth, G. (2015). The 16p11.2 Deletion Mouse Model of Autism Exhibits Altered Cortical Progenitor Proliferation and Brain Cytoarchitecture Linked to the ERK MAPK Pathway. Journal of Neuroscience *35*, 3190-3200.

Rakic, P. (1974). Neurons in rhesus monkey visual cortex: systematic relation between time of origin and eventual disposition. Science *183*, 425-427.

Rauen, K., Chakravarti, A., and Green, E. (2013). The RASopathies. Annual Review of Genomics and Human Genetics, Vol 14 *14*, 355-369.

Rauen, K., Huson, S., Burkitt-Wright, E., Evans, D., Farschtschi, S., Ferner, R., Gutmann, D., Hanemann, C., Kerr, B., Legius, E., *et al.* (2015). Recent Developments in Neurofibromatoses and RASopathies: Management, Diagnosis and Current and Future Therapeutic Avenues. American Journal of Medical Genetics Part a *167*, 1-10.

Razzaque, M.A., Nishizawa, T., Komoike, Y., Yagi, H., Furutani, M., Amo, R., Kamisago, M., Momma, K., Katayama, H., Nakagawa, M., *et al.* (2007). Germline gain-of-function mutations in RAF1 cause Noonan syndrome. Nat Genet *39*, 1013-1017.

Rhee, Y.H., Yi, S.H., Kim, J.Y., Chang, M.Y., Jo, A.Y., Kim, J., Park, C.H., Cho, J.Y., Choi, Y.J., Sun, W., *et al.* (2016). Neural stem cells secrete factors facilitating brain regeneration upon constitutive Raf-Erk activation. Sci Rep *6*, 32025.

Rizvi, T., Akunuru, S., de Courten-Myers, G., Switzer, R., Nordlund, M., and Ratner, N. (1999). Region-specific astrogliosis in brains of mice heterozygous for mutations in the neurofibromatosis type 1 (Nf1) tumor suppressor. Brain Research *816*, 111-123.

Roberts, A.E., Araki, T., Swanson, K.D., Montgomery, K.T., Schiripo, T.A., Joshi, V.A., Li, L., Yassin, Y., Tamburino, A.M., Neel, B.G., *et al.* (2007). Germline gain-of-function mutations in SOS1 cause Noonan syndrome. Nat Genet *39*, 70-74.

Rodriguez-Viciana, P., Rauen, K., Balch, W., Der, C., and Hall, A. (2008). Biochemical characterization of novel germline BRAF and MEK mutations in cardio-facio-cutaneous syndrome. Small Gtpases in Disease, Part a *438*, 277-289.

Rodriguez-Viciana, P., Tetsu, O., Tidyman, W., Estep, A., Conger, B., Cruz, M., McCormick, F., and Rauen, K. (2006). Germline mutations in genes within the MAPK pathway cause cardio-facio-cutaneous syndrome. Science *311*, 1287-1290.

Rojas-Leguizamón, M., Baroja, J.L., Sanabria, F., and Orduña, V. (2018). Response-inhibition capacity in spontaneously hypertensive and Wistar rats: acquisition of fixed minimum interval performance and responsiveness to D-amphetamine. Behav Pharmacol *29*, 668-675.

Rooney, G.E., Goodwin, A.F., Depeille, P., Sharir, A., Schofield, C.M., Yeh, E., Roose, J.P., Klein, O.D., Rauen, K.A., Weiss, L.A., *et al.* (2016). Human iPS Cell-Derived Neurons Uncover the Impact of Increased Ras Signaling in Costello Syndrome. J Neurosci *36*, 142-152.

Rosato-Siri, M., Zambello, E., Mutinelli, C., Garbati, N., Benedetti, R., Aldegheri, L., Graziani, F., Virginio, C., Alvaro, G., and Large, C. (2015). A Novel Modulator of Kv3 Potassium Channels Regulates the Firing of Parvalbumin-Positive Cortical Interneurons. Journal of Pharmacology and Experimental Therapeutics *354*, 251-260.

Roth, B. (2016). DREADDs for Neuroscientists. Neuron *89*, 683-694.

Rudy, B., Fishell, G., Lee, S., and Hjerling-Leffler, J. (2011). Three groups of interneurons account for nearly 100% of neocortical GABAergic neurons. Dev Neurobiol *71*, 45-61.

Rudy, B., and McBain, C. (2001). Kv3 channels: voltage-gated K+ channels designed for high-frequency repetitive firing. Trends in Neurosciences *24*, 517-526.

Sahara, S., Yanagawa, Y., O'Leary, D., and Stevens, C. (2012). The Fraction of Cortical GABAergic Neurons Is Constant from Near the Start of Cortical Neurogenesis to Adulthood. Journal of Neuroscience *32*, 4755-4761.

Saitta, S.C., Harris, S.E., Gaeth, A.P., Driscoll, D.A., McDonald-McGinn, D.M., Maisenbacher, M.K., Yersak, J.M., Chakraborty, P.K., Hacker, A.M., Zackai, E.H., *et al.* (2004). Aberrant interchromosomal exchanges are the predominant cause of the 22q11.2 deletion. Hum Mol Genet *13*, 417-428.

Samuels, I., Karlo, J., Faruzzi, A., Pickering, K., Herrup, K., Sweatt, J., Saitta, S., and Landreth, G. (2008). Deletion of ERK2 mitogen-activated protein kinase identifies its key roles in cortical neurogenesis and cognitive function. Journal of Neuroscience *28*, 6983-6995.

Samuels, I., Saitta, S., and Landreth, G. (2009). MAP'ing CNS Development and Cognition: An ERKsome Process. Neuron *61*, 160-167.

Sanchez-Ortiz, E., Cho, W., Nazarenko, I., Mo, W., Chen, J., and Parada, L. (2014). NF1 regulation of RAS/ERK signaling is required for appropriate granule neuron progenitor expansion and migration in cerebellar development. Genes & Development *28*, 2407-2420.

Sandberg, M., Taher, L., Hu, J., Black, B.L., Nord, A.S., and Rubenstein, J.L.R. (2018). Genomic analysis of transcriptional networks directing progression of cell states during MGE development. Neural Dev *13*, 21.

Schreiber, J., Grimbergen, L.A., Overwater, I., Vaart, T.V., Stedehouder, J., Schuhmacher, A.J., Guerra, C., Kushner, S.A., Jaarsma, D., and Elgersma, Y. (2017). Mechanisms underlying cognitive deficits in a mouse model for Costello Syndrome are distinct from other RASopathy mouse models. Sci Rep *7*, 1256.

Seidman, L.J., Valera, E.M., Makris, N., Monuteaux, M.C., Boriel, D.L., Kelkar, K., Kennedy, D.N., Caviness, V.S., Bush, G., Aleardi, M., *et al.* (2006). Dorsolateral prefrontal and anterior cingulate cortex volumetric abnormalities in adults with attention-deficit/hyperactivity disorder identified by magnetic resonance imaging. Biol Psychiatry *60*, 1071-1080.

Selby, L., Zhang, C., and Sun, Q.Q. (2007). Major defects in neocortical GABAergic inhibitory circuits in mice lacking the fragile X mental retardation protein. Neurosci Lett *412*, 227-232.

Silverman, J.L., Yang, M., Lord, C., and Crawley, J.N. (2010). Behavioural phenotyping assays for mouse models of autism. Nat Rev Neurosci *11*, 490-502.

Sorg, B.A., Berretta, S., Blacktop, J.M., Fawcett, J.W., Kitagawa, H., Kwok, J.C., and Miquel, M. (2016). Casting a Wide Net: Role of Perineuronal Nets in Neural Plasticity. J Neurosci *36*, 11459-11468.

Soriano, E., Del Rio, J.A., Ferrer, I., Auladell, C., De Lecea, L., and Alcantara, S. (1992). Late appearance of parvalbumin-immunoreactive neurons in the rodent cerebral cortex does not follow an 'inside-out' sequence. Neurosci Lett *142*, 147-150.

Southwell, D., Paredes, M., Galvao, R., Jones, D., Froemke, R., Sebe, J., Alfaro-Cervello, C., Tang, Y., Garcia-Verdugo, J., Rubenstein, J., *et al.* (2012). Intrinsically determined cell death of developing cortical interneurons. Nature *491*, 109-U172.

Stanco, A., Pla, R., Vogt, D., Chen, Y., Mandal, S., Walker, J., Hunt, R., Lindtner, S., Erdman, C., Pieper, A., *et al.* (2014). NPAS1 Represses the Generation of Specific Subtypes of Cortical Interneurons. Neuron *84*, 940-953.

Stanco, A., Szekeres, C., Patel, N., Rao, S., Campbell, K., Kreidberg, J., Polleux, F., and Anton, E. (2009). Netrin-1-alpha 3 beta 1 integrin interactions regulate the migration of interneurons through the cortical marginal zone. Proceedings of the National Academy of Sciences of the United States of America *106*, 7595-7600.

Steullet, P., Cabungcal, J.H., Coyle, J., Didriksen, M., Gill, K., Grace, A.A., Hensch, T.K., LaMantia, A.S., Lindemann, L., Maynard, T.M., *et al.* (2017). Oxidative stress-driven parvalbumin interneuron impairment as a common mechanism in models of schizophrenia. Mol Psychiatry *22*, 936-943.

STEWARD, O., TORRE, E., TOMASULO, R., and LOTHMAN, E. (1992). SEIZURES AND THE REGULATION OF ASTROGLIAL GENE-EXPRESSION. Epilepsy Research, 197-209.

Stringer, J. (1996). Repeated seizures increase GFAP and vimentin in the hippocampus. Brain Research *717*, 147-153.

Sussel, L., Marin, O., Kimura, S., and Rubenstein, J. (1999). Loss of Nkx2.1 homeobox gene function results in a ventral to dorsal molecular respecification within the basal telencephalon: evidence for a transformation of the pallidum into the striatum. Development *126*, 3359-3370.

Suzuki, S., al-Noori, S., Butt, S.A., and Pham, T.A. (2004). Regulation of the CREB signaling cascade in the visual cortex by visual experience and neuronal activity. J Comp Neurol *479*, 70-83.

Sznajer, Y., Keren, B., Baumann, C., Pereira, S., Alberti, C., Elion, J., Cavé, H., and Verloes, A. (2007). The spectrum of cardiac anomalies in Noonan syndrome as a result of mutations in the PTPN11 gene. Pediatrics *119*, e1325-1331.

Tamamaki, N., Fujimori, K.E., and Takauji, R. (1997). Origin and route of tangentially migrating neurons in the developing neocortical intermediate zone. J Neurosci *17*, 8313-8323.

Tartaglia, M., Gelb, B., and Zenker, M. (2011). Noonan syndrome and clinically related disorders. Best Practice & Research Clinical Endocrinology & Metabolism *25*, 161-179.

Tartaglia, M., Kalidas, K., Shaw, A., Song, X., Musat, D., van der Burgt, I., Brunner, H., Bertola, D., Crosby, A., Ion, A., *et al.* (2002). PTPN11 mutations in Noonan syndrome: molecular spectrum, genotype-phenotype correlation, and phenotypic heterogeneity. American Journal of Human Genetics *70*, 1555-1563.

Tartaglia, M., Mehler, E., Goldberg, R., Zampino, G., Brunner, H., Kremer, H., van der Burgt, I., Crosby, A., Ion, A., Jeffery, S., *et al.* (2001). Mutations in PTPN11, encoding the protein tyrosine phosphatase SHP-2, cause Noonan syndrome. Nature Genetics *29*, 465-468.

Thomas, G.M., and Huganir, R.L. (2004). MAPK cascade signalling and synaptic plasticity. Nat Rev Neurosci *5*, 173-183.

Tidyman, W., and Rauen, K. (2016). Pathogenetics of the RASopathies. Human Molecular Genetics *25*, R123-R132.

Tidyman, W.E., and Rauen, K.A. (2009). The RASopathies: developmental syndromes of Ras/MAPK pathway dysregulation. Curr Opin Genet Dev *19*, 230-236.

Tien, A.C., Tsai, H.H., Molofsky, A.V., McMahon, M., Foo, L.C., Kaul, A., Dougherty, J.D., Heintz, N., Gutmann, D.H., Barres, B.A., *et al.* (2012). Regulated temporal-spatial astrocyte precursor cell proliferation involves BRAF signalling in mammalian spinal cord. Development *139*, 2477-2487.

Titus, H.E., López-Juárez, A., Silbak, S.H., Rizvi, T.A., Bogard, M., and Ratner, N. (2017). Oligodendrocyte RasG12V expressed in its endogenous locus disrupts myelin structure through increased MAPK, nitric oxide, and notch signaling. Glia *65*, 1990-2002.

Toyoda, R., Assimacopoulos, S., Wilcoxon, J., Taylor, A., Feldman, P., Suzuki-Hirano, A., Shimogori, T., and Grove, E.A. (2010). FGF8 acts as a classic diffusible morphogen to pattern the neocortex. Development *137*, 3439-3448.

Tyssowski, K.M., DeStefino, N.R., Cho, J.H., Dunn, C.J., Poston, R.G., Carty, C.E., Jones, R.D., Chang, S.M., Romeo, P., Wurzelmann, M.K., *et al.* (2018). Different Neuronal Activity Patterns Induce Different Gene Expression Programs. Neuron *98*, 530-546.e511.

van der Vaart, T., Plasschaert, E., Rietman, A.B., Renard, M., Oostenbrink, R., Vogels, A., de Wit, M.C., Descheemaeker, M.J., Vergouwe, Y., Catsman-Berrevoets, C.E., *et al.* (2013). Simvastatin for cognitive deficits and behavioural problems in patients with neurofibromatosis type 1 (NF1-SIMCODA): a randomised, placebo-controlled trial. Lancet Neurol *12*, 1076-1083.

Vithayathil, J., Pucilowska, J., and Landreth, G.E. (2018). ERK/MAPK signaling and autism spectrum disorders. Prog Brain Res *241*, 63-112.

Vong, L., Ye, C., Yang, Z., Choi, B., Chua, S., and Lowell, B.B. (2011). Leptin action on GABAergic neurons prevents obesity and reduces inhibitory tone to POMC neurons. Neuron *71*, 142-154.

Vorstman, J.A., Staal, W.G., van Daalen, E., van Engeland, H., Hochstenbach, P.F., and Franke, L. (2006). Identification of novel autism candidate regions through analysis of reported cytogenetic abnormalities associated with autism. Mol Psychiatry *11*, 1, 18-28.

Walsh, K.S., Vélez, J.I., Kardel, P.G., Imas, D.M., Muenke, M., Packer, R.J., Castellanos, F.X., and Acosta, M.T. (2013). Symptomatology of autism spectrum disorder in a population with neurofibromatosis type 1. Dev Med Child Neurol *55*, 131-138.

Wamsley, B., and Fishell, G. (2017). Genetic and activity-dependent mechanisms underlying interneuron diversity. Nature Reviews Neuroscience *18*, 299-309.

Wang, S.Z., Dulin, J., Wu, H., Hurlock, E., Lee, S.E., Jansson, K., and Lu, Q.R. (2006). An oligodendrocyte-specific zinc-finger transcription regulator cooperates with Olig2 to promote oligodendrocyte differentiation. Development *133*, 3389-3398.

Wang, Y., Dye, C., Sohal, V., Long, J., Estrada, R., Roztocil, T., Lufkin, T., Deisseroth, K., Baraban, S., and Rubenstein, J. (2010). Dlx5 and Dlx6 Regulate the Development of Parvalbumin-Expressing Cortical Interneurons. Journal of Neuroscience *30*, 5334-5345.

Ware, C.B., Horowitz, M.C., Renshaw, B.R., Hunt, J.S., Liggitt, D., Koblar, S.A., Gliniak, B.C., McKenna, H.J., Papayannopoulou, T., and Thoma, B. (1995). Targeted disruption of the low-affinity leukemia inhibitory factor receptor gene causes placental, skeletal, neural and metabolic defects and results in perinatal death. Development *121*, 1283-1299.

Watterson, E., Mazur, G.J., and Sanabria, F. (2015). Validation of a method to assess ADHD-related impulsivity in animal models. J Neurosci Methods *252*, 36-47.

Wichterle, H., Garcia-Verdugo, J.M., Herrera, D.G., and Alvarez-Buylla, A. (1999). Young neurons from medial ganglionic eminence disperse in adult and embryonic brain. Nat Neurosci *2*, 461-466.

Wichterle, H., Turnbull, D., Nery, S., Fishell, G., and Alvarez-Buylla, A. (2001). In utero fate mapping reveals distinct migratory pathways and fates of neurons born in the mammalian basal forebrain. Development *128*, 3759-3771.

Wonders, C., and Anderson, S. (2006). The origin and specification of cortical interneurons. Nature Reviews Neuroscience *7*, 687-696.

Wu, G.Y., Deisseroth, K., and Tsien, R.W. (2001). Activity-dependent CREB phosphorylation: convergence of a fast, sensitive calmodulin kinase pathway and a slow, less sensitive mitogen-activated protein kinase pathway. Proc Natl Acad Sci U S A *98*, 2808-2813.

Wu, X., Simpson, J., Hong, J., Kim, K., Thavarajah, N., Backx, P., Neel, B., and Araki, T. (2011). MEK-ERK pathway modulation ameliorates disease phenotypes in a mouse model of Noonan syndrome associated with the Raf1(L613V) mutation. Journal of Clinical Investigation *121*, 1009-1025.

Wu, X., Yin, J., Simpson, J., Kim, K.H., Gu, S., Hong, J.H., Bayliss, P., Backx, P.H., Neel, B.G., and Araki, T. (2012). Increased BRAF heterodimerization is the common pathogenic mechanism for noonan syndrome-associated RAF1 mutants. Mol Cell Biol *32*, 3872-3890.

Xing, L., Larsen, R., Bjorklund, G., Li, X., Wu, Y., Philpot, B., Snider, W., and Newbern, J. (2016). Layer specific and general requirements for ERK/MAPK signaling in the developing neocortex. Elife *5*.

Xu, Q., Liu, Y.Y., Wang, X., Tan, G.H., Li, H.P., Hulbert, S.W., Li, C.Y., Hu, C.C., Xiong, Z.Q., Xu, X., *et al.* (2018). Autism-associated CHD8 deficiency impairs axon development and migration of cortical neurons. Mol Autism *9*, 65.

Xu, X., Miller, E.C., and Pozzo-Miller, L. (2014). Dendritic spine dysgenesis in Rett syndrome. Front Neuroanat *8*, 97.

Yashiro, K., Riday, T.T., Condon, K.H., Roberts, A.C., Bernardo, D.R., Prakash, R., Weinberg, R.J., Ehlers, M.D., and Philpot, B.D. (2009). Ube3a is required for experience-dependent maturation of the neocortex. Nat Neurosci *12*, 777-783.

Yassin, L., Benedetti, B.L., Jouhanneau, J.S., Wen, J.A., Poulet, J.F., and Barth, A.L. (2010). An embedded subnetwork of highly active neurons in the neocortex. Neuron *68*, 1043-1050.

Yoon, G., Rosenberg, J., Blaser, S., and Rauen, K. (2007). Neurological complications of cardio-facio-cutaneous syndrome. Developmental Medicine and Child Neurology *49*, 894-899.

Zenker, M., Buheitel, G., Rauch, R., Koenig, R., Bosse, K., Kress, W., Tietze, H.U., Doerr, H.G., Hofbeck, M., Singer, H., *et al.* (2004). Genotype-phenotype correlations in Noonan syndrome. J Pediatr *144*, 368-374.

Zhang, Z.W., Zak, J.D., and Liu, H. (2010). MeCP2 is required for normal development of GABAergic circuits in the thalamus. J Neurophysiol *103*, 2470-2481.

Zhu, Y., Harada, T., Liu, L., Lush, M., Guignard, F., Harada, C., Burns, D., Bajenaru, M., Gutmann, D., and Parada, L. (2005). Inactivation of NF1 in CNS causes increased glial progenitor proliferation and optic glioma formation. Development *132*, 5577-5588.

Zhu, Y., Romero, M.I., Ghosh, P., Ye, Z., Charnay, P., Rushing, E.J., Marth, J.D., and Parada, L.F. (2001). Ablation of NF1 function in neurons induces abnormal development of cerebral cortex and reactive gliosis in the brain. Genes Dev *15*, 859-876.

Zimmer, G., Garcez, P., Rudolph, J., Niehage, R., Weth, F., Lent, R., and Bolz, J. (2008). Ephrin-A5 acts as a repulsive cue for migrating cortical interneurons. European Journal of Neuroscience *28*, 62-73.

APPENDIX A

CURRICULUM VITAE

Michael C. Holter, Ph.D.

School of Life Sciences
Arizona State University
Tempe, AZ 85287-4501

Education

08/2014 – present	**Ph.D., Neuroscience** Arizona State University, Tempe, AZ Advisor: Jason Newbern Thesis Defense: October 31, 2019
09/2010 – 06/2014	**B.A., Biology/Neuroscience** Carleton College, Northfield, MN

Research Interests

My research and career interests are centered on the biological mechanisms underlying neural circuit development and neurodevelopmental disorders. My goals include 1) understanding how diverse cell types of the cerebral cortex are specified under normal conditions, 2) how aberrant cell signaling and transcriptional processes disrupt formation of cortical circuitry, and 3) how mutations of diverse genetic etiology drive disorders such as Autism Spectrum Disorder (ASD). Given my expertise in developmental neurobiology, genetics, and cell signaling, I am well-positioned to address questions regarding ASD pathology.

Awards

- *2017 Travel Award,* ASU Graduate and Professional Student Association
- *2018 Travel Award,* ASU Graduate and Professional Student Association
- *Graduate Research Excellence Award 2018,* ASU CLAS
- *2019 Travel Award,* ASU Graduate and Professional Student Association

Peer-Reviewed Publications

In Submission/Published

Holter M, Bjorklund GR, Nishimura KJ, Gupta T, Hewitt LT, Nichols JD, Shah S, Martinez JS, Marsh S, Sanabria F, Treiman D, Snider WD, Anderson TR, Newbern JM. (2018) ERK/MAPK hyperactivation in embryonic GABAergic neurons promotes cortical Parvalbumin neuron death and increases cortical excitability. *In review at PNAS.*

- *I found that gain-of-function ERK/MAPK signaling leads to the apoptotic death of post-mitotic cortical parvalbumin (PV) interneuron precursors in the subpallial mantle zones. Surviving PV interneurons exhibited significant increases in perineuronal net formation.*

Mutant mice had significant defects in prefrontal cortex function, which is linked to ADHD-like phenotypes. Under consideration, PNAS 09/2019.

Holter M, Hewitt LT, Koebele S, Xing L, Judd J, Araki T, Neel B, Snider WD, Conrad C, Bimonte-Nelson H, Newbern JM. (2019) The Noonan Syndrome-linked *Raf1*^{L613V} mutation drives increased glial number and enhanced learning. *PLOS Genetics.* PMCID: PMC6502435

- *Here we provide the first characterization of the nervous system carrying the Noonan Syndrome Raf1*^{L613V} *mutation. I discovered increases in glial number and altered glial development and collaborated with multiple groups to show the first germline RASopathy mouse model with enhanced learning.*

Der-Ghazarian T, Charmchi D, Noudali S, Scott S, **Holter M**, Newbern J, and Neisewander J. (2019). Neural circuits associated with 5-HT1B receptor agonist inhibition of methamphetamine seeking in the conditioned place preference model. *ACS Chemical Neuroscience*. PMCID: PMC31042352

- *Designed and assisted in the collection of quantitative histochemical images of C-Fos across multiple brain regions.*

Aoidi R, Houde N, Landry-Truchon K, **Holter M**, Jacquet K, Charron L, Krishnaswami SR, Yu BD, Rauen KA, Bisson N, Newbern JM, and Charron J. (2018) *Mek1*^{Y130C} mice recapitulate aspects of the human Cardio-Facio-Cutaneous syndrome. *Disease Models and Mechanisms*. 11(3). PMCID: PMC5897723

- *Assisted in mouse brain immunohistochemistry and analysis reported in figures 6 and 7. I wrote and discussed the results in the primary manuscript. Mek1*^{Y130C} *mice exhibited glial number increases in the cortex further implicating altered glial development across multiple RASopathy mutations.*

In Preparation

Holter M, Martinez JS, Nichols JD, Anderson TR, Newbern JM. Activity-dependent GABAergic circuit development requires ERK/MAPK signaling and alters excitatory drive. *In preparation.*

Conference Posters

Holter M, Fry N, Bjorklund G, Nishimura K, Martinez J, Nichols J, Anderson T, Newbern JM (2019). Cortical GABAergic interneurons require ERK/MAPK for postnatal maturation and function. Ann. Soc. For Neuroscience Meeting.

Holter M, Bjorklund GR, Shah SA, Nishimura K, Newbern JM (2018). Constitutively active MEK1 signaling drives selective death of cortical parvalbumin-expressing

interneurons in mouse embryonic brain development. Ann. Soc. For Neuroscience Meeting. Poster Program No. 550.05

Holter M, Bjorklund GR, Shah SA, Nichols JD, Martinez JS, Anderson TR, Newbern JM (2017) Functions of ERK/MAPK signaling in GABAergic neuron development and identity. Ann. Soc. for Neuroscience Meeting. Poster Program No. 653.20

Gipson-Reichardt C, Powell G, Del-Franco A, **Holter M**, Garcia R, Vannan A, Neisewander J (2017) Developmental Nicotine Exposure Induces Persistent Alterations in Accumbens Glutamatergic Circuitry. 72nd Ann. Meeting of the Soc. of Biological Psychiatry. Abstract No. 801.

Holter M, Hewitt LT, Koebele SV, Judd J, Wedwick C, Bimonte-Nelson HA, Conrad CD, Neel BG, Araki T, Snider WD, Newbern JM (2016) The Noonan Syndrome-linked *Raf1*^{L613V} mutation drives increased glial number and alterations in learning. Ann. Soc. for Neuroscience Meeting. Poster Program No. 32.12/D11

Aoidi R, **Holter M**, Newbern JM, Charron J (2016) Mice carrying the Mek1Y130C mutation present cardio-facio-cutaneous phenotype. Soc. for Developmental Biology Meeting Aug 4-8, Boston, MA. Program Abstract #211

Shah S, **Holter M**, Newbern JM (2016) Hyperactivation of ERK/MAPK Leads to Altered Cortical GABAergic Neuron Number and Morphology. 23rd Annual ASU Undergraduate Poster Symposium, Tempe, AZ, April 17th

Service and Outreach

Arizona State University Homecoming Booth - Brain Awareness Table	2014 – 2018
Brain Fair - Kyrene Monte Vista Elementary School	March 2016
University of Arizona and Cox Connect 2 STEM - Brain Awareness	Jan. 2017
Archway Classical Academy Arete – Outreach Event Organizer	Feb. 2018

Teaching Assistantships

ASU BIO 467, Spring 2017 – Neurobiology:
enrollment – 100
ASU BIO 282, Spring 2018 – Conceptual Approach for Bio Majors II:
enrollment – 25
ASU BIO 351, Fall 2018 – Developmental Biology:
enrollment – 297
ASU BIO 351, Fall 2019 – Developmental Biology:
enrollment – 298

Invited Seminars

Arizona State University Department of Psychology – Summer 2016
"The Noonan Syndrome-linked Raf1^{L613V} mutation drives increased glial number and altered learning"

Arizona State University 8th Annual Neuroscience Symposia – Spring 2018
"ERK/MAPK hyperactivation in embryonic GABAergic neurons promotes cortical Parvalbumin neuron death and increases cortical excitability"

Professional Memberships

Society for Neuroscience	2015 – present
Graduate Association of Interdisciplinary Neuroscience Students	2017 – 2018
Student Representative to ASU Neuroscience Executive Board	2017 – 2019